Reference
84-4

U.S. Department
of Transportation
**Federal Railroad
Administration**

Structure and Properties of Thermite Welds in Premium Rails

Office of Research and
Development
Washington DC 20590

L. C. Schroeder
D. R. Poirier

The Department of Metallurgical Engineering
The University of Arizona
Tucson AZ 85721

DOT/FRA/ORD-85/02
DOT-TSC-FRA-84-4

December 1985
Final Report

Technical Report Documentation Page

1. Report No.	2. Government Accession No.	3. Recipient's Catalog No.
DOT/FRA/ORD-85/02		

4. Title and Subtitle	5. Report Date
STRUCTURE AND PROPERTIES OF THERMITE WELDS IN PREMIUM RAILS	December 1985
	6. Performing Organization Code: DTS-76
7. Author(s): L.C. Schroeder and D.R. Poirier	8. Performing Organization Report No.: DOT-TSC-FRA-84-4
9. Performing Organization Name and Address: *The Department of Metallurgical Engineering, The University of Arizona, Tucson, AZ 85721	10. Work Unit No. (TRAIS): RR519/R5304
	11. Contract or Grant No.: DOT-TSC-1567
12. Sponsoring Agency Name and Address: U.S. Department of Transportation, Federal Railroad Administration, Office of Research and Development, Washington, DC 20590	13. Type of Report and Period Covered: Final Report
	14. Sponsoring Agency Code: RRD-10

15. Supplementary Notes

*Under contract to: U.S. Department of Transportation, Research and Special Programs Administration, Transportation Systems Center, Cambridge MA 02142

16. Abstract

Thermite welds were used to join combinations of premium rails and AREA Controlled Cooled Carbon rails (i.e., standard rails). The premium rails comprised head-hardened rails and CrMo, CrV and Cr alloy rails. A major objective was to determine the feasibility of joining premium rails to each other and to standard rails with the thermite welding process. The objective was met in that metallurgically sound welds were produced using either "standard" or "alloy" thermite charges. Other objectives were to determine mechanical properties and metallurgical structures of the weld-metal and of the heat-affected zones. The "alloy" weld-metal was stronger than "standard" weld metal but had less tensile ductility. Both types exhibit ductilities of only 2-6 percent reduction in area and impact energies of only 1.5-2.8 Joules at 20°C. Tensile and impact specimens, which straddled the region of minimum hardness at the outer edge of the heat affected zone, show tensile ductilities of 19-60 percent reduction in area and only 2.6-6.9 Joules for impact energy. In addition, temperature in the rail near the weld metal was measured as four of the welds were produced; in a fifth, temperatures in the weld metal, itself, were measured. Finally, residual stresses were determined, and their effect on fatigue strength of welded rail is discussed.

17. Key Words	18. Distribution Statement
Rail, Thermite-Welding, Premium Rails, Mechanical Properties, Residual Stresses	DOCUMENT IS AVAILABLE TO THE PUBLIC THROUGH THE NATIONAL TECHNICAL INFORMATION SERVICE, SPRINGFIELD, VIRGINIA 22161

19. Security Classif. (of this report)	20. Security Classif. (of this page)	21. No. of Pages	22. Price
UNCLASSIFIED	UNCLASSIFIED	122	

Form DOT F 1700.7 (8-72) Reproduction of completed page authorized

PREFACE

This report was prepared by L. C. Schroeder and D. R. Poirier of the Department of Metallurgical Engineering, The University of Arizona. The technical monitor was Mr. James Morris of the Transportation Systems Center in Cambridge, Massachusetts. Dr. Roger K. Steele, then of the Federal Railroad Administration, Transportation Test Center in Pueblo, Colorado graciously arranged for the thermite-welding at the FAST facility in Pueblo. Messrs. Morris and Steele generously made themselves available for technical consultation for the duration of the project. Their assistance is gratefully acknowledged.

METRIC CONVERSION FACTORS

Approximate Conversions to Metric Measures

Symbol	When You Know	Multiply by	To Find	Symbol
		LENGTH		
in	inches	*2.5	centimeters	cm
ft	feet	30	centimeters	cm
yd	yards	0.9	meters	m
mi	miles	1.6	kilometers	km
		AREA		
in^2	square inches	6.5	square centimeters	cm^2
ft^2	square feet	0.09	square meters	m^2
yd^2	square yards	0.8	square meters	m^2
mi^2	square miles	2.6	square kilometers	km^2
	acres	0.4	hectares	ha
		MASS (weight)		
oz	ounces	28	grams	g
lb	pounds	0.45	kilograms	kg
	short tons (2000 lb)	0.9	tonnes	t
		VOLUME		
tsp	teaspoons	5	milliliters	ml
Tbsp	tablespoons	15	milliliters	ml
fl oz	fluid ounces	30	milliliters	ml
c	cups	0.24	liters	l
pt	pints	0.47	liters	l
qt	quarts	0.95	liters	l
gal	gallons	3.8	liters	l
ft^3	cubic feet	0.03	cubic meters	m^3
yd^3	cubic yards	0.76	cubic meters	m^3
		TEMPERATURE (exact)		
°F	Fahrenheit temperature	5/9 (after subtracting 32)	Celsius temperature	°C

*1 in = 2.54 (exactly). For other exact conversions and more detailed tables, see NBS Misc. Publ. 286, Units of Weights and Measures, Price $2.25, SD Catalog No. C13.10:286.

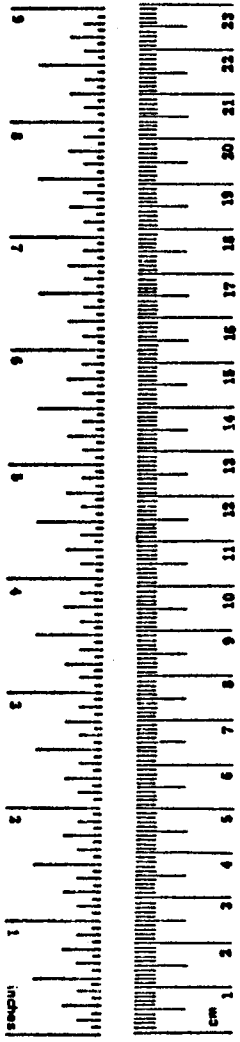

Approximate Conversions from Metric Measures

Symbol	When You Know	Multiply by	To Find	Symbol
		LENGTH		
mm	millimeters	0.04	inches	in
cm	centimeters	0.4	inches	in
m	meters	3.3	feet	ft
m	meters	1.1	yards	yd
km	kilometers	0.6	miles	mi
		AREA		
cm^2	square centimeters	0.16	square inches	in^2
m^2	square meters	1.2	square yards	yd^2
km^2	square kilometers	0.4	square miles	mi^2
ha	hectares (10,000 m^2)	2.5	acres	
		MASS (weight)		
g	grams	0.035	ounces	oz
kg	kilograms	2.2	pounds	lb
t	tonnes (1000 kg)	1.1	short tons	
		VOLUME		
ml	milliliters	0.03	fluid ounces	fl oz
l	liters	2.1	pints	pt
l	liters	1.06	quarts	qt
l	liters	0.26	gallons	gal
m^3	cubic meters	35	cubic feet	ft^3
m^3	cubic meters	1.3	cubic yards	yd^3
		TEMPERATURE (exact)		
°C	Celsius temperature	9/5 (then add 32)	Fahrenheit temperature	°F

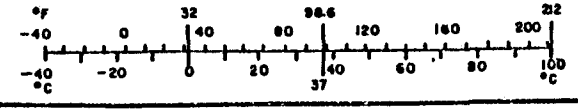

TABLE OF CONTENTS

TABLE OF CONTENTS (CONT.)

LIST OF ILLUSTRATIONS

LIST OF ILLUSTRATIONS

LIST OF TABLES

EXECUTIVE SUMMARY

This report covers the results of a study on the thermite-welding of premium rails; the premium rails comprised head-hardened rails and CrMo, CrV and Cr alloy rails. The work was conducted to establish thermite welding procedures applicable to premium rails and to determine mechanical properties of the welds. The work was under the direction of the Transportation Systems Center. The welds were produced at the Facility for Accelerated Services Testing (FAST) then operated by the Federal Railroad Administration at the Transportation Test Center in Pueblo, Colorado.

Fourteen thermite welds were produced using various combinations of premium rails and AREA Controlled Cooled Carbon rails (i.e., standard rails) on both sides of the welds. The welding was done with weld metal from "standard" and "alloy" thermite charges. Because a major objective of the research was to determine the feasibility of joining premium rails to each other and to standard rails, normal procedures for thermite welding of rails were employed. The objective was met in that metallurgically sound welds were produced using either "standard" or "alloy" thermite charges.

Other objectives of the program were to determine mechanical properties and metallurgical structures of the weld-metal and of the heat-affected zones of the welds. It is shown that "alloy" weld metal is stronger than "standard" weld metal but has slightly less tensile ductility. Both types exhibit ductilities of only 2-6 percent reduction in area and impact energies of only 1.5-2.8 Joules at 20^{o}C, and their fractures show transgranular cleavage with small amounts of microporosity. Moreover, there is 0.24-0.49 volume percent of microinclusions which is enough to be a contributory factor in the brittle behavior of weld metal. From the welded rails, tensile and impact specimens, which straddled the region of minimum hardness along the outer edge of the heat affected zone were prepared in that region of minimum hardness, tensile ductilities

were 19-60 percent reduction in area for these longitudinal specimens, and the impact energies were only 2.6-6.9 Joules. In addition to evaluating the mechanical properties, temperatures in the rail near the weld metal were measured as four of the welds were produced; in a fifth, temperatures in the weld metal, itself, were measured. Finally residual stresses in one of the welds were determined, and the effect of the residual stresses on fatigue strength of welded rail is discussed.

This study showed that premium rails can be joined together or joined to standard rails by thermite-welding, without the introduction of brittle constituents. The mechanical properties of the weld metal found in this study compare with previously published properties of thermite-weld metal. However, this study and the previous study show that the weld metal in thermite welds exhibit low tensile ductility and low impact toughness. Accordingly, it is recommended that future research be directed to process- and alloy-modifications which could improve the mechanical properties.

1. INTRODUCTION

The aluminothermic process is credited to Goldschmidt for his development in 1898 of a process for reducing iron and other metals from their oxides by igniting mixtures of the oxides and powdered aluminum (1, 2)*. The first, and still the most common application of the aluminothermic process, is to the thermite welding of railroad rails (3). As early as 1908, Goldschmidt (4) mentioned the existence of 200,000 thermite rail-welds in Europe. Thermite rail-welds were not introduced to the U.S. railways until the 1930s when the concept of continuous-welded rail (CWR) was being developed as a means to permit higher speeds and car loadings on rails.

Typical CWR consists of rail "strings," 439 meters (1440 feet) in length, that are fabricated by the electric-flash butt (EFB) welding of individual rail "lengths." The lengths are steel mill products, which are hot rolled from ingots or continuously cast billets and are typically 12 meters (39 feet) in length. The fabricated strings are transported to the track site and layed at an ambient temperature that avoids excessive thermal stresses which can arise from fluctuations of the ambient temperature. The joining of the strings requires a thermite weld every 439 meters (1440 feet). Also, CWR is repaired by removing damaged or worn segments of rail and by thermite welding the repair sections in place.

1.1 STATEMENT OF THE PROBLEM

Since the development of the rail systems in this country, the sizes of the rolling stock and of the trains have been steadily increasing. Today, for example, 124 MN (14,000 ton) unit coal trains with 0.9 MN (100 ton) cars are not uncommon. However, the

*References are listed on page 47.

basic design of the track and roadbed system has not changed significantly since the early 1900s. The net effect is a substantial increase in the service stresses to which rails, welds and related components are subjected.

Based on a summary of the status of thermite welding of rail by Hauser (5,6) and on an evaluation of mechanical properties by Myers (7), the weld metal in thermite welds exhibits low ductility, impact energy and fatigue strength. Typical properties are only 1-3 percent reduction in area and 2.7 - 5.4 J (2-4 ft-lb_f) in Charpy impact energy at room temperature (7). These low mechanical properties were attributed to undesirable microstructures and to a high concentration of nonmetallic inclusions in the weld metal. According to Hauser (5,6), the most common mode of weld failure in service is due to fatigue cracks that nucleate at sites of porosity and/or inclusions in the weld metal and in regions which do not completely fuse the parent rail.

The failure rates among various types of rail welds are greater for thermite welds than for EFB welds; specifically the expected life of a thermite weld is about half that of an EFB weld (5,6). Also, since the process of thermite welding of rails has remained almost unchanged since its development, it is expected that the high stresses associated with current service have significantly reduced the fatigue life and critical flaw size of thermite welds in service.

1.2 OBJECTIVE OF THIS STUDY

Although there are alternatives to the thermite process for in-track welding of rails (such as in-track EFB, gas-pressure welding, arc and electroslag welding and variations thereof), the thermite process is widely used, and will probably continue to be so, in spite of its shortcomings. This is due primarily to the low costs of the equipment and to the ease and speed of installation of on-site thermite welds (5,6). Thus, the overall objectives of this

study are to evaluate the properties of thermite welds in rails, to determine the causes of poor properties so that the probability of weld failures will be reduced, and to evaluate the applicability of the thermite process to joining of premium rail steels - both of alloy and heat-treated type.

The study involves the evaluation of fourteen thermite welds produced at the DOT-FAST* facility at Pueblo, Colorado. The welds include variations in rail and weld chemistry, length of preheat period, and method of postcooling. Time-temperature data at various locations in the rail were obtained for the complete cycles of several welds. In addition, thermal data were obtained for the filler metal for one of the welds. Impact energy, tensile properties and hardness were measured for the weld metal and the heat-affected zones for thirteen of the welds. One weld was evaluated for residual stresses produced by the welding operation, and macro and microstructures from representative welds were studied. Thus the study can be considered as an evaluation of the current state of the art of the thermite welding process to the joining of premium steels such as alloy and head-hardened rail steels.

*DOT-FAST is the acronym for Department of Transportation Facility for Accelerated Service Testing.

2. REVIEW OF RELATED STUDIES

2.1 APPLICATIONS OF THE ALUMINOTHERMIC PROCESS

Since its inception, the most widespread use of the aluminothermic process has been the thermite welding of ferrous alloys (3). There have been many applications in the extraction of refractory metals and in steel castings as a riser and feeding aid (1,2). A process has been developed by Mehra et al (1) for the production of molybdenum from calcium molybdate by aluminothermic reduction; molybdenum has also been reduced from its oxide by aluminum (8). The aluminothermic reaction has also been applied to the production of ferrochrome, ferrocolumbium, ferrotungsten and other ferroalloys (9-11). If not economically competitive themselves, these processes appear as valuable aids in optimizing ore, reducing agent and flux combinations for large scale reduction operations (8-10). With suitable fluxing agents, binders and excess aluminum, the aluminothermic reaction can be used to produce refractory linings (2). Only enough iron oxide is used to initiate the reaction, and once initiated, the aluminum reacts with the atmosphere to produce the refractory alumina. The fluxing agents aid in binding the alumina into the shape of a refractory vessel or mold.

2.2 ALTERNATIVE REDUCTANTS TO ALUMINUM

Studies on the use of reducing agents, other than aluminum, were made by Belitkus (12). One of the factors involved in the selection of a reductant for a particular metal oxide is the requirement that the reaction have a free energy change amenable to a high yield of the reaction products. The reaction should also be exothermic in order to produce the superheat necessary to sustain the reaction and to minimize oxide and reductant contamination in the metal produced. Some alternative reductants to aluminum are calcium, magnesium, silicon, carbon and hydrogen (12, 13). For the

latter three, the heat of reaction is insufficient to sustain a reaction without external heat. The relatively low boiling points of calcium and of magnesium (1482°C and 1103°C, respectively) coupled with the high melting points of their oxides (2480° and 2800°C, respectively) require that the reactions be conducted in pressure-tight vessels and at high temperatures to insure complete reaction and metal-slag separation. Aluminum, while having a lower heat of formation of the oxide than calcium and magnesium, is the optimum choice as a reductant because it has a boiling point of 2467°C, an oxide melting point of 2045°C and a heat formation of the oxide which is adequate for sustaining the reactions.

2.3 ADDITIVES THAT AFFECT THE ALUMINOTHERMIC PROCESS

Aluminothermic charges for producing iron or iron-alloy welds are composed of aluminum powder, a finely divided ore or iron oxide, usually a flux, and often a thermal booster. Alloy elements are usually introduced in the form of ferroalloy pellets dispersed throughout the charge. Relatively pure iron pellets may also be present to reduce the amount of superheat produced.

The most common reactions used in formulating thermite rail-weld mixtures involve the reduction of Fe_3O_4 and/or Fe_2O_3 to produce the molten iron filler-metal (5,14); mixtures of these oxides and FeO may also be used (15). The reduction of Fe_3O_4 by aluminum liberates 79.9 kcal per mole of iron produced for an adiabatic reaction temperature (ART) of 3088°C, whereas Delachaux (15) gives the ART for Fe_3O_4 reduction as 2590°C. In view of these discrepancies, the ART and energy liberated were calculated for the Fe_3O_4 reaction. Utilizing data from Kubaschewski and Alcock (16), U.S. Steel Corp. (17) and the JANAF tables (18), the ART for the reduction of Fe_3O_4 by aluminum was determined as 2697°C with the energy liberated as 89.2 kcal/mole of iron produced.

The amount of aluminum is usually 10-15 percent in excess of the stoichiometric amount for completion of the reaction. This has

been found to result in the highest yield of the desired metal product (1,8,9,12,19). The need for excess aluminum is attributed to mechanical segregation of the oxide and aluminum particles prior to ignition and to the desirability of producing weld metal with about 0.4 percent aluminum (20).

The metal product of an aluminothermic reaction should be free of the alumina-rich slag which forms. The metal-slag separation requires time, and time available for separation is directly related to the amount of heat available from the aluminothermic reaction. If the reaction proceeds too slowly then there is more heat-loss to the surroundings, and the reaction temperature is too low, thereby producing a molten metal with little superheat. The rate of the reaction is most noticeably affected by changes in the particle size and the amount of excess aluminum (9).

When very fine aluminum particles (less than 6-10 m diameter) are used, the reaction proceeds rapidly due to a high reactant surface area. These reactions closely approach adiabatic conditions and yield the highest peak reaction temperature. However, it has been demonstrated that these reactions do not yield the highest purity of metal product (9). It is thought that the aluminum reacts so rapidly that secondary reactions, such as reaction of the alumina with the fluxing agent or the thermal booster (if present), do not have time to go to completion during the brief period when the maximum superheat is available for the metal slag separation. It is also thought that the violence of the reaction blows much of the fine aluminum out of the reaction vessel, thus reducing the amount available for reduction of the oxide (20).

Reactions involving aluminum particles of greater than 1000μm diameter result in a product which contains slag since the reaction rate is slow enough that heat losses result in a low peak temperature. For good metal-slag separation, a high peak temperature and adequate time at that temperature are required. A

suitable condition occurs with aluminum particles with a mean diameter in the range of 10-1000μm (9).

A commonly used flux is calcium oxide, CaO. It is usually added in quantities to produce a 70-80 percent alumina slag with a melting point of 1800°C (12). While the use of flux lowers the melting point of the slag, heat is absorbed from the reaction to raise the CaO to the reaction temperature of the alumina. This reduces the amount of superheat available to the metal product. If the heat of reaction is insufficient to produce good metal-slag separation, a thermal booster such as sodium chlorate may be added to the charge. The sodium chlorate reacts with the excess aluminum to yield about 2200 kcal per kg of reactants. An additional product of this reaction is sodium chloride which separates into the slag phase. An alternative to a thermal booster is preheating of the aluminothermic charge.

2.4 THERMITE RAIL-WELDS

The adiabatic reaction temperature (ART) of iron oxide and aluminum powder is in the range of 2600-3100°C, as discussed above; the most reliable estimate for the ART is 2700°C. Regardless of the reaction employed, heat losses reduce the temperature of the molten iron to about 2000°C before the weld is actually poured (6). Flux and alloy additions further reduce this temperature. In practice, weld charges are designed to produce a molten steel with a superheat of 400-500°C above the freezing temperature of the steel (14).

According to Ashton (20), precise control of the composition of a thermite charge is necessary so that, after the reaction, about 0.4 percent excess aluminum is in the molten weld metal. Not enough aluminum can cause the loss of the alloying elements and the oxidation of carbon and manganese, resulting in a weld with poor mechanical properties. This condition can also result in a very violent reaction due to the evolution of carbon monoxide. Typically, a large portion of the manganese from ferromanganese

pellets is lost to the slag; however, an excess of aluminum increases the recovery of manganese significantly. On the other hand, discretion must be exercised since excessive aluminum can lead to weld embrittlement.

Another critical factor in the production of an acceptable thermite weld is the "taptime" or the interval from ignition of the reaction until the crucible is tapped (i.e., when the weld is poured). Ashton (20) summarizes the sequence of events as: ignition to 15 seconds, vigorous reaction occurs; 15-25 seconds, vigorous reaction ceases and slag rises; 25 seconds on, slag separation nearing completion and loss of superheat is beginning. The optimum taptime is thus 20-25 seconds. Data on the failure load of the bend tests of welded rail sections versus taptime support this. The failure load shows a maximum at a taptime of about 22 seconds (20).

In addition to the above factors, the production of a good weld in the field involves the mechanics of proper rail cutting and end preparation, rail alignment, mold placement and proper preheating. Accordingly, the railways have standard procedures for thermite welding in the field (e.g., see the Appendix) and trained crews to implement those procedures. Despite such precautions, many failures of thermite-welds are attributed to faulty installation and welding.

Even though a thermite weld is installed according to recommended procedures, its mechanical properties are usually lower than those of the parent rail. From Sonon et al (21), control-cooled (CC) standard rail has an average yield strength of 483 MPa (70 ksi), a tensile strength of 910 MPa (132 ksi), an elongation of 11 percent (2.54 cm or 1 in. gage) and a reduction of area of 14 percent. By comparison, typical values for thermite weld metal are a tensile strength of 793 MPa (115 ksi), an elongation of 1-3 percent (12.7 cm or 5 in. gage length) and a reduction of area of 1-3 percent as reported by Myers (7), Geiger (22) and Myers et al

(24). The impact toughness (Charpy key-hole specimens) is also very low; at 20°C it is approximately 2.7 J and at 149°C, 9.5 J (7,24).

Specimens used in the latter three works (7,22,24) were removed from the weld-metal. However, mechanical properties of welds in rail are usually reported in terms of the results of bend tests conducted on rather long lengths of welded rail. Results collected by Hauser (5) and made available by the Atchison, Topeka and Santa Fe (AT&SF) Railway Company (23) are given in Table 1. These include properties of rail, thermite welds and electric flash butt (EFB) welds. EFB welds are plant welds and are included in the table because such welds are considered to be more reliable in service than thermite welds. The data collected from Hauser (5) are from four point bend tests with a 122 cm (48 in.) span; the loads are applied symmetrically at points 15 cm (6 in.) on both sides of the weld. The data of A.T. & S.F. are from a three point bend test, 122 cm (48 in.) span, in which one load is applied at the weld itself. In all cases, the rail is so-called "CC standard rail".

The scatter that was noted for the bend test results reported by Hauser (5) for thermite welded rails appeared to offset the effect of loading with the head or base down. However, the method of loading, 4-point or 3-point, does affect the results, particularly for thermite welds. The 4-point method subjects the weld to pure bending, whereas the 3-point method introduces a shear stress in the weld. In any case the conclusion is that, even though a thermite welded rail may sometimes sustain a load greater than a rail or an EFB weld, it does not have the ductility necessary to deflect significantly before failure. This fact is significant because thermite welds are placed in track in the span between two ties and therefore do not have base support and are subject to the high flexural loads and deflections that occur in service.

2.5 WELD INTEGRITY

Most of what follows is a review of the literature on factors which contribute to embrittlement, cracking, and/or lack of toughness and ductility in steel welds. To adequately cover these topics, the scope of this discussion is not restricted to thermite welds because there is a paucity of literature on the mechanical properties and microstructures of such welds.

The most extensive work on the metallurgical structure and mechanical properties of thermite welds in rails is that reported by Myers et al (24). Their study included macrostructures and microstructures of welds, as well as mechanical properties which consisted of hardness traverses across welds and tensile properties and Charpy impact energies of the weld metal. The major conclusions of that study follow:

1. The weld metal exhibited low tensile ductility and low impact energy. The fractures of the tensile and impact specimens were almost completely brittle.

2. The microstructures of the weld metal in some of the welds showed intragranular Widmanstatten ferrite and upper bainite in other welds. These constituents were thought to be at least partly responsible for the brittle behavior of the weld metal.

3. Columnar dendrites aligned in the direction of heat flow (i.e., the axial direction of the rail) comprised the cast structure of the weld metal. Microporosity and numerous inclusions were observed, and these heterogeneities were significant contributing factors for the low tensile ductility and impact energy of the weld metal.

4. Grain boundary precipitates were not observed on extraction replicas when viewed under a transmission electron microscope so that the brittleness of the weld metal could not be attributed to grain boundary embrittlement due to

such precipitates. However, grain boundary segregation without precipitation could not be eliminated as a contributing factor.

Ezhov (25) studied the welding of steel castings of variable thickness (100-400mm) with a parent structure of very fine pearlite and tempered martensite in which transgranular cracking was encountered in the heat-affected zones (HAZ) of the welds in the thickest sections. The cracks occurred in the martensitic structure of greatest hardness of the HAZ. Further, inclusions were noted and were found to be of the same type in both thick and thin areas (MnS, sulfides with aluminates, silicates and oxides), but the inclusions were coarser and more populous in the thicker sections. Crack initiation was influenced by the presence of the inclusions, but this did not fully explain why the structure of highest strength (martensite) failed preferentially. Ezhov (25) also observed that martensite, tempered or untempered, was much more susceptible to hydrogen embrittlement than was very fine pearlite. Given the same concentration of diffused hydrogen, the fracture strength of the former was about half that of the latter. For welds in the thick sections of the castings, the concentration of hydrogen was greater in the martensite structure of the HAZ than in the parent material or the weld metal. Hydrogen was not detected in welds in the thin sections of the castings. Ezhov (25) concluded, therefore, that the primary cause of weld failure was contamination of the martensite structures in the HAZ by diffused hydrogen encountered in the welding process (such as from moisture).

Heller and Beck (26), in a study of flame cutting and welding of rails, found that the element which deleteriously influenced tensile and impact properties of the HAZ and fusion zone the most was carbon, followed by manganese. These elements increased the hardenability of steel, and manganese promotes microsegregation in the form of banding. The banding was found to have significant influence on the transformation products in the HAZ, particularly adjacent to the fusion zone. This segration is detrimental in that

it promotes the formation of martensite in this region which is subject to brittle fractures.

Another degrading factor is the grain coarsening that occurs in the HAZ just adjacent to the weld. When it occurs, the grain coarsening increases the tendency to brittle fracture. The high austenitizing temperatures from the welding operation promote formation of the coarse grains and, coupled with rapid cooling rates in the region, promote the formation of brittle martensite (26,27).

Heller and Beck (26) also observed hydrogen absorption in some thermite welds. After weld solidification, the composition of hydrogen was approximately equal to the maximum solubility in austenite (26). If the cool-down rate is too rapid, i.e., the weld metal does not have time to give up sufficient hydrogen to the rail steel, cold cracking of the weld may occur (26,28). On the other hand, diffusion of hydrogen into the HAZ of the rail steel may result in exceeding the critical content; this can produce cold cracking in this region of the HAZ which is adjacent to the fusion zone (26). Heller and Beck (26) strongly recommend that the thermite kits be moisture free and the welds cool slowly enough to allow hydrogen, if present, to diffuse extensively so that a critical concentration does not occur in any one area of the weld or rail.

For welds in low carbon steels, Lebdev (29) observed grain boundary segregation of sulfur and phosphorus in the weld metal and the extent of the segregation was controlled by the solidification cooling rate of the weld metal. For cooling rates less than 250 ^{o}C/s, sulfur and phosphorus diffused to the grain boundaries so that the compositions of these elements were greater at the grain boundaries than at the center of the grains. For cooling rates greater than 250 ^{o}C/s the diffusion process was sufficiently inhibited to the extent that the distribution of sulfur and of phosphorus was uniform within the grains. A reduction in the level of segregation resulted in welds with an increased resistance to solidification or hot cracking and a greater weld strength.

In the welding of high-strength steels with weld metal of similar composition, Makarov (30) observed cold cracking in the weld metal. When the steels had martensitic structure, these cracks were located on the prior austenitic grain boundaries. Resistance to cold cracking depended on the shape, dimensions and chemical inhomogeneity of these boundaries. Makarov (30) found that additions of elements such as Mo, W(<1 %), Ni (>3.5 %), Si and Cu increased the resistance to cold cracking whereas C, Mn, Cr and Co reduced it. In welds which resisted cold cracking, the solidification structure of the weld metal was equiaxed and had a small austenitic grain size with minimum segregation at the grain boundaries. Molybdenum had the most pronounced effect on promoting an equiaxial solidification structure and, thereby, improving resistance to cold cracking.

Boniszewski (31) found effects of inclusion level and certain alloying additions on grain boundary strength with respect to the susceptibility of welds in ferritic steels to reheat cracking during post weld heat treatment. Reheat cracking is a form of creep-rupture which occurs at the prior austenitic grain boundaries. Steels conctaining Cr, Mo and V, individually or in combination, were found to be most susceptible to reheat cracking. Impurities such as P, residual elements (Cu, As, Sb) and some deoxidants (Al) were also detrimental; other deoxidants such as Ti, Zr, Ca and Ce were beneficial or neutral. Steels with lower inclusion contents had a decreased susceptibility to reheat cracking.

Boniszewski (31) and McPherson (32) in separate studies have shown that grain boundary segregation in prior austenite and residual stresses cause reduced impact energy, lower fracture toughness and reheat cracking during stress-relief for welds in ferritic steels. Welds in steels containing small amounts of vanadium appear particularly susceptible to HAZ reheat cracking (32). Similarly, Joshi and Stein (33) and Marcus et al (34) have attributed the temper embrittlement of low alloy steels to grain

boundary segregation in prior austenite; impurities such as Sb, P, Sn and As as well as the alloying elements, Ni and Cr, segregated to the boundaries. The Cr may form grain boundary carbides, and the combined presence of Cr and Ni leads to more extensive grain boundary segregation of Sb, Sn and P. Joshi (35) attributed the segregation to grain boundaries to the lowering of the energy of high-energy grain boundaries by segregates and precipitates. In quenched steels, these are the prior austenitic boundaries. In some cases tempering results in more grain boundary segregation and embrittlement of these boundaries.

According to Farrar and Dolby (36), lamellar tearing in welded steel plate is related to the transverse ductility of the plate, and, in turn, the transverse ductility is inversely related to the inclusion content of the plate. If the volume fraction of inclusions is 0.01, the percent reduction of area is 10 percent or less for short transverse specimens, whereas to achieve a percent reduction in area of 50 percent, the volume fraction of inclusions must be less than 0.002. The percent reduction in area approaches zero as the volume fraction of inclusions exceeds 0.015. The ductility is also a function of the strength level of the steel; smaller inclusions become more significant in high-strength steels.

Rittinger and Fehervari (37) found that welds of microalloyed steels were more sensitive to lamellar tearing than silicon-killed steels. This is attributed to the presence of low-melting sulfides and sulfonitride eutectics as inclusions. It was noted than an excess of microalloy elements in solid solution reduced weld toughness and that the best results were obtained when these elements were combined as nitrides.

Oono et al (38) have shown that the addition of calcium to rolled steel products changes the shape of the sulfide inclusions from elongated to spherical. This results in almost isotropic properties, significantly improved resistance to lamellar tearing and improved toughness of the HAZ in welds of this material.

Acicular ferrite is a microstructural constituent which correlates with high strength and toughness in high strength low alloy (HSLA) steels and with a high resistance to cleavage fracture of weld deposits in low-alloy steel (39,40). Abson et al (39) confirmed that inclusions in weld metal strongly influence the nucleation of ferrite from austenite and determine the extent of the desirable acicular ferrite. The inclusions not only serve as nucleation sites for ferrite at austenite boundaries but also nucleation sites of acicular ferrite within the austenite grains. It was noted that a decrease of oxygen in the weld from 0.02 to 0.01 percent (i.e., a reduction in the number of inclusions), virtually eliminated the nucleation of acicular ferrite and resulted in a bainitic structure which was more brittle (39). On the other hand an increase in oxygen from 0.03 to 0.06 percent, resulted in predominantly side-plate structures with little or no acicular ferrite. In contrast, with 0.06 percent oxygen in a deposit produced under an alumina based flux, the structure was substantially acicular ferrite. Changes in sulfur content only changed the microstructure slightly as compared to changes in oxygen. It was concluded that there is an optimum level of oxygen and to a lesser extent, sulfur, and hence a volume fraction of inclusions, that results in the acicular ferrite structure.

Since a thermite weld can be considered to be a steel casting in that a molten charge is poured into a mold around the gap between the rail ends, it is noteworthy to consider findings pertaining to the metallurgy of cast steel. For example, it is known that the impact properties of steel castings are improved by additions of calcium silicide, rare earth metals and aluminum (41). The former spherodize inclusions, and the aluminum is a deoxidant. In the same study, it was also shown that barium and strontium silicides produce the same effect as calcium silicide and rare earth metals. When these silicides are used in correct proportions with aluminum, the low temperature impact properties of steel castings are noticeably improved (41). Aleksandrov (42) found that similar results are

obtained for welds when Ca, Y, Ce and other rare earth metals are introduced into the weld metal. It was noted that calcium must be introduced in the form of a "silico-calcium" ferroalloy (Ca, Si, Al and Fe) to produce a noticeable improvement in the low temperature impact strength of the deposit.

2.6 RESIDUAL STRESSES IN WELDS

During welding, the weld metal and the HAZ are at temperatures substantially above that of the unaffected parent metal (14). The areas of the weld which solidify first are plastic and exert little stress on nearby material; however, as cooling and shrinkage progress, increasing stress is exerted by the weld metal on the adjacent cooler metal where the stresses can approach the yield strength of the base metal and HAZ (14,43). Since the region that solidifies first shrinks more rapidly than surrounding areas, it is typically placed in a state of residual tensile stress, and the regions that solidify last are under compressive stress. The maximum (absolute) residual stresses occur in the weld metal and HAZ (32). In addition to solidification and cooling effects, residual stresses may be produced in steel welds at relatively low temperatures by the martensitic transformation since it involves an increase in specific volume.

The residual stress state can vary from uniaxial to triaxial depending on the weld geometry and complexity (14,43,44). In most cases, the residual stresses are deleterious. For example, residual stresses in weldments may produce distortion, and they can cause premature weld failure either through the promotion of brittle fracture or the initiation and propagation of fatigue cracks during service loading (14,43,44). In addition, tensile residual stresses contribute to the corrosion failure of welds (14).

A beneficial effect of residual stresses was observed by Kapadia and Imhoff (45) who conducted linear elastic fracture mechanics (LEFM) studies of electroslag welds of two steels. They

found that the crack growth rates in the weld metal were similar to or up to five times slower than in the parent metal if the residual stresses were compressive. This retardation effect was most pronounced at low stress intensity ranges and was significantly greater in the coarse grained region of the HAZ and in the fusion zone as compared to the weld metal. It was noted that marked variations in microstructure of the HAZ and weld metal did not significantly affect growth rates in these respective regions; however, they did affect the topography of the fracture surface. In a separate study, Kapadia (46) attributed the retardation effects to residual compressive stresses in the HAZ and in the fusion zone. He concluded that the benefit of these stresses would diminish under service conditions of high tensile mean loading or after a postweld stress-relief heat treatment.

In a study by Dohse (47), the residual stresses in nonwelded rails (50 kg/m) and in thermite welded rails (with and without vertical reinforcing ribs) were determined. He noted that the residual stress pattern in the rail itself was tensile in the head and base with compressive stresses in the web. This stress state is found in roller straightened rail but not in hot rolled rail directly after rolling. This pattern was reversed in thermite welds of the rails. No significant difference was noted between welds with and without the reinforcing ribs. For the nonwelded rail, (rail height: 152.4 mm), the maximum longitudinal stresses were +83 MPa (+12 ksi) along the top of the head, +138 MPa (+20 ksi) along the underside of the base, and -145 MPa (-21 ksi) in the web 105 mm from the base.

For the thermite welds, typical residual stresses were as shown in Figure 1. Along the weld centerline, the average of the maximum longitudinal stresses were -108 MPa (-16 ksi) on the top of the head, -98 MPa (-14 ksi) on the underside of the base and +206 MPa (+30 ksi) in the web 60 mm (reinforcing ribs) and 85 mm (without ribs) from the base. The vertical residual stresses were a maximum of +196 to +254 MPa (28 to 37 ksi) at the web-weld center. The

longitudinal stresses decreased slowly with distance from the weld whereas the vertical stresses were completely relieved at 80 mm from the weld center. The vertical residual tensile stresses were considered to be insignificant due to the high compressive service loads. Dohse (47) concluded that the weld residual stress pattern is actually of benefit in service since the base, which is subject to tensile service stress, is prestressed in compression. Heller and Beck (26), confirmed Dohse's findings in a later study. However in these studies, the residual stresses in the HAZ's of these welds were not investigated. Thus the residual compressive stresses in the base may be beneficial in avoiding base initiated failure but would not beneficially influence failure occurrence in other regions of the rail, i.e., the web where residual tensile stresses can exist.

Krauss (48) determined the residual stress levels in an EFB weld of head-hardened rail, 68 kg/m, (136 lb/yd), that had been subjected to 1.2 GN (135 million gross tons) of service loading. His findings agree with Dohse; the base and head area of the weld are in compression while the web is in tension. Measurements taken approximately 3.6 cm from the weld vertical centerline indicate this area follows the weld stress pattern; however, at about 7.3 cm from the weld center the head and web residual stresses vary from about zero to compressive regardless of orientation. Longitudinal stresses at about 8.1 cm above the base were +416 MPa (+60 ksi) at the weld center line, +352 MPa (+51 ksi) averaged for the left and right side of the weld at 3.6 cm from the weld centerline, and zero MPa (0 ksi) at 7.3 cm from the weld center. Corresponding vertical stresses were +281 MPa (+41 ksi), +269 MPa (39 ksi), and -69 MPa (-10 ksi).

3. EXPERIMENTAL PROCEDURES

Fourteen thermite welds were produced at the DOT-FAST facility in Pueblo, Colorado. Welding was performed inside a building to shield against the wind. The procedures were according to standard field practice (Appendix). A thorough analysis of these welds which included mechanical properties, macro and microstructures, residual stresses and thermal history during the welding cycle, was conducted. The fourteen test welds were produced acccording to the test matrix outlined in Table 2 using the rail and weld metallurgies of Table 3. The welds all employed the Orgotherm SKV (self-tapping) process in which two lengths of 68 kg/m (136 lb/yd) rail, (each of 1.2 m (4 ft) length), were welded with a gap of 24 mm (15/16 inches). As is indicated in Table 2, the test variables were rail and weld chemistries, rail preheat time and postweld condition. All other procedures were the same as applied in the field (see Appendix). The mold configuration and the flow pattern of the molten steel are shown in Figure 2.

In welds 1 through 4, fifteen thermocouples were placed in one rail according to the schematic of Figure 3. Thermocouples 1-5 in weld 4 were platinum-rhodium 90 percent Pt, 10 percent Rh (AWG 30) in alumina tubing; all others were chromel-alumel (AWG 20) in a glass-fiber insulation. After the production of weld 4, the first for which thermal data were recorded, it was determined the chromel-alumel thermocouples were adequate to withstand the peak temperatures, and these were used exclusively thereafter.

For weld 9, three thermocouples were placed in the center of the weld gap by means of holes bored in one mold half, Figure 4. These locations were approximately centered in the head, the web and the base. The thermocouples were tungsten (W)-rhenium (Re) type and were made from 95 percent W, 5 percent Re, 74 percent W, and 26 percent Re wires (AWG 24) that had been sealed from the atmosphere in alumina tubing while in argon.

Additional protection was provided by sheathing them in closed-end quartz tubes, which were inserted through the holes in the mold.

Thermal data were recorded by means of a "Datalogger" data acquisition system. In addition, the output from thermocouples 1-5 in welds 1-4 were simultaneously recorded on a "Brush 481" stripchart recorder to provide a check of the data. The outputs of the three thermocouples in the weld metal of weld 9 were simultaneously recorded by both units. The time to read all thermocouples once for the Datalogger was 7-8 seconds for welds 1-4 and 2-3 seconds for weld 9. The stripchart provided a continuous record. For all welds, thermal data were recorded at the start of preheat and continued for about 1.5 hours after weld completion.

Preheat was done with an oxy-propane torch with a reducing flame according to the standard practice for making thermite welds in rails. The "muffle" referred to in the experimental schedule, Table 2, was a clamshell box about 30 cm (12 in.) in length which was insulated with about 2.5 cm (1 in.) of fiber insulation in the top and sides. The bottom of the muffle, which locked the unit in place, did not contain insulation. The muffle was contoured to fit the rail profile, and was placed over the hot weld immediately after the sprue and risers were removed, and the weld was ground. The purpose of the muffle was to retard the cooling rate of the weld.

All completed welds were cut to a length of 30 cm (12 in.) with the weld metal centered. With the exception of weld 11, these lengths were sectioned longitudinally to provide a full-depth macroetch. The sections were etched in a boiling solution of 1 part of concentrated hydrochloric acid to 1 part of water for approximately 45 minutes.

Rockwell "C" hardness profiles were determined on tranverses which went across the welds and were arbitrarily selected at 2.5 cm (1 in.) below the running surface of the center of the heads as indicated in Figure 5. These profiles extended a minimum of 7.6 cm

(3 in.) in both directions from the center of the weld metal until the original hardness of the rail material was encountered.

Tensile test bars and Charpy V-notch specimens were removed from the locations shown in Figure 5. The tensile specimens were reduced size, ASTM standard bars with a diameter of 0.64 cm (0.25 in.) and a gage length of 2.5 cm (1 in.). The Charpy V-notch specimens were standard size according to ASTM specifications. Note that the specimens in the HAZ of the welds straddle the narrow soft region of the HAZ and, as a result, contain a structure and a hardness gradient (e.g., see Figures 7-9).

Specimens for microstructural analyses were taken at essentially the same location as the Rockwell hardness profile; refer to Figure 5. Two samples, each 7.6 cm (3 in.) in length, were taken from each weld. Each sample contained the structure gradient from the center of the weld metal to the unaffected rail. Specimens were prepared using standard metallographic procedures and etched with a 1:1 solution of 2 percent Nital and 2 percent Picral. This was followed by vapor deposition of a carbon layer and then a gold layer. Microstrucures were examined in an ISI model IIIA scanning electron microscope (SEM) equipped with a PGT-System III energy dispersive spectrum (EDS) analyzer.

The SEM was also used to examine the fractured surfaces of all tensile and impact specimens. Elemental analyses were done on several inclusions, and unusual surface features which were encountered while viewing the fractures and microstructure samples.

Finally, several samples of weld metal from the location of the microstructural specimens were quantitatively analyzed for inclusions in a quantitative image analyzer. These analyses were on weld metal specimens which were carefuly prepared to preserve the inclusions. Each field of view was an area of 0.25 mm^2 examined at a magnification of 400X. Size distribution and volume fraction of inclusions were determined for welds 5-7 and 12-14. Ten fields of

view were selected at random and evaluated for each specimen. Fields containing obvious microporosity were purposely avoided.

Residual stresses as a result of welding were measured in weld 11 which was left intact for this purpose. Measurements were taken at various locations in the weld metal and the HAZ as shown in Figure 6. The blind-hole technique was employed using rosette strain gages (Micro-Measurements EA-06-062RE-102) designed for this purpose (52).

Each of the three elements of a rosette was made the active element of a quarter-bridge circuit. Leads were 1.2 m (48 in.) lengths of copper wire (AWG 16) twisted together to reduce interference. Three leads were used for each element. Two leads were attached to the same end of the active element and to the signal input and internal dummy gage of a nullmeter and switching unit. The third lead, connected to the excitation potential, completed the active element circuit. Thermal drift was not observed after gage attachment.

After setup and nulling of the gages, a 1.6 mm (0.062 in.) diameter hole was bored in the center of the rosette, and the changes in the three gage readings were recorded to determine the residual stresses in the immediate vicinity of the rosette. Virtually complete stress relief occurs at a hole depth/diameter ratio of 1 (52). For all rosettes, the holes were bored accordingly, and then rebored to increase the ratio to 1.5 and the gage values recorded to determine if stress gradients normal to the surface existed. No significant changes were observed.

The boring of flat-bottom holes was accomplished with an end mill which was centered over the rosette by using a centering scope. Thermal drift due to localized heating from boring was checked by reading the gages immediately after boring and then checking for a change in the readings with time. In no case was drift observed.

4. RESULTS AND DISCUSSIONS

4.1 MECHANICAL PROPERTIES

4.1.1 Hardness Profiles

Hardness measurements were taken across both heat affected zones and the weld metal of thirteen of the welds; weld 11 was excluded from this study. The data are shown in Figures 7-10 and Table 4. Nominal chemistries of the weld metal and of the rail for each weld are given in Table 3.

Figure 7 presents the hardness profiles of welds 1, 4, and 7 which are between two alloy rails, a standard and an alloy rail, and a head-hardened and an alloy rail, respectively. In all cases except for the head-hardened (HH) rail of weld 7, the maximum hardness is observed in the HAZ and often just beyond the edge of the fusion zone. In all welds, minimum hardness is at the outer edge of the HAZ. The profiles for welds 1 and 4 are typical for all welds between alloy rails and between a standard rail and an alloy rail. However, the hardness profile for weld 7 is atypical because of the region of low hardness in the HAZ and adjacent to the fusion zone in the head-hardened rail. This was the only weld which exhibited this behavior and may be due to the heating and cooling effect of welding on the hardening imparted to the head of the rail. Specifically, the irregularity in the shape of the hardness profile is possibly the result of a mixed structure. The HH rail is AREA standard rail in which the head has been induction heat treated. The depth of this "cap" terminates at 12 to 15 mm below the running-surface, and although the hardness profile, at 25 mm, should be below the fully hardened region, microstructures observed at 25 mm were not entirely uniform.

Figures 8 and 9 summarize the range of hardness deviations observed in the heat affected zones of the five types of rails. No

effect of preheat time on hardness and only a slight effect of the application of the muffle to retard cooling on hardness was observed; thus the data are presented as a range of hardness for a given type of rail. All of the heat affected zones are included in Figures 8 and 9 except the HAZ of the CrMo side of weld 7.

The hardness for the heat affected zones are summarized in Table 4. From these data, it appears that the effect of retarding cooling by application of the muffle is to decrease the maximum hardness by approximately 1-3 R_C points in the alloy rails. However, it is difficult to make any statement regarding the effect of the muffle on the hardness in the standard and in the head-hardened rails because of the small number of test welds with these rails.

Figure 10 summarizes the hardness of the weld metal in the thirteen welds for which hardness profiles were measured. The most noticeable effect is that weld metal produced from so-called "alloy" thermite-steel has a hardness of 28-34 R_C at the center and 32-38 R_C near the fusion zone. This is significantly harder than the weld metal produced from the "standard" thermite-steel which varies in hardness from 20 to 27 R_C.

Another effect is that of preheat time. As indicated above, preheat has no significant effect on the hardness within the HAZ. For the weld metal, however, a preheat of 3 minutes causes the weld metal to be about 2-5 R_C points softer at the center; this is evident in Figure 10. Finally, Figure 10 shows that the longer preheat increases the width of the weld metal by approximately 25 percent. This is true for the welds produced using "alloy thermite-steel," but there are not enough data to draw the same conclusion when a weld is produced using "standard" thermite-steel.

4.1.2 Impact Properties

Impact properties were determined with Charpy V-notch specimens. Specimens were taken from the weld metal and from the

transitional region between the HAZ and the unaffected rail on each side of the weld as shown in Figure 5. The impact energies are tabulated in Table 5.

The impact energies do not show any trends associated with variations in preheating time or with retardation of cooling rates. In the weld metal the impact energy is only 1.5 to 2.8 Joules (1.1 to 2.1 ft-lb_f) with only slightly better properties in the welds using the standard mix for the thermite steel.

The specimens in the heat affected zones incorporated about 50 percent of the HAZ and 50 percent of the unaffected rail, as indicated in Figure 5. This location was selected because it includes the weakest metal at the edge of the HAZ. With the exception of the B-specimen in weld 9, the fractures did, in fact, reveal approximately 50 percent of the cross section to be in the HAZ and this was further verified by lightly etching the fractured impact specimens to reveal the HAZ. Given the scatter typically associated with the impact energy, no trends can be associated with rail chemistry, preheating time or retardation of cooling. An exception appears to be the low energies of the HAZ of the head-hardened rail (welds 7 and 8). These energies, 2.8 and 2.6 Joules, are lower than the remaining energies which range from 4.3 to 6.9 Joules. Weld 9, with one side of the HAZ at 9.6 Joules is another exception, but this is due to the fact that approximately 90 percent of the fracture surface was within the unaffected rail. The low energies in welds 7 and 8 are unexplainable; however; these are also the head hardened rails which exhibited the unusual hardness profiles in Figure 9.

4.1.3 Tensile Properties

Tensile properties were determined with reduced size tensile bars (6.4 mm dia. with 25.4 mm gage length). Specimens were taken from across the weld metal and across the HAZ on each side of the weld as shown in Figure 5. The tensile properties are given in

Table 6. These data show that the weld metal prepared from "alloy mix" is consistently harder (268-314 BHN) than weld metal prepared from "standard mix" (227-255 BHN). Accordingly, the "alloy mix" is usually stronger (approximately 15-20 ksi) with slightly less reduction in area than exhibited by the "standard mix".

It is difficult to draw conclusions from the tensile properties of the specimens removed from the heat affected zones as given in Table 6. Apparently the steep gradient in hardness, where hardness is a minimum at the outer edge of the HAZ, causes the yield strength to be rather unpredictable. For example, the yield strengths among the CrMo rails vary from a low of 510 MPa (74 ksi) to a high of 820 MPa (119 ksi), yet there are no significant differences among their respective hardness profiles. The Cr rails and CrV rails have yields which vary between 531 MPa (77 ksi) and 593 MPa (86 ksi), and the standard rails and the head-hardened have yield strengths between 462 MPa (67 ksi) and 552 MPa (80 ksi).

The variation of tensile strength is less than the variation of yield strength in the specimens from the heat-affected zones. All of the alloy rails (CrMo, Cr and CrV) have tensile strengths which are in the range 883-1000 MPa (128-145 ksi); the tensile strength of the standard and head-hardened rails is in the range of 855-883 MPa (124-128 ksi). In all rails, the tensile specimens exhibit significant ductility (17 to 61 percent reduction in area) which far exceeds the weld metal (2 to 6 percent reduction in area).

4.1.4 Fractography of Impact and Tensile Specimens

The fracture surfaces of the impact and tensile specimens were examined by scanning electron microscope with an energy dispersive spectrum analyzer (SEM/EDS) system. The SEM mode was used to study the fractures, and when atypical features on the fractures were encountered, the EDS was employed to gather qualitative chemical analyses. The results of the fractographic analyses are presented

in the order of observations of the fractures of the Charpy V-notch (CVN) specimens and then descriptions of the fractures of the tensile specimens. Each group is discussed in terms of the specimens removed from the HAZ and from the weld-metal, respectively.

4.1.4.1 Charpy V-notch Specimens in the HAZ - Two-thirds of the CVN specimens straddled the regions of minimum hardness in the HAZ with the notch oriented such that the crack propagated across the thickness of the rail in a direction perpendicular to the rolling direction. Figure 5 shows the specimens; according to the classification in Hertzberg (53), the specimen orientations were T-S (width long transverse-thickness short transverse).

Since part of the cross-section of each specimen was in the rail beyond the HAZ and the remainder was in the HAZ, the fractures had a duplex appearance which was apparent when examined visually and with the SEM. Figure 11 shows a fracture at a low magnification which is typical of the fractures observed for all welds. The material beyond the HAZ (the original rail in Figure 11) has a faceted fracture which is coarser in appearance than the more fibrous fracture within the HAZ. At a higher magnification, the fracture in the "original rail", Figure 12a, is mostly cleavage with some intergranular separation on surfaces which are almost normal to the major crack. In the lower-right corner, an elongated MnS inclusion which has partially separated from the matrix can be seen. Figure 12a is typical of fractures of rail steel; e.g., see Park and Bernstein (54). Figure 12b shows the fracture appearance in the region of minimum hardness. The major portion of the fracture has details finer than those of Figure 12a with an appearance described as quasi-cleavage (55), with some regions of intergranular separations similar to those in Figure 12a.

According to Table 5, specimen 1-B shows an energy absorbed of 5.7 J. Feddersen and Broek (56) report values of about 2.7-5.4 J for rail steels at 20°C. Thus, the energy absorbed by the fracture

shown in Figures 11 and 12 is comparable to the impact energies for unwelded rail. The lowest impact energy of a HAZ shown in Table 5 is 2.6 J for specimen 8-B. This specimen was removed from a head-hardened rail. The fracture appearance on the rail side of the region of minimum hardness, Figure 13a, is similar to Figure 12a except that the transgranular facets are larger which is consistent with less energy absorbed in an impact test. A MnS inclusion is also present in this fractograph, Figure 13a. In the HAZ portion, Figure 13b, the fracture is similar to Figure 12b; of course, in both instances partial spheroidization has occurred and the minimum hardnesses are approximately equal.

As indicated above, MnS inclusions, elongated in the direction of rolling, were often seen in the fracture surfaces of the rail material; e.g., see Figures 12a and 13a. In all but four fractures of the twenty-six impact specimens for the region of minimum hardness in Table 5, a region of easy separation in the rail was evident. An example is shown in Figure 14 which is a fractograph from the CrV side of weld 4. The easy separation occurs on the side opposite the notch. In this case, the region of easy separation was detected in about 10-15 percent of the HAZ side of the region of minimum hardness where the pearlite has partially spheroidized. Among the welds in which this was seen, it occurred always on the side opposite the notch and predominantly in the HAZ side regardless of the type of rail.

4.1.4.2 Charpy V-notch Specimens in the Weld Metal - For the most part, the appearance of these fractures was similar to the fractures of unwelded rail with transgranular cleavage and some evidence of intergranular separations, Figure 15. They all show transgranular fracture and brittleness regardless of weld metal chemistry, preheat time, or cooling rate. Although not evident in the fractographs of Figure 15, small amounts of microporosity were observed when the specimens were studied with the SEM. Small inclusions were observed on the facets which can be seen in Figure 15. The inclusions in all

impact specimens were qualitatively analyzed with the EDS system which showed predominatly Al with lesser amounts of Mn, S, and Si. Presumably the inclusions are rich in Al_2O_3 and contain SiO_2 and MnS.

4.1.4.3 Tensile Specimens in the HAZ - The tensile specimens were oriented longitudinally across the region of minimum hardness in the head portion of the rails as shown in Figure 5. Although collectively as a group, these fractures were more complex than those of the CVN specimens, the fractures occurred in the regions of minimum hardness. Four types of fractures were noted: (1) cleavage with a small shear lip, Figure 16a; (2) cleavage with a fibrous central-region and no shear lip, Figure 16b; (3) "cup and cone" fractures, Figures 17a and 17b; and (4) "cup and cone" with radial features, Figures 18a and 18b.

Table 7 summarizes the specimens according to the above classification. It shows that the failures of types 1 and 2 have ductilities in the range of 16.8-29.4 percent reduction in area and that types 3 and 4 have ductilities in the range of 43.2-61.2 percent reduction in area with one exception at 33 percent (tensile specimen 1-B).

Table 8 summarizes the distribution of rail types according to the observed fractures. The number of specimens is small (the greatest number is 13 for CrMo), but it appears that the failures of the CrMo rails are among the fractures of high ductility with the exception of one specimen (12-A). That particular specimen necked, but the fracture was displaced slightly from the location of the minimum area. The three specimens from the standard rails failed with low ductility (type 2), the head-hardened with high ductility and the Cr and CrV rails had failures of high and low ductilities.

Figures 19a and 19b show the fractures of a low-ductility and of a high-ductility specimen, respectively. Figure 19a is a type 2 fracture at the transition between the central-fibrous region (the

lower portion of the fractograph) and the region of a transgranular cleavage (the upper portion of the fractograph). Figure 19b is an example which shows the details of a radial feature. Along the "cliff" which goes across most of the fractograph, one can see evidence of the inclusions elongated in the rolling direction. There are numerous secondary cracks and also many holes resulting from the separation of the matrix from the inclusions. Many of these holes were qualitatively analyzed with the EDS, and Mn and S were always detected in significant amounts. Since the inclusions in the rails are elongated in the rolling direction, rather high ductility is observed because the tensile specimens are oriented longitudinally. Were specimens oriented transverse to the rolling direction, then ductility would be expected to be significantly less.

4.1.4.4 Tensile Specimens in the Weld Metal - The mode of fracture of the tensile specimens removed from the weld metal for all of the welds was essentially cleavage which corresponds to the low ductilities reported in Table 6. Figures 20a and 20b show the fractures of alloy weld metal and standard weld metal, respectively. On the right side of Figure 20b, there is a large region showing the separation of an as-cast columnar structure. Tensile bars were removed from five welds prepared from standard weld metal, and their fractures all displayed one or two of these features which occupied about 10-25 percent of the fracture area. None of the tensile specimens from alloy welds showed these features. At a greater magnification, it is clear that the as-cast grain boundaries have separated; this can be seen in Figure 21. In Figure 21b, much of the surface of the grain boundary is smooth with rough areas corresponding to the dendrite arms shown in Figure 21a. Before fracture, neighboring columnar grains were bridged at the rough areas; fracture merely tore the "bridges" and produced the roughness.

The direction of the as-cast columnar structure exposed in Figures 20b and 21 corresponds closely to the dendrite direction (in the location of the test bar) shown in Figure 22. The tensile specimens were removed from the head portion where the dendrites are oriented at approximately 45° to the horizontal, and this corresponds to the large regions of easy separation in the fractures of standard weld metal. The absence of similar features in alloy weld-metal is not understood at this time.

Further evidence that the regions of easy separation are as-cast columnar structure boundaries is given in Table 9. The regions were analyzed semi-quantitatively and found to contain high concentrations of many elements. These analyses are similar to the analyses shown in Table 10 which are from the exposed surfaces of dendrite arms found in the interdendritic areas of microporosity in Figure 23. Since microporosity occurs between dendrite arms, then it follows that the exposed surfaces of the dendrite arms in Figure 23 would exhibit segregation; as-cast grain boundaries (between neighboring arrays of similarly oriented dendrites) also would be expected to exhibit segregation. The segregation is particularly evident for Ni, Cu, Zn, and Al in the welds.

4.2 STRUCTURAL ANALYSES

4.2.1 Macrostructures

The weld macrostructures appeared independent of all weld parameters except preheat time. Preheat time affected the extent of melt back or the width of the weld deposit. At the location of the hardness profile, the deposit width was 45-58 mm for the standard preheat and 64-74 mm for the long preheat with the exception of weld 6. Weld 6 was subjected to a long preheat but displayed a deposit width of 46 mm. A possible explanation for this discrepancy is a suppressed reaction temperature and thus reduced superheat. Also,

weld 6 was the first weld of the day (ambient temperature was only -1°C) so that inadequate preheating of the reaction crucible could have contributed to a loss of superheat.

Overall, with the exception of weld 6, the weld deposits for the long preheats were 20-30 percent wider than for the standard preheat. At all locations, growth of primary dendrite arms was essentially perpendicular to the fusion zone. These effects are shown in the representative macroetchs of Figures 24 and 25.

For all welds, the dendritic structure was columnar with the dendrites growing from both fusion zones and meeting in the weld center. From the weld base to about the head-web area, the primary dendrite arms were essentially parallel to the longitudinal axis of the rail. In the head-web and head areas, the primary arms were oriented at an upward angle of about 45°. This is due to the head, with the pouring cup located directly above it, having the greatest melt-back. This results in solidification proceeding inward and upward towards the cup as reflected by the dendrite growth direction.

Some macroetches displayed slight pitting along the weld centerline; however, this was not attributed to porosity. Rather, the pitting was determined to be due to preferential etching of segregation along the centerline. Weld 14 displayed a slight depression along the top of the weld metal. This was caused by improper removal of the pouring cup and sprue from the weld.

Welds 7, 11 and 14 exhibited macroinclusions in the weld. In welds 11 and 14 these inclusions were located at about the web center along the fusion zone approximately where the mold for the weld had contacted the rail. They were about 6 mm in diameter and had the appearance of the slag. Weld 7 displayed a similar inclusion in the top of the base. Also, a black iron oxide inclusion of similar size was noted in this region. In addition, a large alumina/silicate inclusion, 10 mm x 6 mm x 6 mm deep was noted in the web-center of this weld, where contact with the mold surface

occurs. These inclusions were not analyzed but had the glassy appearance and color of the alumina slag with evidence of fused and unfused silica. The silicate/alumina inclusions are attributed to trapped alumina slag and sand particles from the mold that either were washed from the mold walls during the pour or were not blown from the mold prior to welding. The iron oxide is probably unreacted material from the thermite charge.

The width of the HAZ was essentially constant for all welds at 30-33 mm. The HAZ's of the welds with a long preheat were abut 2 mm wider than the HAZ's of welds produced with standard preheat. Otherwise, the width of the HAZ was essentially independent of the welding parameters.

4.2.2 Microstructures

The microstructures of the welds were determined by examining specimens for each weld but only at the approximate mid-height of the rail head. The examination started in the parent metal on one side, passed through the HAZ and weld metal and continued through the HAZ and into the parent metal on the other side. In no instance was a martensitic structure observed.

The microstructures were characterized after consulting Smith and Fletcher (57) for the appearance of constituents found in rail steels. A constituent which they identified as transitional pearlite is harder than lamellar pearlite and other pearlitic morphologies (57). Bainite has a coarser carbide distribution than transitional pearlite, so that its hardness is intermediate between transitional pearlite and all other pearlite morphologies. However, after characterizing the microstructures according to the sum of transitional pearlite and bainite, no correlation between hardness and the amount of those constituents was clearly evident. Therefore, in this report no distinctions are made among lamellar pearlite, transitional pearlite and distorted pearlite; together they are classified as pearlite.

With regards to the weld metal, all microstructures were pearlitic and some had bainite. When present, the volume fraction of bainite was 0.05-0.10 based on the field of view. Typical microstructures are shown in Figures 26 and 27. The major difference between alloy weld metal and standard weld metal is the proeutectoid ferrite, evident in Figure 28, which was present in standard weld metal in all cases but which was not seen in any of the alloy weld metal specimens.

Structures observed at the fusion zone were similar to those of the interior of the weld metal with two exceptions: (1) proeutectoid ferrite was absent or present in lesser amounts in the standard welds and (2) somewhat more welds, especially among the alloy welds, exhibited bainite and the volume fraction of bainite was as much as 0.25 when present.

The parent rails, themselves, were also pearlitic; in three alloy rails and one standard rail small amounts of bainite, based on the field of view, were observed. Even in the HAZ's, which were harder than the parent rails (Figures 8 and 9), only small amounts of bainite (0.05-0.10 volume fraction) were observed in six alloy rails and two standard rails. Of course in the outer edge of the HAZ's, where minimum hardness was observed, it was consistently observed that the pearlite had undergone significant spheroidzation as shown in Figure 29.

Finally some large inclusions, 200-500 μm in diameter, were observed along the fusion zone in welds 6 and 10, Figure 30. In weld 6, the EDS analysis indicated that inclusions were rich in alumina and silica. The inclusions in weld 10 also contained alumina and silica with a significant amount of manganese sulfide.

4.2.3 Inclusion Evaluation

Quantitative image analysis was performed on the weld metal in six welds for the purpose of determining inclusion volume fraction. The location of the inclusion evaluation surface was close to the

location of the center of tensile bars and was approximately at the center of the weld, 2.5 cm below the running surface and parallel to the surface.

The parameters and results of the evaluation are listed in Table 11. The fields of view were selected at random with the exception that when microporosity was observed in a field, this field was disregarded and another selected. The volume fraction of inclusions for a sample was based on the mean inclusion area and the total observations for that sample. Confidence limits were established using the basic definitions of expected value and variance for the volume fraction and the Student's t-distribution (58).

Inclusion content varied from 0.24 percent to 0.49 percent and seemed to be independent of welding process variables. Table 11 also indicates that the welds with the higher volume fraction of inclusions have the larger inclusions with the greater dispersion (standard deviation from the mean size).

Welds 5 and 6 represented the standard weld composition after standard and long preheats, respectively. Weld 7, a standard weld, was evaluated because several macroinclusions were observed during sectioning for the macroetch. Among these three welds, no obvious differences were noted on the micro-level, Table 11. Welds 13 and 14 represent alloy weld metal for standard and long preheats, respectively. Weld 12, an alloy weld, was produced with a premature tap, and as a result, a high inclusion level was expected. As evident in Table 11, this was not the case. Thus these measurements indicate that the inclusion level is approximately 0.2 - 0.5 volume percent in thermite welds. This factor alone, could account for, at least in part, the lower fracture ductilities of the tensile specimens reported in Table 6 (59).

4.3 THERMAL MEASUREMENTS

Thermocouples were positioned in the rails of welds 1-4 and in the weld metal of weld 9. Figure 31 shows the temperature as a function of time for weld 1. The numbers on the curves refer to the thermocouples located at the respective positions shown in Figure 3. The locations nearest to the rail end (thermocouples 1-5), of course, respond most rapidly and achieve the greatest peak temperatures after the molten charge is tapped at 145 s. As expected, all curves exhibit peak temperatures, as ordinarily exhibited by welds, and some of the curves show thermal arrests or retardation of cooling due to the transformation of austenite upon cooling through the temperature range of 1000°K to 810°K (1340°F to 1000°F). Curve 2 shows a sudden increase of temperature at about 370 seconds. This occurred right after the excess metal on the top of the weld had been removed by chiseling and when the risers on both sides of the weld are usually removed by knocking (Appendix). A variation of the process, which was employed in this case, is to remove the risers by torch cutting which is the probable reason for the abrupt increase at about 370 seconds for thermocouple 2. By placing the muffle on the weld (750 s), the cooling rate is increased initially and then stabilized. The increase is evident for the thermocouples located in the rail head (thermocouples 1, 6 and 11).

Figure 32 shows the measured temperatures in the weld metal of weld 9. At 125 s, the preheating torch was removed, and the charge was tapped at 150 s. During preheat the temperatures shown in Figure 32 do not reflect the true preheat rail temperature due to the combined effects from the gas flame and radiant energy from the heated rail ends. These temperatures dropped as soon as the torch was removed just prior to tapping at 150 seconds, and, of course, increased very rapidly as the thermite charge was tapped.

Thermocouple output was monitored continuously by the strip chart recorder and at discrete intervals (every 2-3 seconds) by the data acquisition system. Data from each system were in agreement

except for the peak temperatures at tapping. The strip chart data, being continuous, were used for these peak temperatures. It is difficult to ascertain the exact temperature at tapping, but the maximum recorded temperature was 2140°K (3400°F) at position A in the rail-head, so we know that the tapping temperature was at least of that magnitude. While all three thermocouples indicate tapping temperatures well above the liquidus, cooling at the web and base positions was very rapid so that the true tapping temperatures at these positions were probably not recorded.

The heaviest mass of weld metal is in the rail-head, and so the thermal arrest at approximately 1760°K (2700°F) and 250 seconds shown for the head is the arrest closest to the liquidus temperature of the weld metal. The corresponding portions of the other two curves show arrests at lower temperatures when the heat of solidification was evolved in the regions which were solidifying more slowly. Consequently, the indications of freezing on these cooling curves are below the liquidus temperature of the alloy. The curves for the head and base also show evidence of the transformation of austenite at 950°K (1250°F) during cooling.

Figures 33-35 summarize important features derived from the thermal measurements for welds 1-4. Figure 33 shows the temperature distribution in the head, web and base locations of the rails at the end of the preheating period. At a given distance from the end of the rail, preheat temperature is almost uniform from the head down to the base so the curves show no distinction among the thermocouples' positions in the vertical sense. In Figure 33, data are combined for welds 1, 2 and 4 because they were preheated for the same period (2 minutes). A longer preheat of 3 minutes (weld 3) increases the preheat temperature distribution somewhat, and causes an increase in the width of the weld metal region and a decrease in cooling rate through the critical range for the austenite transformation. Both curves are extrapolated to the rail end (zero distance) by assuming that log $(T-T_a)$ vs $(x/\ 2\sqrt{\alpha\tau})$ is linear for $(x/\sqrt{2\ \alpha\tau})$ <0.5

where x = distance from the end of the rail,

α = thermal diffusivity,

τ = time,

T = temperature at x, and

T_a = ambient temperature.

This assumes that during preheat, heat flow in the rail is one dimensional, and that the rail is infinitely long with the end heated by a convective environment. Such a solution is available in heat transfer texts (e.g., see Geiger and Poirier (60) or Schneider (61)). By extrapolating to the zero distance, the temperature at the rail end is approximately 1150°K and 1300°K for standard (2 minutes) and long (3 minutes) preheats, respectively.

Figures 34 and 35 show the peak temperatures in welds 1-4. These plots were derived from the maximums of the curves of temperature versus time as shown, for example, in Figure 31 for weld 1. Figure 34a gives peak temperatures for weld 1; peak temperatures are the greatest in the head, and they decrease in a regular manner from the head to the base. The same behavior of peak temperature in welds 2-4 can be seen in Figure 34b and in Figures 35a and 35b.

The effect of a longer preheat is evident for weld 3 (Figure 35b); peak temperatures in this weld are the highest of the four given in Figures 34 and 35.

Finally, Table 12 has been prepared to show the cooling times of the welds as they cooled through the temperature range of 1000°K to 810°K (1340°F to 1000°F); within this range, the austenite transforms. Along with data derived from welds 1-4, data from Figure 32 are included. The latter represents the cooling of the weld metal. Table 12 illustrates that the average cooling times through the specified temperature range are not fully comparable within the weld metal and within the heat affected zones in the head and web regions. However, in the base of the rail the time of cooling is about the same for the weld metal and the rail metal in the HAZ. The slowest cooling shown for these welds is 1380 s in the

weld metal of weld 9. Weld 2 was produced with no muffle, and it, in fact, cooled somewhat faster than did welds 1, 3 and 4. Weld 4, while produced with the muffle, cooled noticeably faster than welds 1 and 3 and, in fact, has rates that approach those of weld 2, while the preheat temperatures of welds 1, 2 and 4 are comparable, Figure 33, the peak temperatures of weld 4, particularly in the head near the rail end, are on the order of 150°K lower than that for welds 1 and 2, Figures 34 and 35a. These lower peak temperatures indicate that the thermite steel for weld 4 was probably tapped at a lower temperature so that cooling from 1000°K to 810°K required less time. This weld was the second of the day (ambient of +6°C) so that crucible preheat should not have been a problem. No adverse effects on the properties of weld 4 were noted. Finally, there is no significant effect of a longer preheat (weld 3) on cooling from 1000°K to 810°K (1340°F to 1000°F), although the width of the zone of weld metal is increased by increasing the time of preheating.

4.4 RESIDUAL STRESSES

Residual stresses were determined by the blind hole technique for weld 11 at the location shown in Figure 6 and 36. The principal stresses and their orientations relative to the vertical centerline are given in Table 13 and shown in Figure 36. In Figure 36, the principal stresses are shown as vectors with lengths proportional to the respective scalars.

The residual stresses for the weld metal, locations E, C, F, D and O, agree with the findings of Dohse (47) and others (26, 48) in that the head and base areas are in compression while the web area exhibits tensile residual stresses. The compressive stresses in the head, head-fillet and base-fillet areas are relatievly high, on the order of -270 MPa, while the tensile stresses in the web are relatively low, on the order of +60 MPa.

A lack of symmetry is noted for the stress fields in the HAZ's on both sides of the weld metal. This is particularly evident in

the locations selected for the web region (L, J, B and H). In going with location L to J, a transition from a compressive-tensile state to a compressive state occurs. At L, the maximum principal stress is +110 MPa and at J, a compressive maximum of -207 MPa occurs. In the opposite side of the weld and in the web HAZ, no tensile stresses are observed at locations B and H. At B, a low compressive state exists, -48 MPa maximum, but at H, a high compressive state occurs, with a maximum of -335 MPa exhibited. The reason for the asymmetry is not known but could be due to differing residual-rolling stresses existing in the rails prior to welding. However, since these stresses were not measured, this is only a hypothesis.

In contrast, the stress fields in the HAZ of the head-fillet area (locations K, I and A, G) are relatively symmetrical. At both K and I, the maximum principal stress is about +145 MPa. At A, the tensile stress is relatively low at +34 MPa while at G a value of +128 MPa is observed. The compressive stress at K is insignificant, and at I the material is in a tensile-tensile state with one principal stress essentially equal to zero. At A and G, the compressive-principal stresses are about -90 MPa.

The residual stresses in the head are compressive. Specifically at location M the maximum compressive stress is -154 MPa, and at location E, on the head running surface, the maximum compressive stress is -285 MPa. Finally at N, the greatest tensile residual stress is observed, +151 MPa.

The residual stresses observed in the HAZ's are considered significant since they approach 25 percent of the yield strength and 15 percent of the ultimate strength of the unwelded rail steel, 600 MPa and 950 MPa, respectively (7). Of more significance is the reduced strength in the region of minimum hardness at the outer region of the HAZ. Tensile data from the standard rail portion of welds 4 and 5, produced under similar conditions as weld 11, show that the yield strength of the outer edge of the HAZ is 474-548 MPa, and the ultimate strength is 857-88[illegible] MPa; these values are

significantly lower than for the unwelded rail. Thus the residual tensile-stresses in the outer edge of the HAZ exceed 25 percent of the yield strength in the web, and they are also significant in the head fillet and base fillet regions.

If the residual stresses are taken to be a mean stress superimposed on alternating stresses imposed during the flexural loading of rail in-service, then the effect of the residual stresses on the fatigue strength can be approximated by the Goodman equation or by the Gerber equation. These equations are given by Hertzberg (62):

$$\text{Goodman equation:} \quad \sigma_a = \sigma_{fat}\left[1 - \frac{\sigma_m}{\sigma_{ts}}\right]$$

$$\text{Gerber equation:} \quad \sigma_a = \sigma_{fat}\left[1 - \left(\frac{\sigma_m}{\sigma_{ts}}\right)^2\right]$$

where

σ_a = fatigue strength in terms of stress amplitude, where $\sigma_m \neq 0$

σ_m = mean stress,

σ_{fat} = fatigue strength in terms of stress amplitude, where $\sigma_m = 0$

σ_{ts} = tensile strength,

σ_{ys} = yield strength.

According to Sato (63), the fatigue limit in the welded zone of high carbon steel is 0.37 of the tensile strength. Table 6 gives values of the tensile strength in the region of minimum hardness in the HAZ; the average values are 865 MPa and 938 MPa for standard (including head hardened) and alloy rail, respectively. The maximum residual stress of 151 MPa (tensile) occurs in the region of minimum hardness (Table 13). Then using σ_m=151 MPa, σ_{fat}=0.37 σ_{ts}, σ_{ts}=865

MPa for standard rail and σ_{ts}=938 MPa for alloy rail, we get σ_a=264 MPa (Goodman) and σ_a=310 MPa (Gerber) for standard rail. For alloy rail, we get σ_a=291 MPa (Goodman) and σ_a=338 MPa (Gerber).

For unwelded rail, assuming no residual stresses and no mean stresses, and that the 0.37 ratio still applies, with σ_{ts}=900 MPa for standard rail and σ_{ts}=1240 MPa for alloy rail, σ_a=330 and 460 MPa, respectively. Therefore, the fatigue strength in the region of minimum hardness appears to be less than the fatigue strength of unwelded rail, and the decrease in fatigue strength is greater for alloy rail. The degradation in fatigue strength due to the residual stresses compared to the total degradation of the fatigue strength in the region of minimum hardness is about 16 pct. according to the Goodman equation and 3 pct. according to the Gerber equation. Thus, it *is* possible that the residual stresses degrade the fatigue strength in the region of minimum hardness. However a greater cause of degradation of the fatigue strength is the general decrease of the mechanical properties caused by coarsening of the metallurgical structure.

5. CONCLUSIONS

Standard rails (i.e., AREA CC rails) and head-hardened rails can be welded to premium rail steels, such as Cr, CrV, and CrMo alloy rails, by the thermite process using either "standard" kits or "alloy" kits for the weld metal. In this study, no martensitic structures were encountered in the heat-affected zones or in the weld metal of any of the welds. Thus, it is concluded that premium rails can be successfully joined in the field by the thermite-welding process.

The following summarizes other important conclusions regarding the hardness, tensile properties, impact energies, and structure of the thermite welds in rails, along with additional conclusions drawn from the thermal measurements and residual stress measurements.

1. "Alloy" weld metal is harder and stronger than "standard" weld metal. Specifically, the hardness of "alloy" weld metal is 28 to 34 R_C, whereas the hardness of "standard" weld metal is in the range of 20 to 27 R_C, depending on pre-heat time. Correspondingly, the yield strength and tensile strength of "alloy" weld metal are about 100 - 150 MPa (15 - 22 ksi) greater than those of "standard" weld metal.

2. Since "alloy" weld metal is stronger than "standard" weld metal, it is not as ductile. However, it is more important to note that weld metal of both types exhibits ductility in the range of only two to six percent.

3. The tensile fractures of the weld metal show transgranular cleavage when examined by SEM. Features observed in the fractures of "standard" weld metal, but not in "alloy" weld metal, are as-cast boundaries of columnar grains which separated very easily. Microporosity in small amounts was also seen in the tensile fractures along with microinclusions rich in Al_2O_3 with SiO_2. MnS is also present. Positive

identification was not carried out, but it is likely that the inclusions are aluminates, silicates, oxysulfides, and sulfides.

4. The impact properties of weld metal are very low. Using Charpy V-notch (CVN) specimens, the energy absorbed is only 1.5 - 2.8 J (1.1 - 2.1 ft-lb_f) at 20°C. Within that range of energy absorbed, "standard" weld metal is slightly better than "alloy" weld metal.

5. The fractures of the CVN specimens, removed from weld metal, predictably indicate brittle failures. The appearance is similar to published fractographs of rail steel with transgranular cleavage. Microporosity and incusions are also apparent in amounts equivalent to those in the tensile fractures.

6. Longitudinal tensile specimens, which straddled the region of minimum hardness along the outer edge of the HAZ, were removed from the welds and tested. The yield strength of such specimens varies widely (from 460 - 820 MPa) due to the steep gradient of hardness at that location. The variation of the ultimate tensile strength is not as great as for the yield strength; it is 850 - 880 MPa for the standard and head-hardened rails and 890 - 960 MPa for the alloy rails.

7. When standard or alloy rail is welded with a "standard" thermite kit, the minimum hardness of the HAZ and of the weld metal are comparable, but the tensile strength of the weld metal is less than that of the outer edge of the HAZ.

8. In the case of welding alloy rails with an "alloy" thermite kit, the minimum hardness in the HAZ is less than the minimum hardness of the weld metal; even so, the tensile strengths compare closely.

9. The impact properties of CVN specimens, which straddle the region of minimum hardness along the outer edge of the HAZ, are very low. The energy absorbed for all specimens is only in the range of 2.6 - 6.9 J.

10. The microstructures of the heat-affected zone and of the weld metal were studied in detail. As expected, the region of minimum hardness in the HAZ has a partially spheroidized structure. All of the remaining structures contain pearlite with small amounts of bainite sometimes noted. In most instances, of course, the hardest material is within the HAZ.

11. Nonmetallic macroinclusions were observed in the weld metal of three welds when they were sectioned, ground, and etched to reveal the macrostructures. Such inclusions were isolated and not seen on fracture surfaces of the tensile bars or CVN specimens used in this study.

12. The microinclusion content in weld metal is 0.24 - 0.49 percent. This volume fraction is high enough to be a contributory factor to the low values of tensile ductility of 2 - 6 percent reduction in area.

13. In four welds, temperatures in the rail were recorded during preheating and welding. These data show that preheat temperature is primarily a function of preheat time and of distance from the weld gap but not of location in the vertical cross-section of the rail. Preheat times of two and three minutes made no important differences in properties or structures of the heat-affected zones. The only effects observed were an increase in the width of the zone of weld metal and a slight decrease in the hardness and strength of weld metal.

14. During the cooling of some welds, a "clamshell" type muffle was wrapped around the weld for the purpose of decreasing the cooling rate. Depending upon the location in the HAZ, the muffle did increase the time in the critical range (1000^{o}K - 810^{o}K) by 15 - 70 percent. The retardation of cooling did not significantly alter the properties of the welds except to reduce the maximum hardness in the HAZ's of alloy rails by about 1 - 3 R_C points.

15. In one weld, temperatures in the weld metal were measured. The molten thermite steel was poured into the mold at a temperature of at least 2140°K (3400°F) and perhaps higher. Solidification of the weld metal proceeded in the order of web, base, and head. In the critical range (1000°K - 810°K), the base and web cooled at rates comparable to those of the HAZ's and the head cooled more slowly than the HAZ.

16. One weld was left intact so that residual stresses could be measured. In the weld metal the principal stresses are compressive (-270 MPa) in the head and base slightly tensile (+60 MPa) in the web. Principal stresses in the HAZ are both compressive and tensile with some tensile stresses as high as +110 to +150 MPa in locations where the ultimate tensile strength is 855 - 1000 MPa. Such residual stresses, when added to the stresses due to flexural loading encountered in service, could contribute to a decrease in fatigue strength of welded rail.

6. REFERENCES

1. Mehra, O.K., D.K. Bose and C.K. Gupta, "Reduction of Calcium Molybdate," Metallurgical Transactions, vol. 4, March 1973, pp. 691-694.

2. Applied Science in the Casting of Metals, ed: K. Strauus, Pergammon Press, Oxford, England, 1970, pp. 443-466.

3. Houldcroft, P.T., Welding Process Technology, Cambridge University Press, London, England, 1977, pp. 188-190.

4. Goldschmidt, H., "Neue Thermitreaktionen (New Thermit Reactions)," Zeitschrift fur Elektrochemie, vol. 14, No. 35, 1908, pp. 558-564.

5. Hauser, D., "Methods for Joining of Rails: Survey Report," Report No. FRA/ORD-77/16, Prepared for the U.S. Department of Transportation, July 1977.

6. Hauser, D., "Welding of Railroad Rails - A Literature and Industry Survey," ASTM Special Technical Publication STP 644, ASTM, Philadelphia, PA, 1978, pp. 118-141.

7. Myers, J., "Evaluation of Thermite-Type Railroad Welds," Master's Thesis, Department of Metallurgical Engineering, University of Arizona, Tucson, AZ, 1979.

8. Gupta, C.K., P.K. Jena, "Reduction of Molybdenum Trioxide by Aluminum," Journal of the Less Common Metals, vol. 14, January 1968, pp. 148-150.

9. Belitskus, D., "Aluminothermic Production of Ferroalloys," Journal of Metals, vol. 25, May 1973, pp. 39-44.

10. "High Temperature Reactions and Processes," Proceedings of the National Symposium, March 1976, Surathkal, India, pp. 89-97.

11. Ibid., pp. 217-222.

12. Belitskus, D., "Aluminothermic Production of Metals and Alloys," Journal of Metals, vol. 24, January 1972, pp. 30-34.

13. Viswanath, R.P., B. Viswanathan, V. Srinivasan and M.V.C. Sastri, "A Differential Thermal Analysis Stuy of the Reduction of Ferric Oxide by Hydrogen," Indian Journal of Technology, vol. 9, November 1971, pp. 439-440.

14. Welding Handbook, 7th edition, vol. 1, American Welding Society, Miami, FL, 1978, pp. 43-44.

15. Delachaux, P., "Soudage Aluminothermique de Pieces D'acier Moule et de Fonte (Aluminothermic Welding of Cast Steel and Cast Iron Parts)," Soud Techn Connexes, vol. 25, no. 1,2, Jan-Feb. 1971, pp. 26-31.

16. Kubaschewski, O., C.B. Alcock, Metallurgical Thermochemistry, 5th edition, Pergamon Press, Oxford, England, 1979.

17. The Making, Shaping and Treating of Steel, 9th edition, United States Steel Corporation, Pittsburgh, PA, 1971.

18. JANAF Thermochemical Tables, Second edition, National Bureau of Standards, June 1971, Sections: Al_2O_3, Fe.

19. Khalil, S.E., M.W. Abdel-Salam, "Studies on Some Factors Affecting the Production of Extra Low-Carbon Ferrochrome from Baramiya Chromite Ore by Aluminothermic Process," Egyptian Journal of Chemistry, vol. 15, no. 4, 1972, pp. 347-359.

20. Ashton, M.E., "Thermit Welding of Rail Steels," Railway Engineer, vol. 2, no. 3, May-June 1977, pp. 40-45.

21. Sonon, D.E., J.V. Pellegrino and J.M. Wandrisco, "A Metallurgical Examination of Control-Cooled, Carbon-Steel Rails with Service Developed Defects," ASTM Special Technical Publication STP 644, ASTM, Philadelphia, PA, 1978, pp. 99-117.

22. Geiger, G., "Structure and Properties of Thermite Welds," Report No. TS-11958-1, Prepared for the Transportation Systems Center, U.S. Department of Transportation, Cambridge, MA, Feb. 1977.

23. Private Communication, Department of Technical Research and Development, A.T. & S.F. Ry. Co., 1001 N.E. Atchison St., Topeka, KS, 66616, 1981.

24. Myers, J., G.H. Geiger and D.R. Poirier, "Structure and Properties of Thermite Rail Welds," Welding Journal-Welding Research Supplement, Aug. 1982, pp. 258-S to 268-S.

25. Ezhov, A.A., "The Development of Cracks in Welded Steel Castings of Unequal Thickness," Welding Production, vol. 23, no. 10, Oct. 1976, pp. 38-41.

26. Heller, W. and G. Beck, "UnwandlungsVerhalten der Schienenstahle und Folgerungen fur das Schweisen und Brennschneiden (Transformation Characteristics of Rail Steels and Consequences for Welding and Flame Cutting)," Archiv fur das Eisenhuttenwesen, vol. 39, no. 5, May 1968, pp. 375-386.

27. DeOliveira, E.Q., "Rail Specifications and Testing," Master's Thesis, Department of Metallurgy, Sheffield University, Sheffield, England, Sept. 1977.

28. Tetelman, A.S., "Fundamental Aspects of Fracture, with Reference to the Cracking of Weldments," Weld Imperfections, Proceedings of a Symposium at Lockheed Palo Alto Research Laboratory, Palo Alto, CA, Sept. 19-21, 1966, Addison-Wesley, pp. 249-275.

29. Lebedev, B.D., "Effect of Solidification Rate on the Character of Distribution of Sulphur and Phosphorus in Welded Joints in Low Carbon Steels," Welding Production, vol. 20, no. 11, Nov. 1973, pp. 12-15.

30. Makarov, E.L., "Influence of Alloying Elements on the Resistance of High-Strength Weld Metal to Cold Cracking," Welding Production, vol. 22, no. 4, April 1975, pp. 13-16.

31. Boniszewski, T., "Metallurgical Aspects of Reheat Cracking of Weldments in Ferritic Steels," Proceedings of the Biennial Conference Organized by the Heat Treatment Committee of the

Iron and Steel Institute 8-9 Dec. 1971 London, I.S.I., 1972, pp. 29-41.

32. McPherson, R., "Research on Stress Relief Heat Treatment of Weldments," Australian Welding Journal, vol. 18, No. 4, July-Aug. 1974, pp. 25-29.

33. Joshi, A. and D.F. Stein, "Temper Embrittlement of Low Alloy Steels," ASTM Special Technical Publication STP 499, ASTM, Philadelphia, PA, 1972, pp. 59-89.

34. Marcus, H.L., L.H. Hackett, Jr., and P.W. Palmberg, "Effect of Solute Elements on Temper Embrittlement of Low Alloy Steels," Ibid., pp. 90-103.

35. Joshi, A., "Segregation at Selective Grain Boundaries and its Role in Temper Embrittlement of Low Alloy Steels," Scripta Metallurgica, vol. 9, 1975, pp. 251-260.

36. Farrar, J.C.M. and R.E. Dolby, Lamellar Tearing in Welded Steel Fabrication, The Welding Institute, Cambridge, England, 1972.

37. Rittinger, J. and A. Fehervari, "The Influence of Microalloying Elements on the Toughness of Steels in Welded Structures," Macroalloying 75, Proceedings of the 1975 Microalloying Conference Oct. 1-3, 1975, Washington, DC, Union Carbide Corporation, 1977, pp. 593-598.

38. Oono, Y., S. Yano and Y. Okamura, "Improvement in Steel Properties by Sulphide Shape Control," Proceedings of the Welding Institute Conference on Trends in Steel and Consumables for Welding, Nov. 13-16, 1978, London, The Welding Institute, Cambridge, England, 1979, pp. 55-68.

39. Abson, J., R.E. Dolby and P.H.M. Hart, "The Role of Nonmetallic Inclusions in Ferrite Nucleation in Carbon Steel Weld Metals," Proceedings of the Welding Institute Conference and Trends in Steel and Consumables for Welding, Nov. 13-16, 1978, London, The Welding Institute, Cambridge, England, 1979, pp. 75-101.

40. Smith, J.E., A.P. Coldren and R.L. Cryderman, "Manganese-Molybdenum-Niobium Acicular Ferrite Steels with High Strength and Toughness," Toward Improved Ductility and Toughness, Climax Molybdenum Co., Conference in Kyoto, Japan, Oct. 25-26, 1971, pp. 119-142.

41. Titarenka, V.A. and A.A. Shalomeev, "Low Carbon Steel for Castings of Superior Quality," Russian Castings Production, no. 5, May 1975, pp. 206-207.

42. Aleksandrov, A.G., "The Effects of Calcium, Yttrium and Cerium on the Structure and Properties of Deposited Metal," Automatic Welding, vol. 30, no. 1, Jan. 1977, pp. 32-34.

43. Gray, T.G.F., J. Spence and R.H. North, Rational Welding Design, Butterworth and Co., London, England, 1975.

44. Hall, W.J., H. Khara, W. Soete and A.A. Wells, Brittle Fracture of Welded Plate, Prentice-Hall, Inc., Englewood Cliffs, NJ, 1967.

45. Kapadia, B.M. and E.J. Imhoff, Jr., "Fatigue-Crack Propagation in Electroslag Weldments," ASTM Special Technical Publication STP 631, ASTM, Philadelphia, PA, 1977, pp. 159-173.

46. Kapadia, B.M., "Influence of Residual Stresses on Fatigue Crack Propagation in Electroslag Welds," ASTM Special Technical Publication STP 648, ASTM, Philadelphia, PA, 1978, pp. 244-260.

47. Dohse, R., "Ermittlung von Eigenspannungen in Aluminothermisch Geschweissten Schienen (The Investigation of Residual Stresses in Alumino-thermally Welded Rails)," Schweissen and Schneiden, vol. 19, no. 10, Oct. 1967, pp. 471-476.

48. Krauss, G., "Residual Stresses in the Weld Area of Head-hardened Rail," Colorado School of Mines, Golden, CO, A Report Prepared for the Transportation Systems Center, U.S. Department of Transportation, Cambridge, MA, April 21, 1980.

49. Steel, R.K., "A Perspectival Review of Rail Behavior at the Facility for Accelerated Service Testing," Prepared for the 19th Annual Conference of Metallurgists, Halifax, Nova Scotia, 24-28, Aug. 1980.

50. Manual for Railway Engineering, American Railway Engineering Association, Ch. 4, 1975.

51. Private communication, Chemetron Railway Products, 111 E. Wacker Drive, Chicago, IL, 60601, 1980.

52 "Measurement of Residual Stresses by the Blind Hole Drilling Method," Technical Data Bulletin T-403, Photolastic, Inc., Malvern, PA, 1977.

53. Hertzberg, R.W., Deformation and Fracture Mechanics of Engineering Materials, John Wiley, New York, 1976, p. 334.

54. Park, Y.J. and I.M. Bernstein, "Mechanism of Cleavage Fracture in Fully Pearlitic 1080 Rail Steel," ASTM Special Technical Publication STP 644, ASTM, Philadelphia, PA, 1978, pp. 287-302.

55. Metals Handbook, 8th edition, vol. 9, American Society for Metals, Metals Park, OH, 1974.

56. Feddersen, C.E. and D. Broek, "Fatigue Crack Propagation in Rail Steels," ASTM Special Technical Publication STP 644, ASTM, Philadelphia, PA, 1978, pp. 414-429.

57. Smith, Y.E. and F.B. Fletcher, "Alloy Steels for High-Strength As-rolled Rails," Ibid., pp. 212-232.

58. Meyer, P.L., Introductory Probability and Statistical Applications, 2nd edition, Addison-Welsey, 1970, pp. 303-311.

59. Hertzberg, R.W., Ibid., p. 337.

60. Geiger, G.H. and D.R. Poirier, Transport Phenomena in Metallurgy, Addison-Wesley, Reading, MA, 1973, pp. 319-321.

61. Schneider, P.J., Conduction Heat Transfer, Addison-Wesley, Reading, MA, 1955, p. 266.

62. Hertzberg, R.W., Ibid., pp. 425-426.

63. Sato, T., "The Effect of Microstructure on the Fatigue and Impact Properties of Welded Zone in High Carbon Steels," Transactions of the Iron and Steel Institute of Japan, vol. 21, no. 4, 1981, pp. 260-269.

APPENDIX - THERMITE WELDING (FIELD WELDING) - TMP 4-021

1. This procedure covers the preparation and process of field welding.

2. (a) Thermite welding is defined as a mixture of finely divided aluminum with an oxide of iron or other metal.

   (b) A proper mixture of aluminum and iron oxide provides sufficient heat to weld steel.

   (c) Welding with heat produced by the reaction of aluminum with a metal oxide, when ignited, the reaction with the thermite mixture develops a temperature approaching 5000°F and produces a filler metal of about 3500°F when introduced into a gap between rail, welds or fuses the ends together.

3. Quick heat welding procedure:

   (i) Oxygen pressure must be set at 71 PSI.

   (ii) Propane pressure must be set at 21 PSI.

   (iii) Weld gap size must be 61/64 inch $\pm$ 1/16 inch.

   (iv) Crucible height must be set 2-1/2 to 3 inches above top of rail.

   (v) Self tapping thimble must fit snugly in throat of crucible liner.

   (vi) Torch height from top of rail shall be 1-1/8 inches to 1-1/4 inches.

4. (a) The rail ends shall be saw cut prior to welding except when approved by the FAST Operations Test Manager whereby the rail ends may be cut with a torch (propane and oxygen).

(b) A torch cut must be slag free and made not more than 60 minutes prior to welding.

(c) An acetylene torch must not be used.

5. (a) In preparation for welding, the rail ends must be crowned 1/32 inch in 18 inches.

(b) Gage rods (rail alignment tools) shall be used as required to achieve perfect longitudinal alignment of the rail ends.

6. Preparation of the crucible:

(i) Crucible liner shall be placed firmly into crucible shell.

(ii) Crucible shall be heated not less than 15 minutes to thoroughly dry.

(iii) The universal clamping device must be properly placed on the rail.

(iv) The mould shoes must be properly applied to the rail ends.

(v) The crucible must be lined accurately with the center of mould shoes for perfect pour.

(vi) The mould shoes must be firmly packed ensuring there is no foreign material in the compound.

(vii) The self-tapping thimble is placed in the crucible liner and the thermite portion is poured directly over the thimble leaving a small mound at top for the igniter.

(viii) Prior to pre-heating, the slag pans must be applied to the mould shoes.

(ix) The pre-heat will take about 2 minutes, a 2 minute count down will begin when the desired flame height is reached which will be approximately 14 to 15 inches above the top of the mould shoes.

(x) Upon completion of the 2 minute pre-heat, the torch is removed from the universal clamp and slag plug placed in center of mould shoes. The crucible is then swung over the center of the mould shoes and ignited.

7. When pour has been made, remove crucible from universal clamp and set in dry place.

8. (a) Approximately 2 to 3 minutes thereafter, the upset metal shall be removed by means of chiseling.

(b) Rail must be finished in manner as specified by the FAST Operations Test Manager.

(c) The large steel risers which are on both sides of the weld starting from the base risers must not be removed until they are cooled.

(d) They shall be removed by knocking risers towards center of rail after it has cooled.

9. Should the upset metal on top of rail be torch cut, caution must be taken not to cut into sand.

10. When making a field weld, a rail puller/expander shall be used when the rail temperature varies more than $5^{o}F$ in an hour.

11. All rail anchors 200 feet each side of the weld must be properly positioned before starting the welding procedure.

12. Line, surface and gage in the field weld area must be accurately maintained.

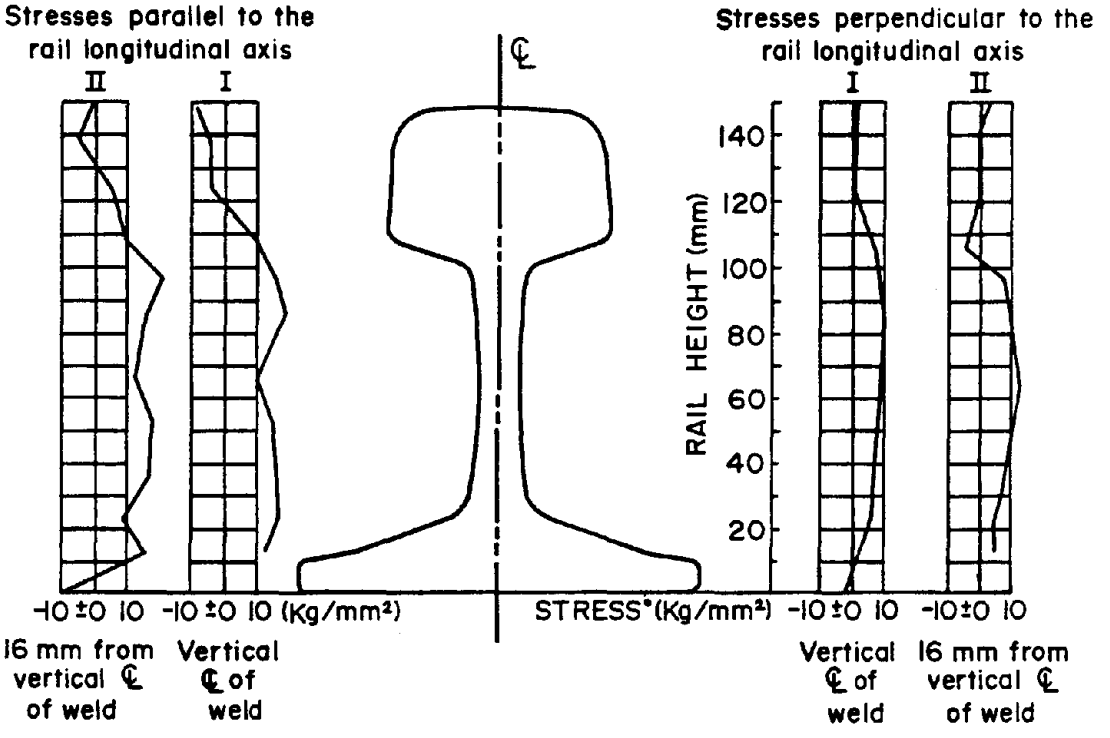

FIGURE 1: RESIDUAL STRESSES IN A NONREINFORCED THERMITE RAIL-WELD; WELD GAP - 24 mm, 50 kg/m RAIL. FROM DOHSE (47).

Preceding page blank

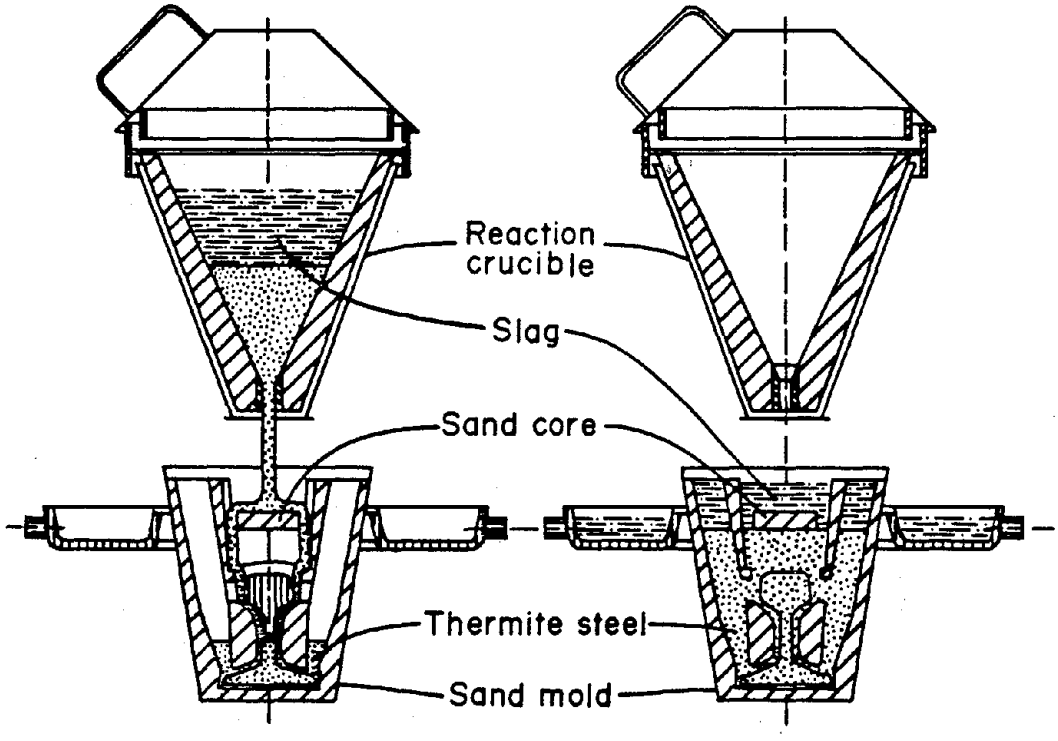

FIGURE 2: MOLD CONFIGURATION AND FLOW PATTERN OF THE MOLTEN STEEL FOR THE THERMITE RAIL-WELDS.

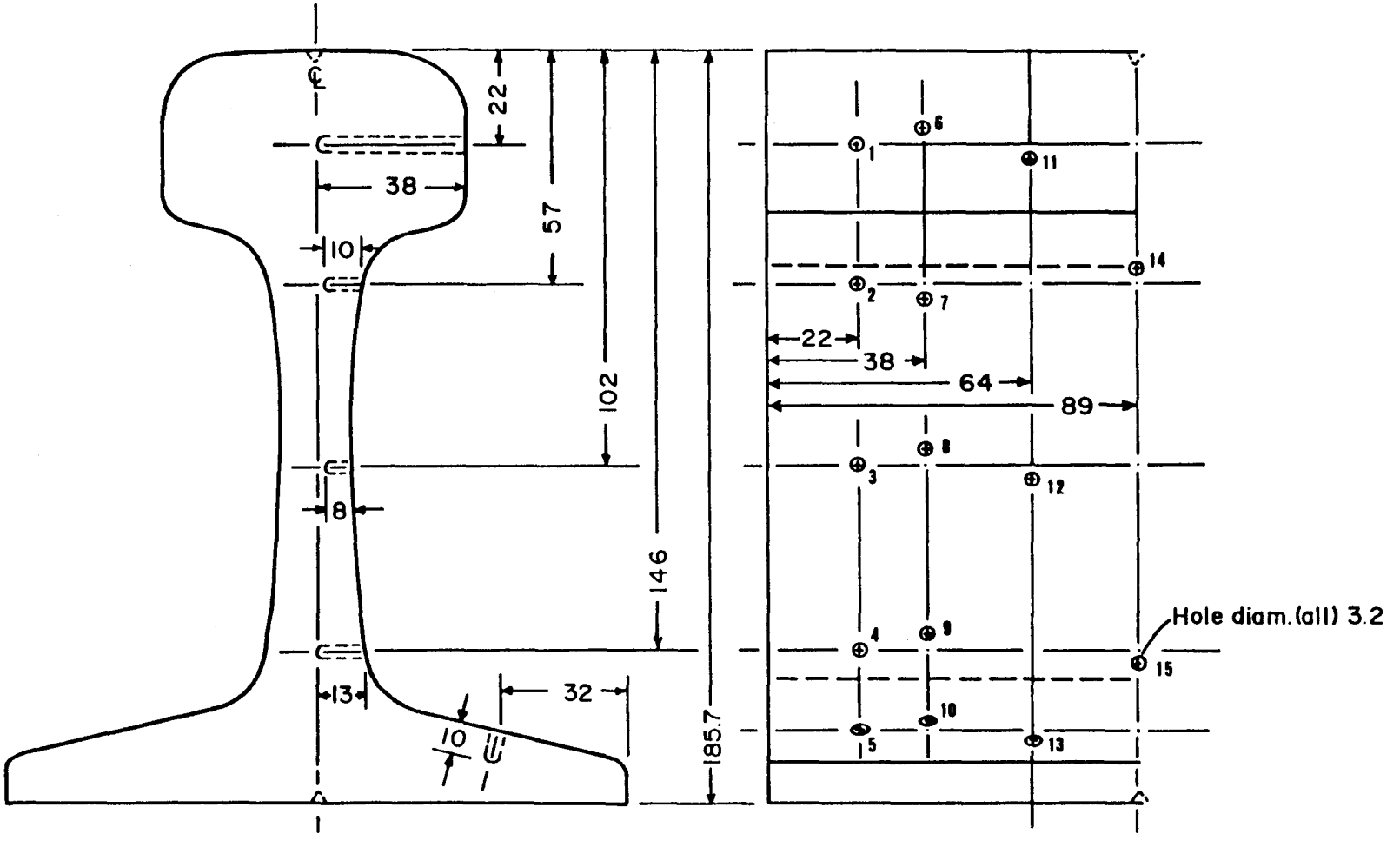

FIGURE 3: THERMOCOUPLE LOCATIONS FOR WELDS 1, 2 and 4. FOR WELD 3, ALL THERMOCOUPLES WERE 3 mm CLOSER TO THE RAIL END. NUMBERS IDENTIFY THE THERMOCOUPLES AND THE DIMENSIONS ARE IN mm. THE RAIL IS 68 kg/m (136 lb/yd RE).

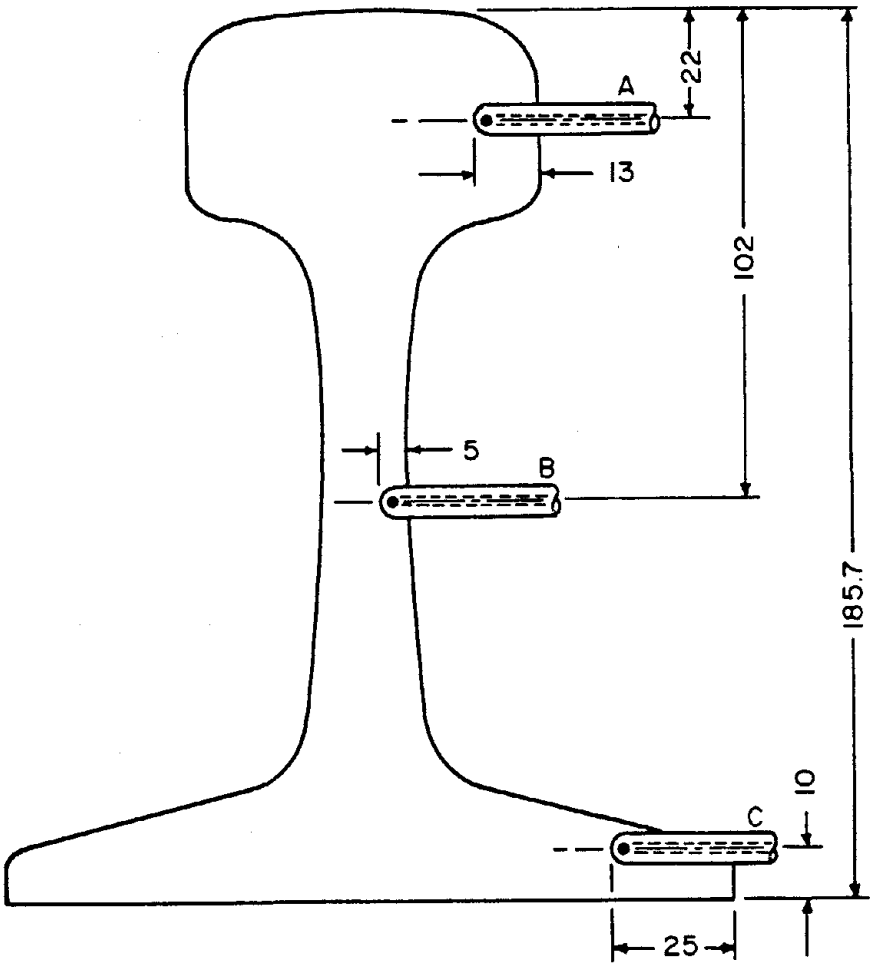

FIGURE 4: LOCATIONS OF THERMOCOUPLES IN THE WELD METAL OF WELD 9. THERMOCOUPLES WERE CENTERED LONGITUDINALLY IN THE 24 mm GAP. A-HEAD, B-WEB, C-BASE. DIMENSIONS IN mm.

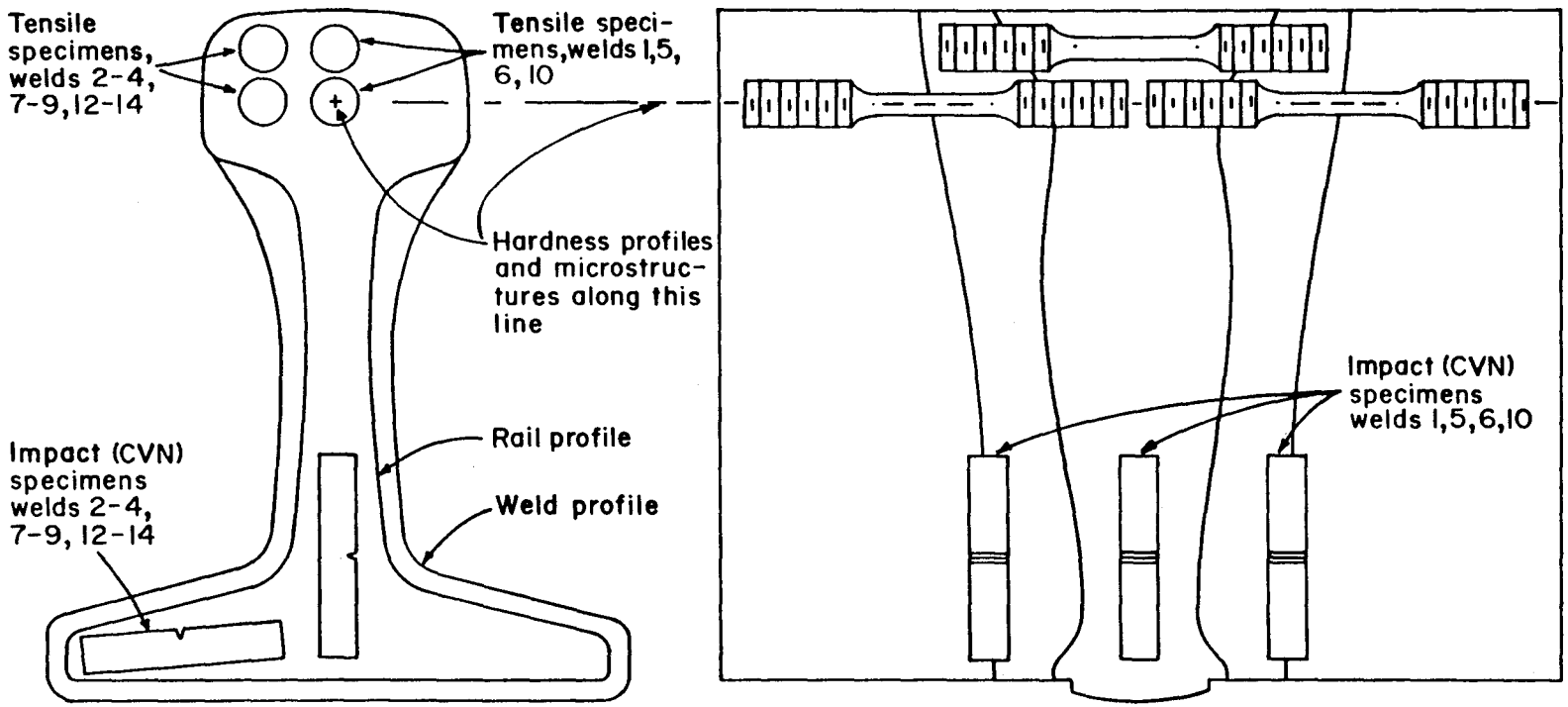

FIGURE 5: LOCATIONS OF TENSILE AND IMPACT SPECIMENS, HARDNESS PROFILES AND MICROSTRUCTURE SPECIMENS IN WELDS. FUSION ZONES AND OUTER EDGES OF THE HAZs ARE INDICATED.

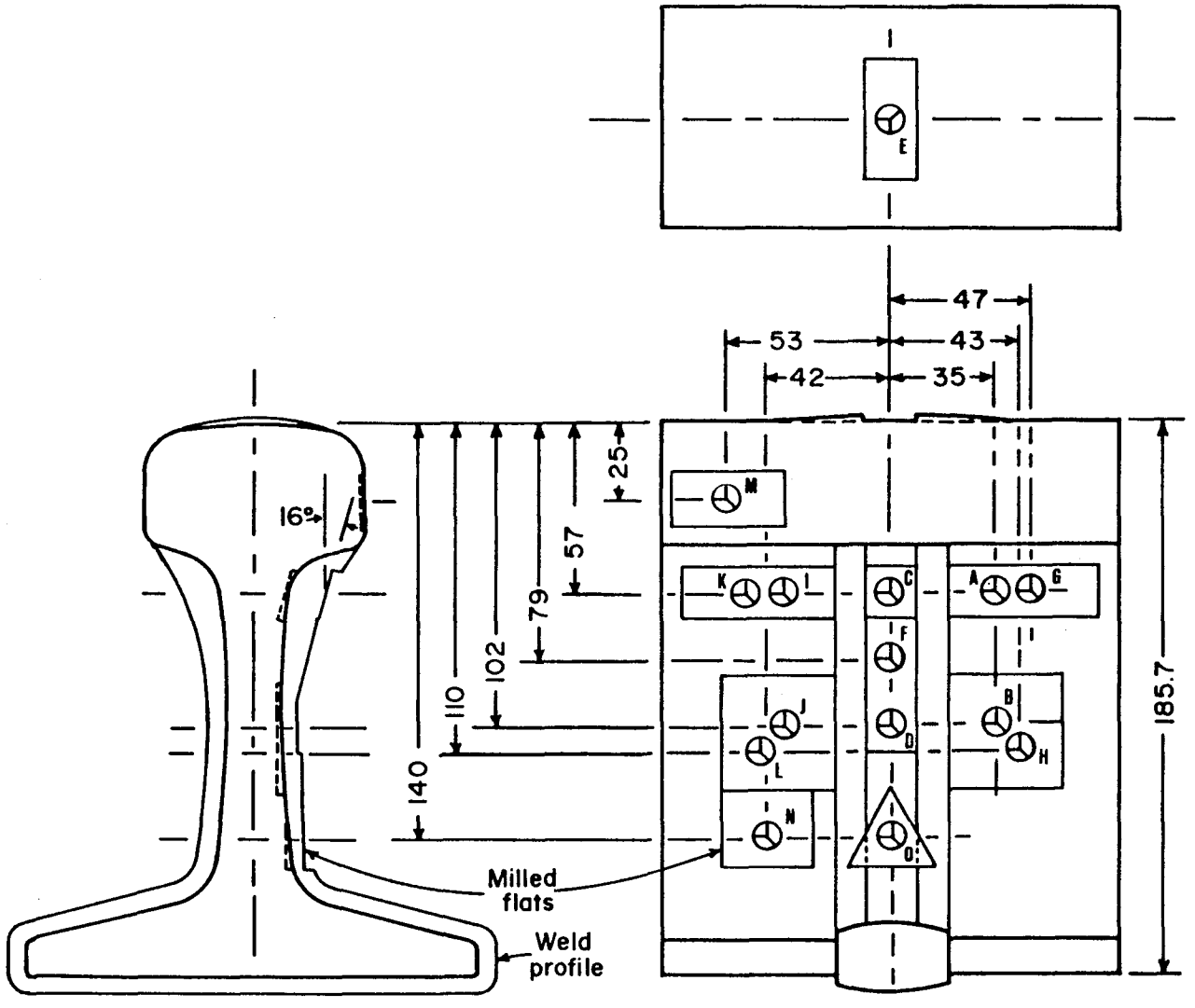

FIGURE 6: LOCATIONS OF STRAIN GAGE ROSETTES FOR RESIDUAL STRESS MEASUREMENTS. LETTERS IDENTIFY LOCATIONS AND THE DIMENSIONS ARE IN mm.

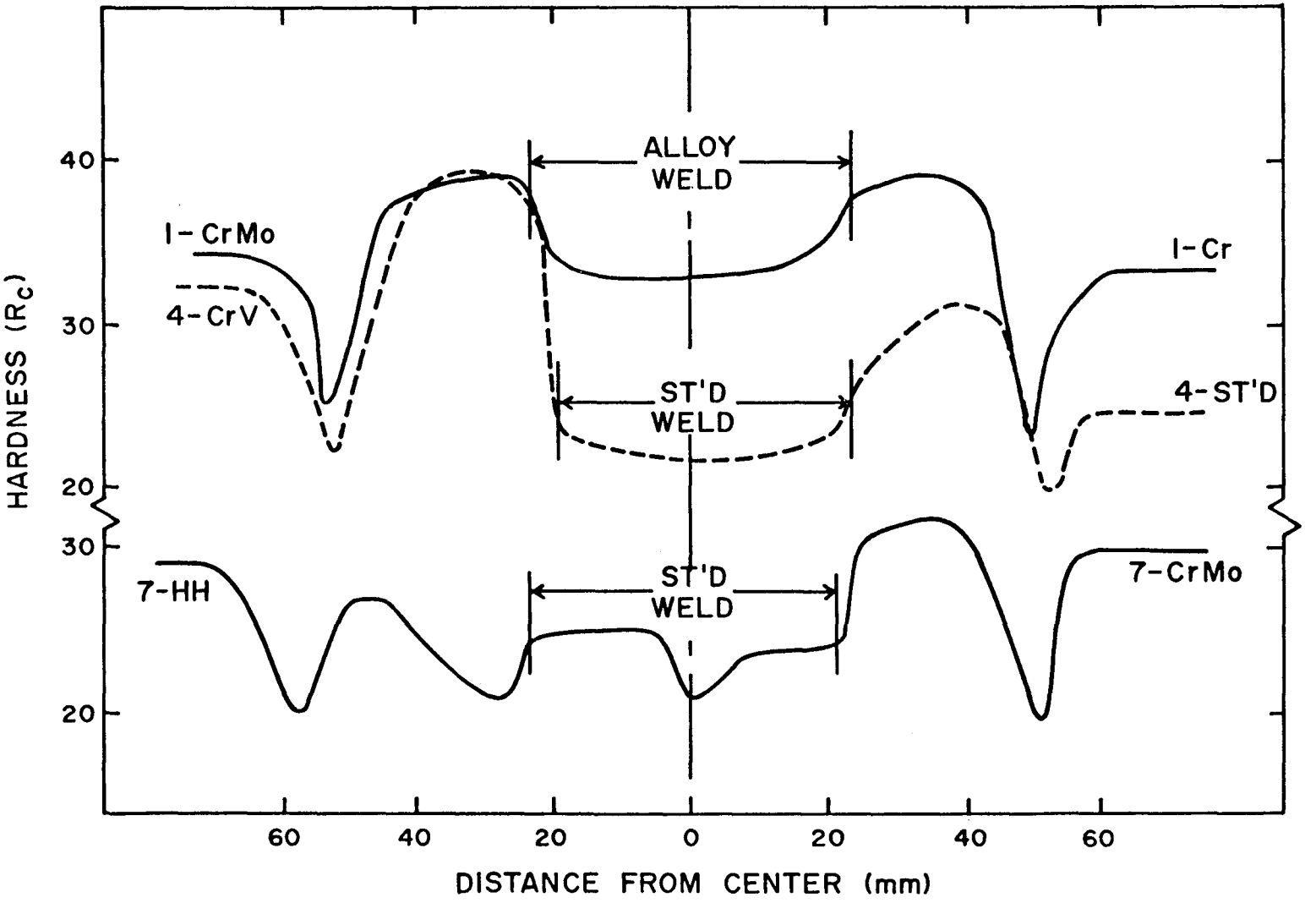

FIGURE 7: HARDNESS PROFILES OF WELDS 1, 4 AND 7.

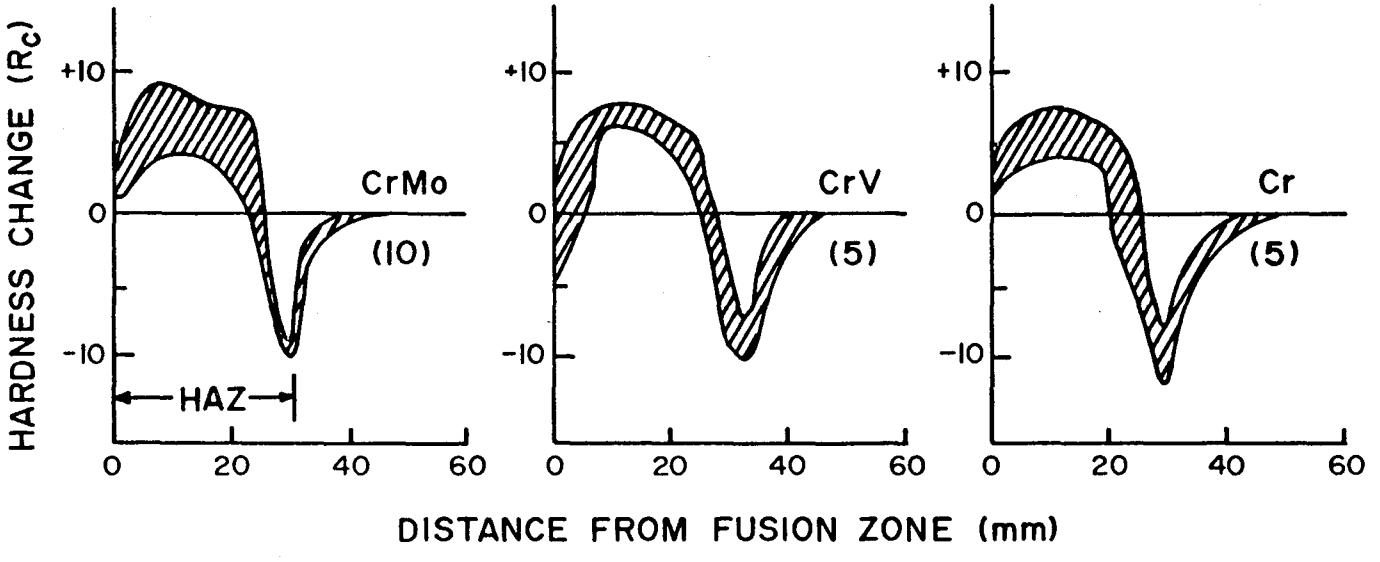

FIGURE 8: HARDNESS VARIATIONS IN THE HAZs OF ALLOY RAILS RELATIVE TO THE HARDNESS OF PARENT RAIL. NUMBERS IN PARENTHESES ARE THE NUMBERS OF RESPECTIVE RAILS.

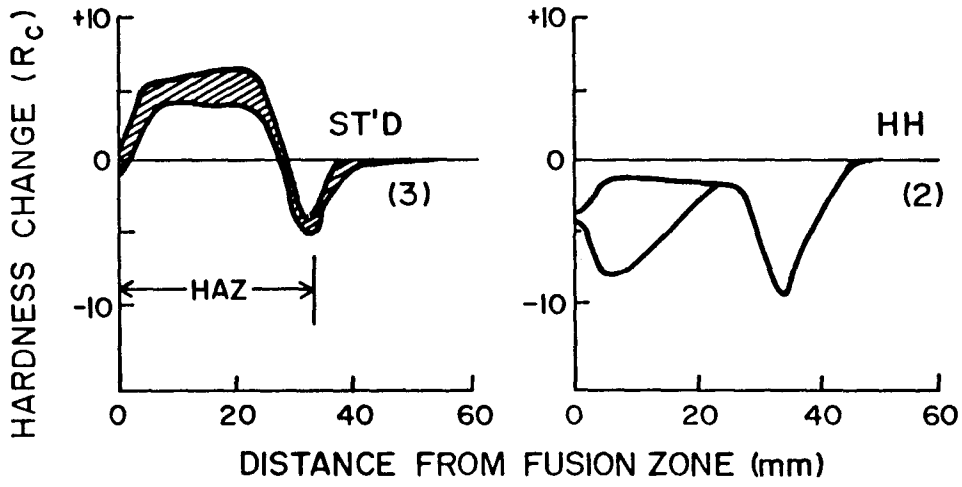

FIGURE 9: HARDNESS VARIATIONS IN THE HAZs OF STANDARD AND OF HEAD-HARDENED RAIL RELATIVE TO THE HARDNESS OF PARENT RAIL. NUMBERS IN PARENTHESES ARE THE NUMBERS OF RESPECTIVE RAILS.

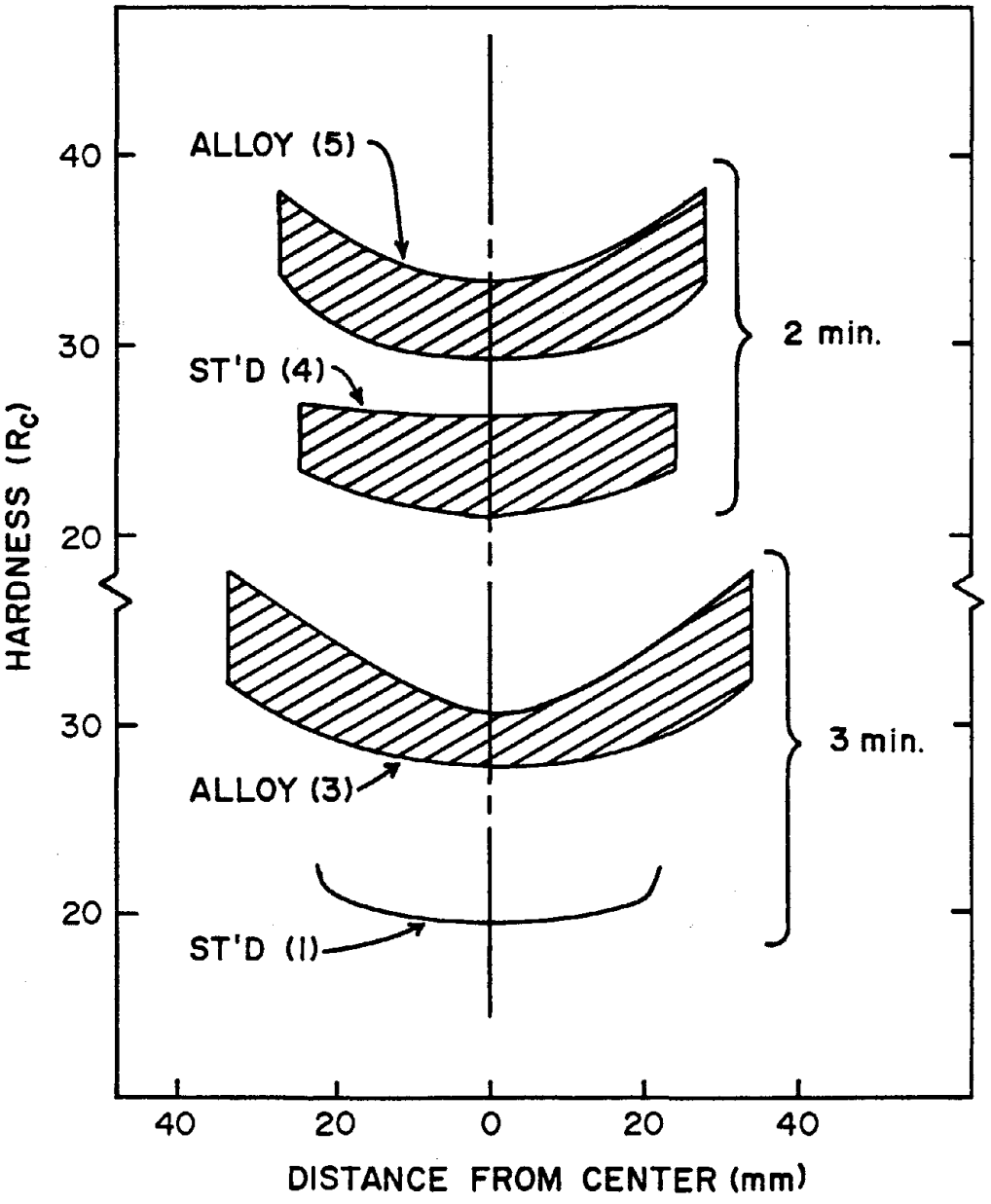

FIGURE 10: HARDNESS OF THE WELD METAL AS A FUNCTION OF PREHEAT TIME AND DISTANCE FROM THE WELD CENTERLINE.

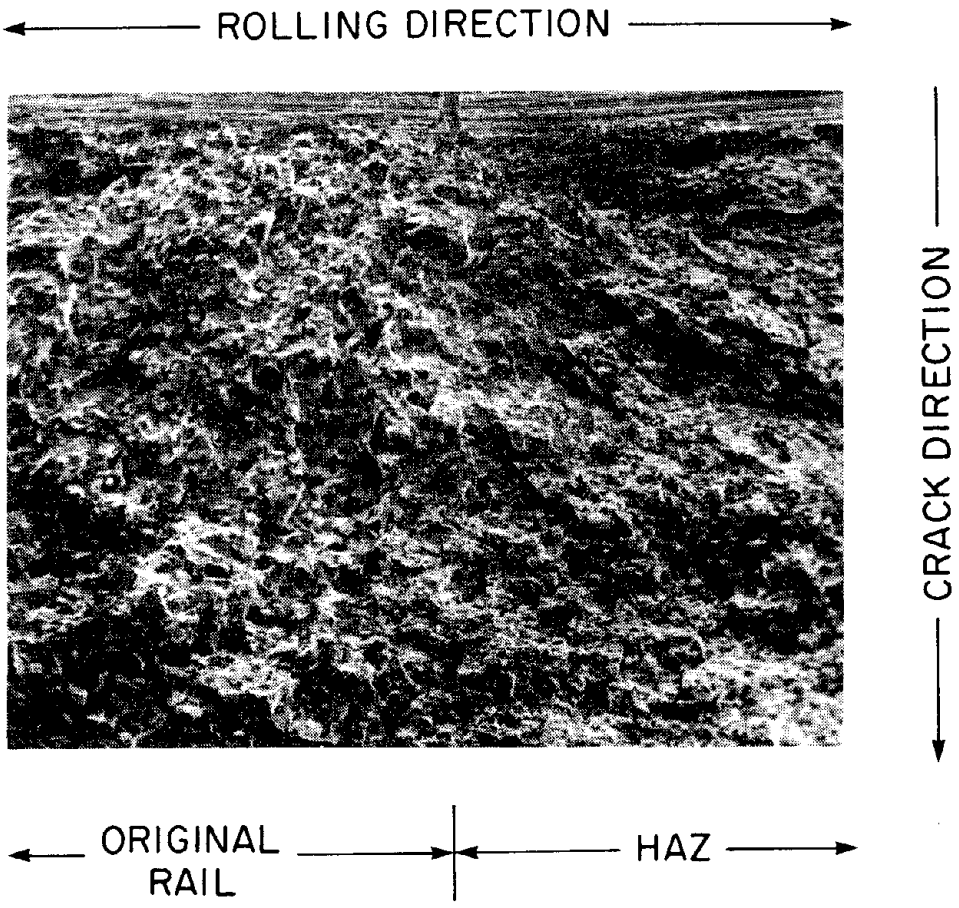

FIGURE 11: FRACTURE OF IMPACT SPECIMEN THROUGH THE REGION OF MINIMUM HARDNESS IN THE HEAT-AFFECTED ZONE. FRACTOGRAPH IS FROM THE CrMo SIDE OF WELD 1. 17X.

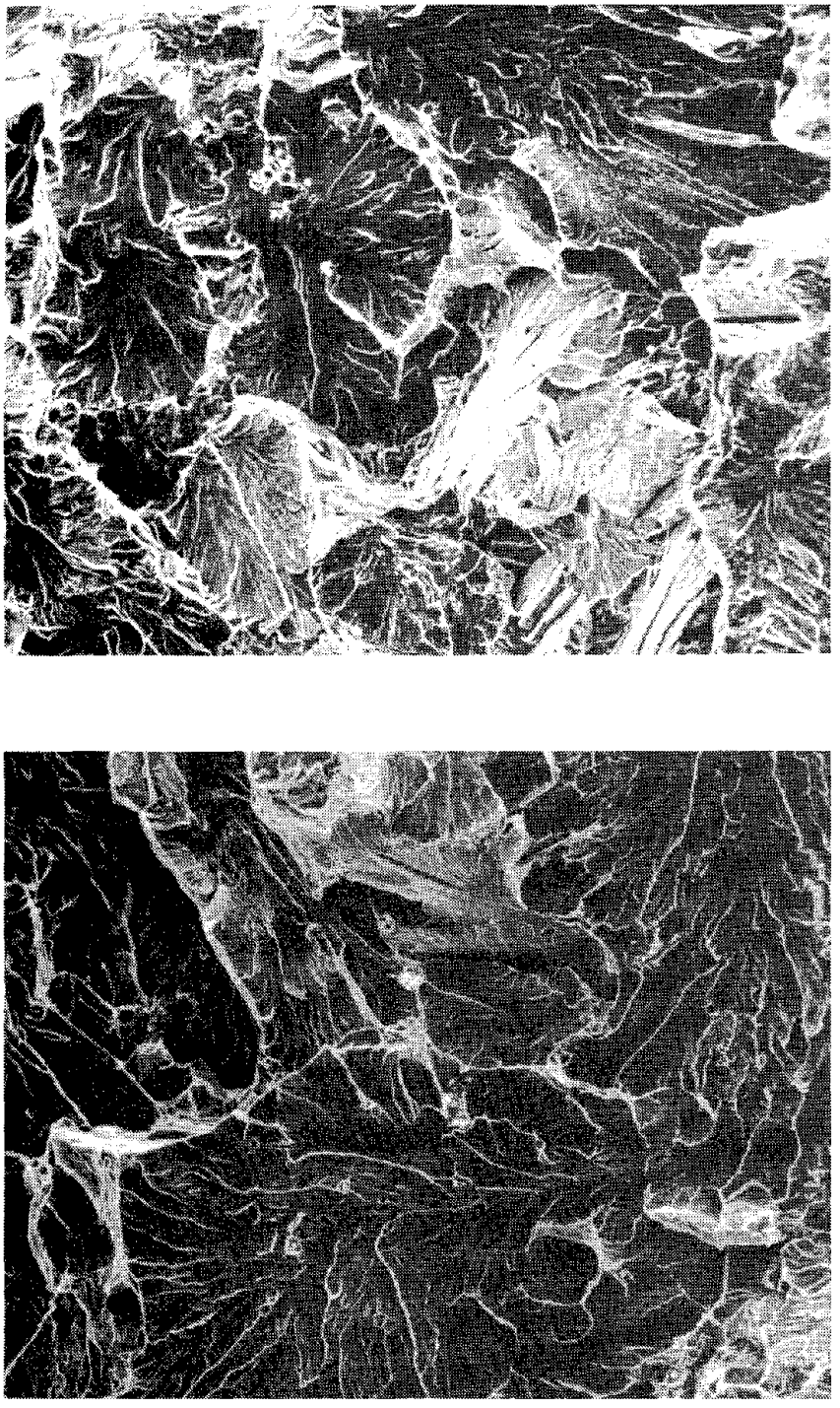

FIGURE 12: FRACTURE SURFACE OF FIGURE 11; (a) ORIGINAL RAIL SIDE; (b) HAZ SIDE. 280X.

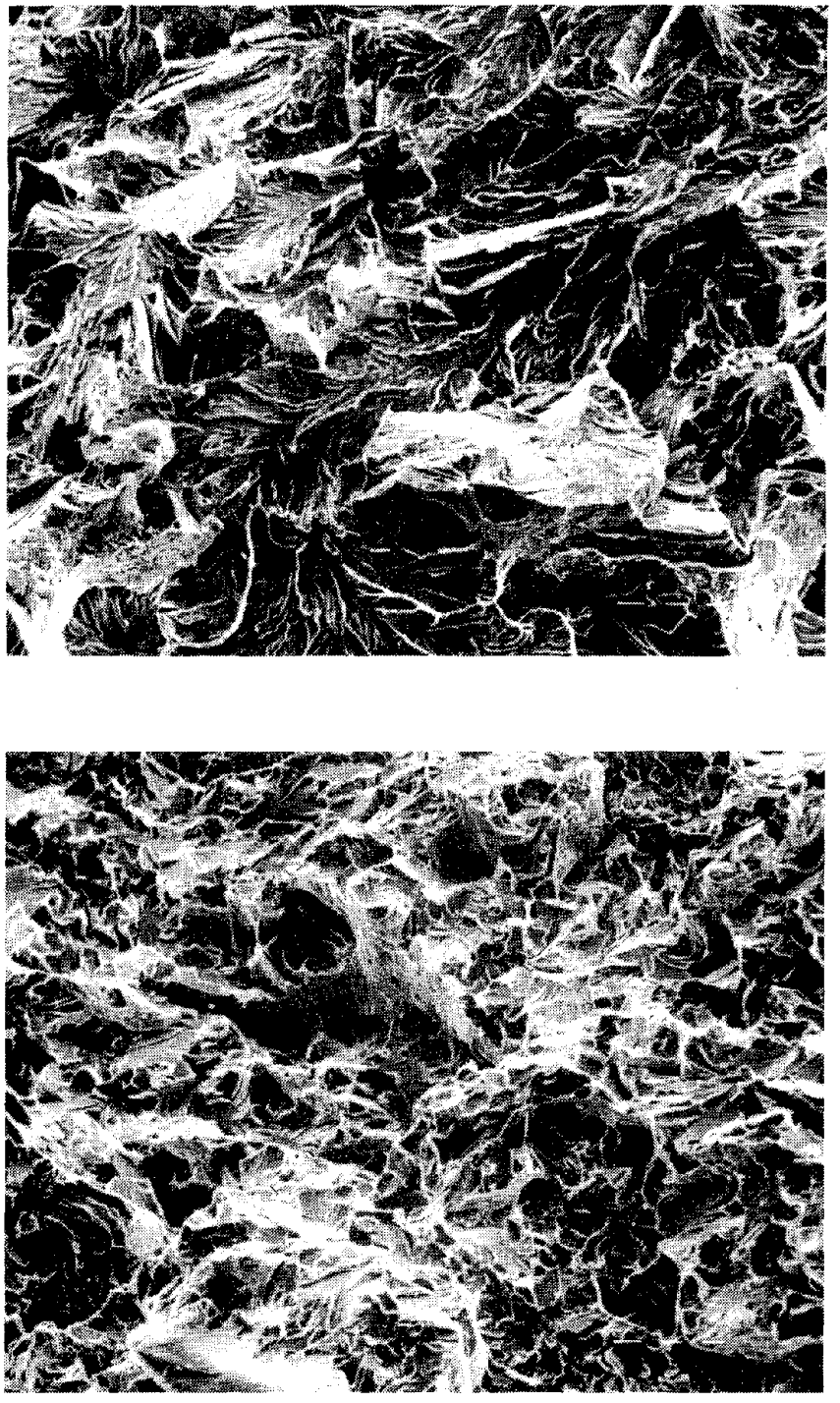

FIGURE 13: FRACTURE OF IMPACT SPECIMEN THROUGH THE REGION OF MINIMUM HARDNESS IN THE HAZ OF THE HEAD-HARDENED RAIL OF WELD 8. (a) ORIGINAL RAIL SIDE; (b) HAZ SIDE. 280X.

FIGURE 14: REGION OF EASY SEPARATION OF THE HAZ SIDE OF THE IMPACT SPECIMEN FROM THE CrV RAIL OF WELD 4. BOTTOM OF THE PHOTOMICROGRAPH IS THE SIDE OPPOSITE THE V-NOTCH. 52X.

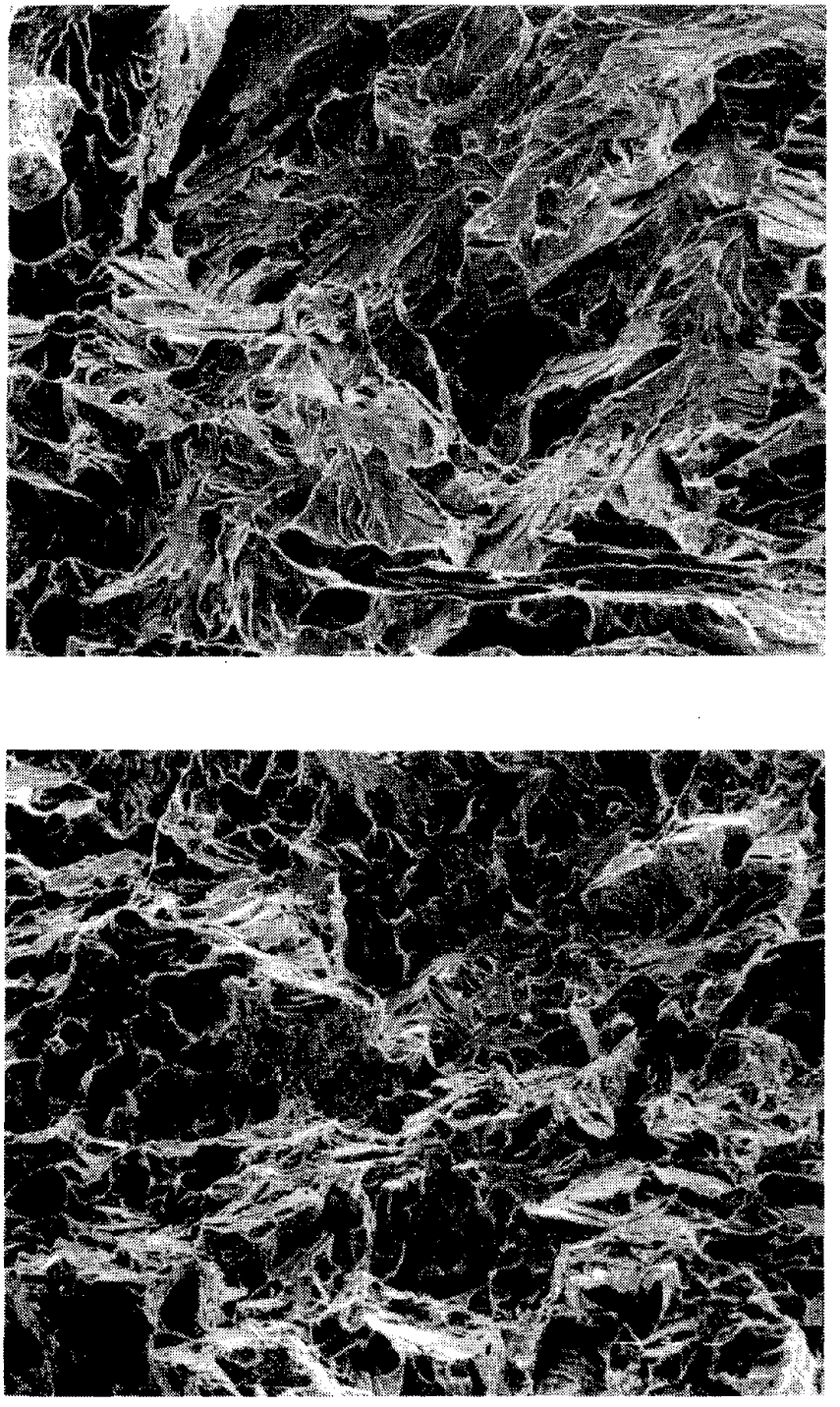

FIGURE 15: FRACTURES OF IMPACT SPECIMENS FROM THE WELD METAL. (a) WELD 1; ALLOY WELD METAL, (b) WELD 8; STANDARD WELD METAL. 280X.

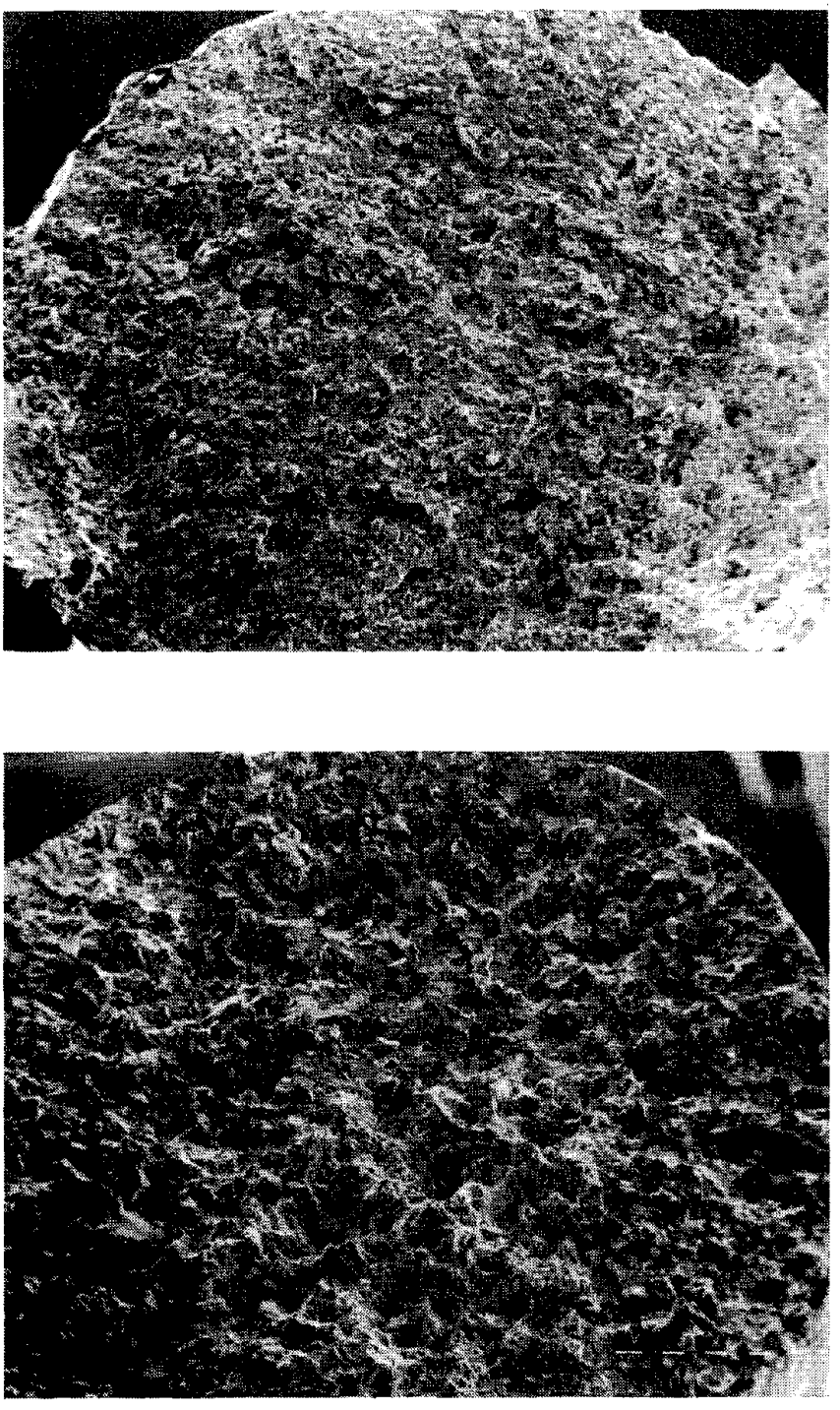

FIGURE 16: LOW DUCTILITY FRACTURES OF TENSILE SPECIMENS IN THE REGION OF MINIMUM HARDNESS. (a) FROM WELD 1 IN THE Cr RAIL, (b) FROM WELD 4 IN THE STANDARD RAIL. 24X.

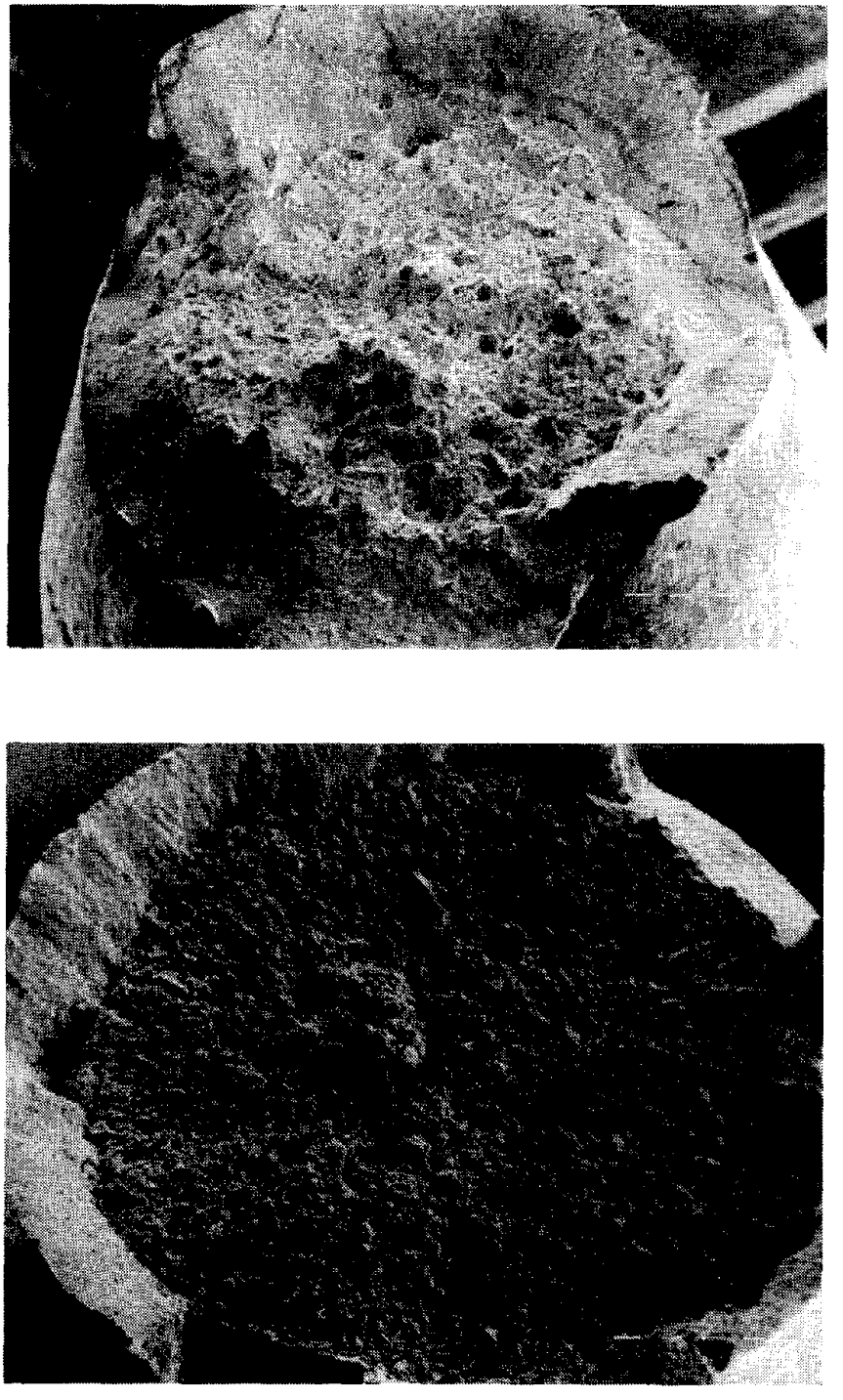

FIGURE 17: "CUP AND CONE" FRACTURES OF TENSILE SPECIMENS IN THE REGION OF MINIMUM HARDNESS. (a) FROM WELD 1 IN THE CrMo RAIL, 23X; (b) FROM WELD 8 IN THE HEAD-HARDENED RAIL, 28X.

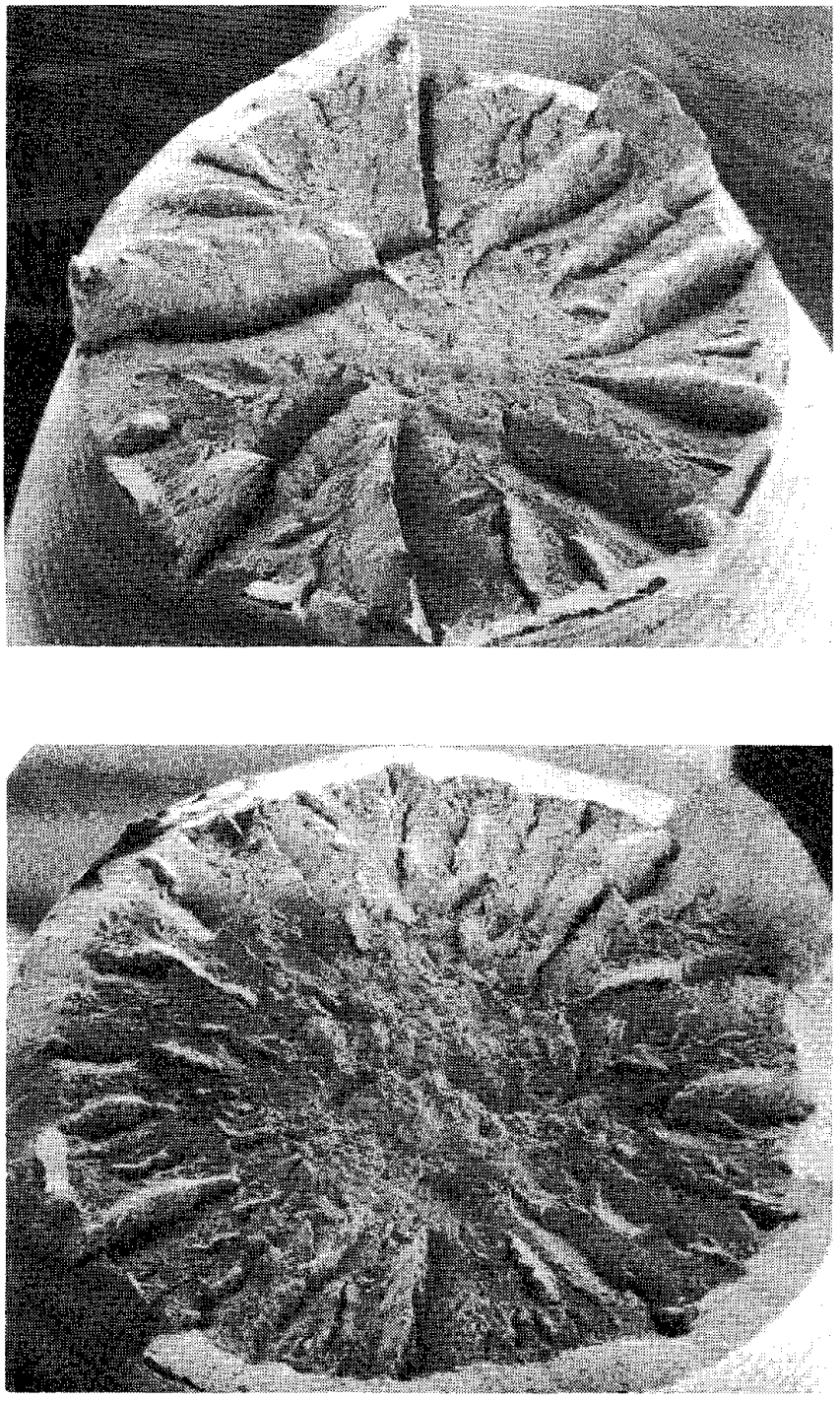

FIGURE 18: "CUP AND CONE" FRACTURES WITH RADIAL FEATURES FROM TENSILE SPECIMENS IN THE REGION OF MINUMUM HARDNESS. (a) FROM WELD 4 IN THE CrV RAIL, 25X; (b) FROM WELD 8 IN THE CrMo RAIL, 29X.

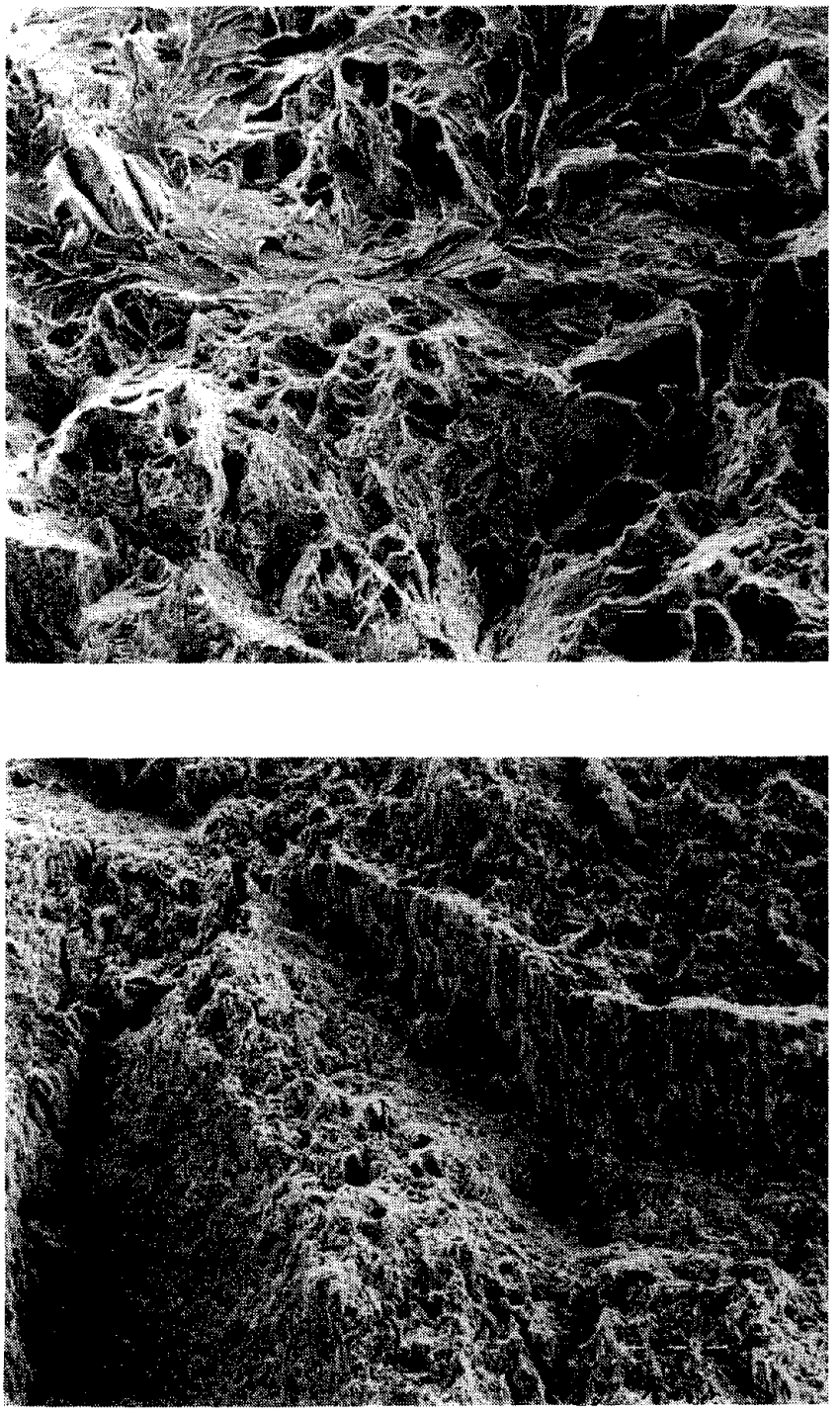

FIGURE 19: TENSILE FRACTURES OF THE HAZ IN THE REGION OF MINIMUM HARDNESS. (a) FROM WELD 4 IN THE STANDARD RAIL, 240X; (b) FROM WELD 4 IN THE CrV rail, 250X.

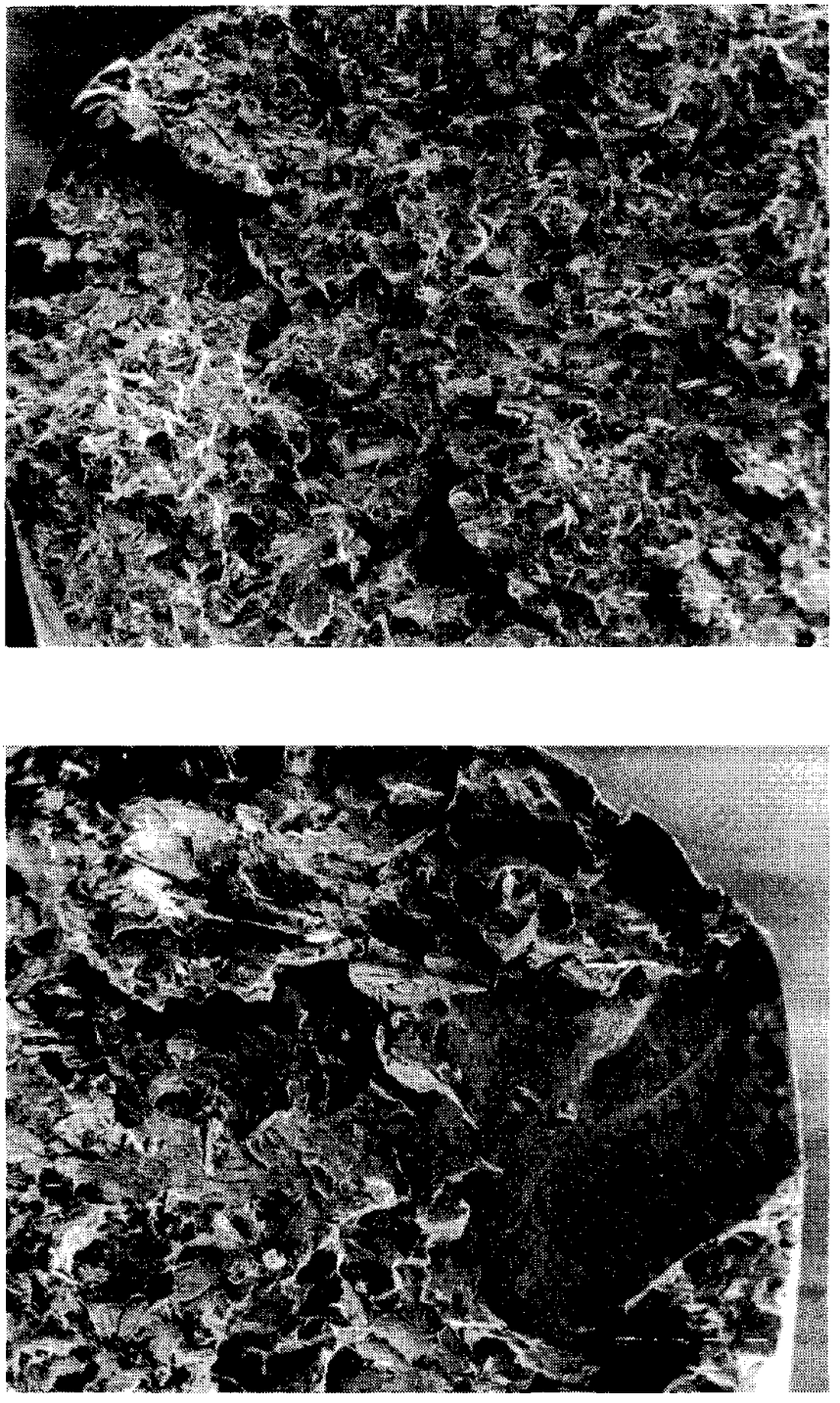

FIGURE 20: FRACTURES OF TENSILE SPECIMENS FROM THE WELD METAL. (a) WELD 3, ALLOY WELD METAL; (b) WELD 4, STANDARD WELD METAL. 25X.

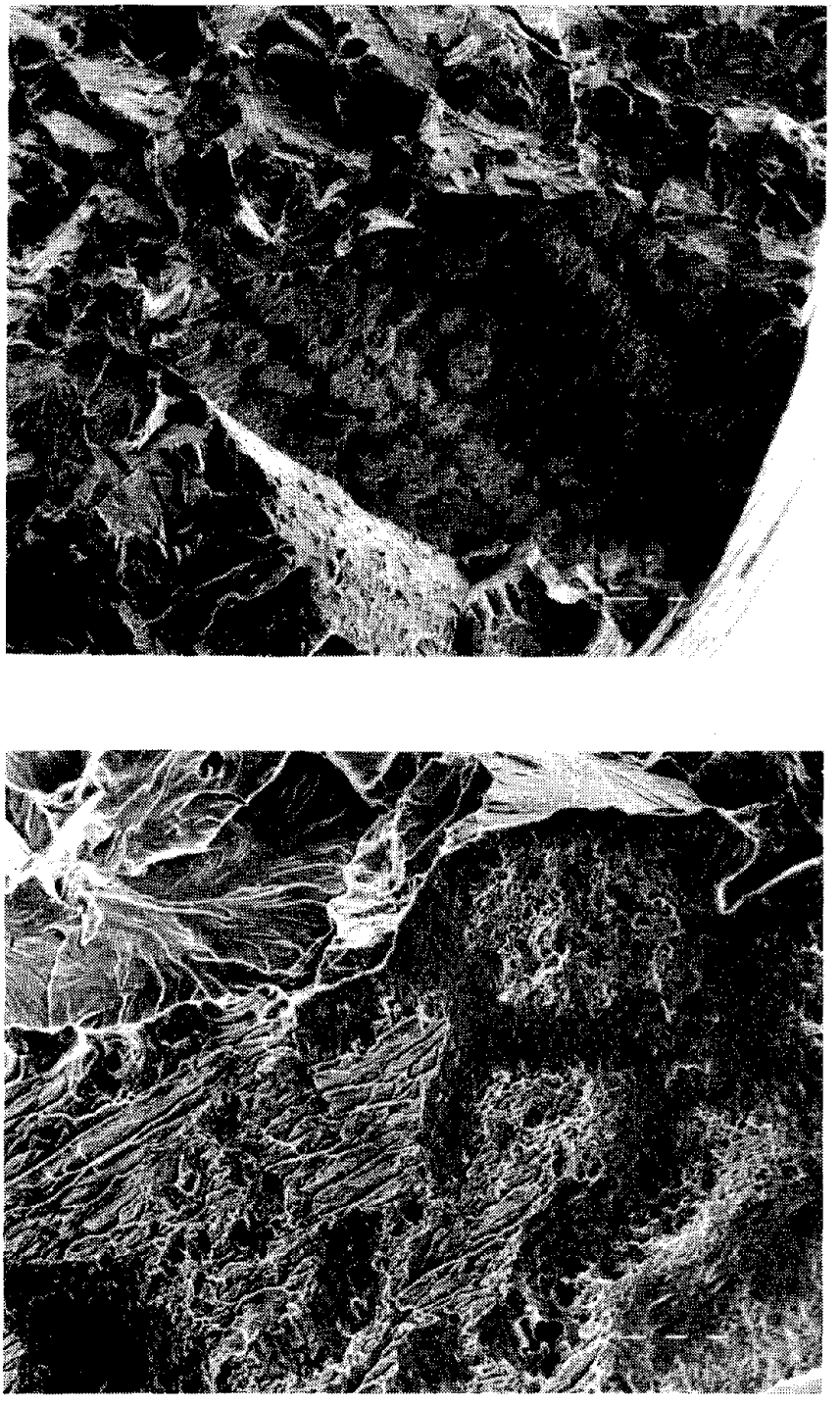

FIGURE 21: FRACTURE OF THE TENSILE SPECIMEN FROM THE STANDARD WELD METAL OF WELD 6. (a) 50X, (b) 270X.

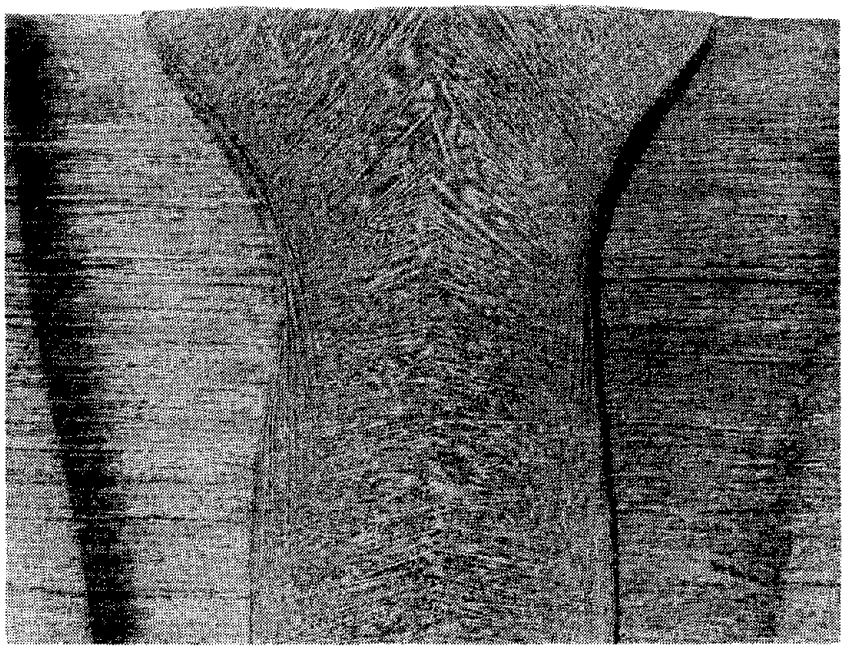

FIGURE 22: MACROSTRUCTURE OF THE HEAD AREA OF WELD 6. 1X.

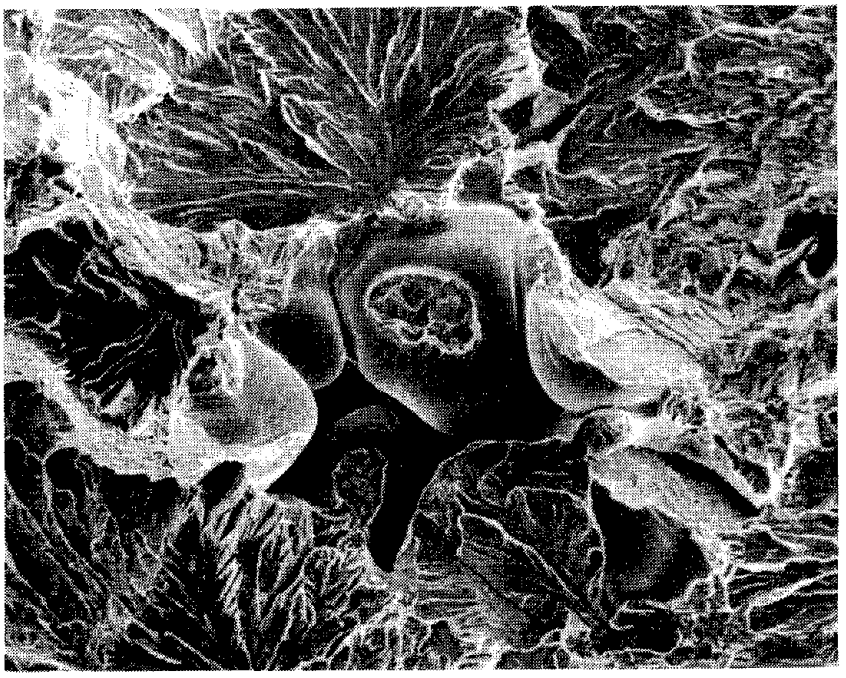

FIGURE 23: TENSILE FRACTURE OF THE ALLOY WELD METAL OF WELD 10 SHOWING MICROPOROSITY. 290X.

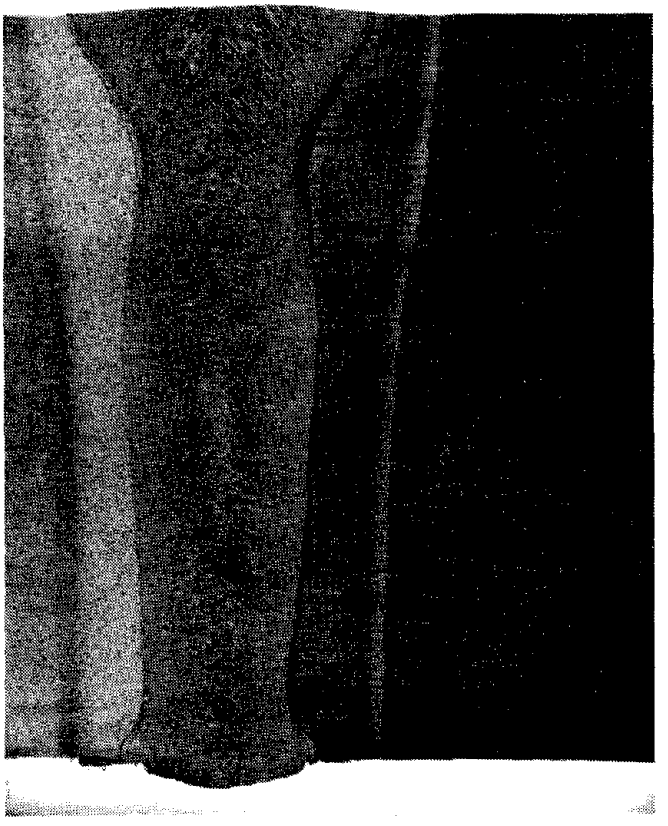

FIGURE 24: MACROSTRUCTURE OF WELD 2, ALLOY WELD METAL. NOTE THE THERMOCOUPLE LOCATIONS. APPROXIMATELY ONE-HALF SIZE.

FIGURE 25: MACROSTRUCTURE OF WELD 10 SHOWING THE EFFECT OF A LONG PREHEAT. APPROXIMATELY ONE-HALF SIZE.

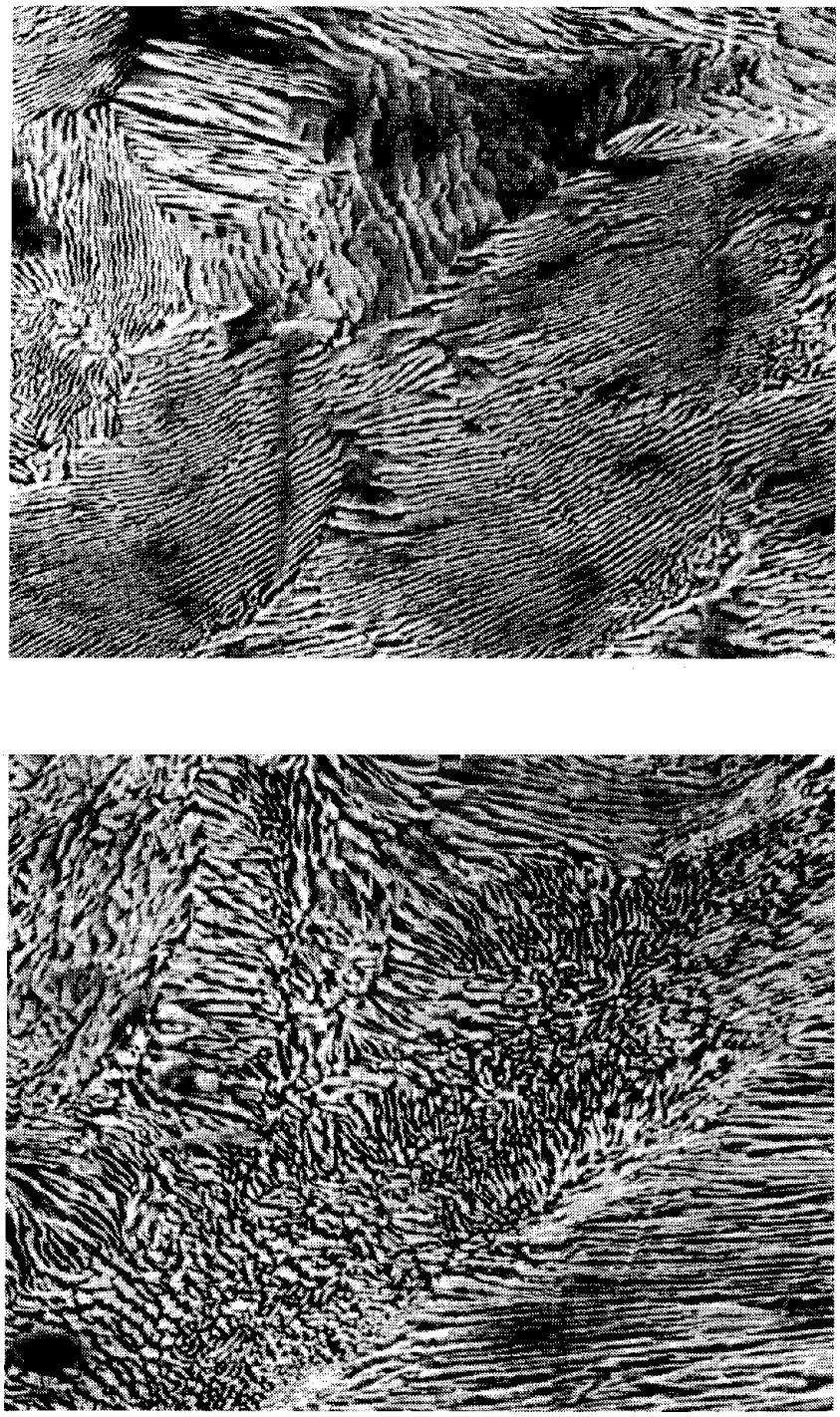

FIGURE 26: PEARLITE (a) AND PEARLITE AND BAINITE (b) IN WELD METAL OF WELD 14. 4500X.

FIGURE 27: VERY FINE PEARLITE IN THE HAZ OF THE Cr RAIL OF WELD 1. 4500X.

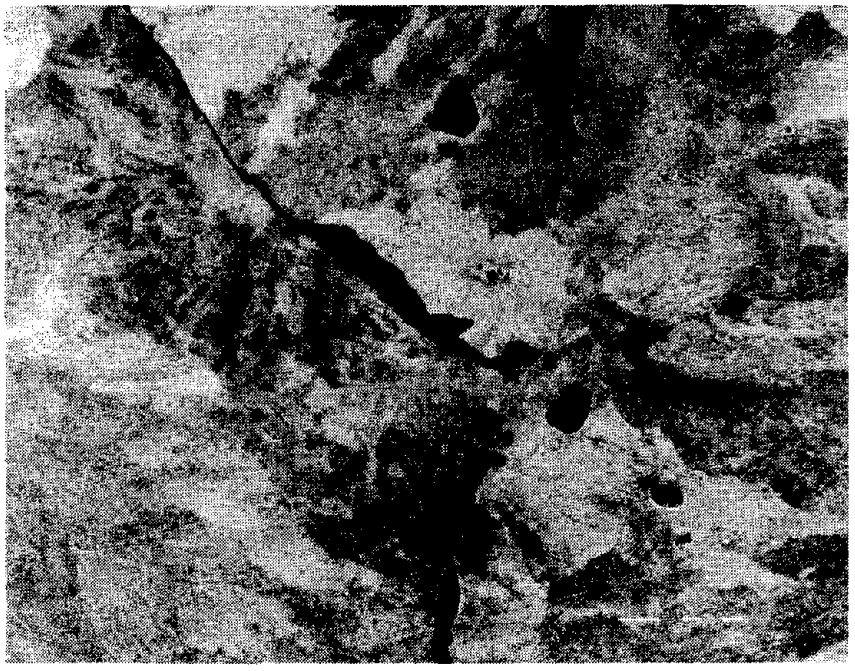

FIGURE 28: PROEUTECTOID FERRITE IN THE WELD METAL OF WELD 6. 450X.

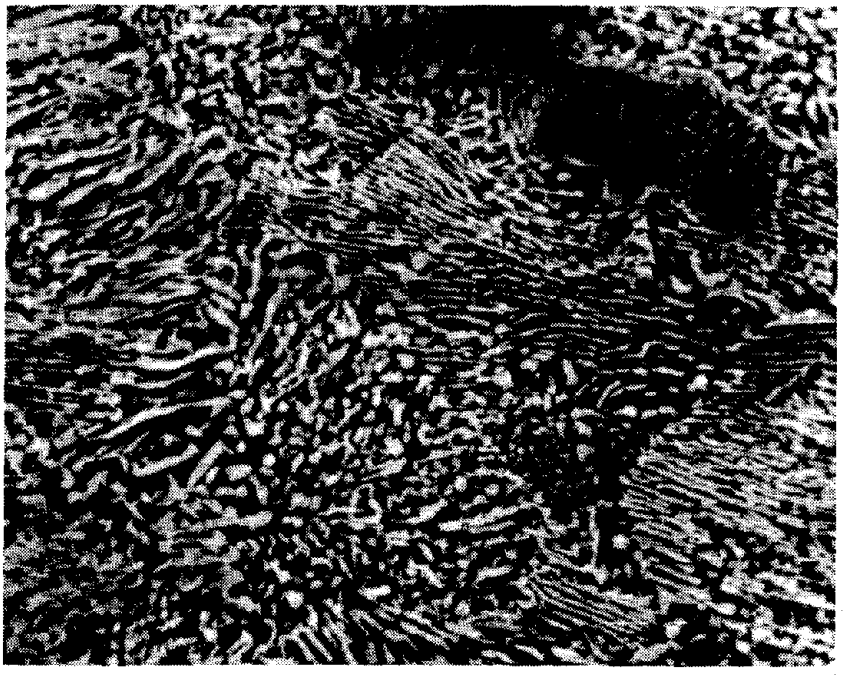

FIGURE 29: SPHEROIDITE AND DEGENERATIVE PEARLITE IN THE OUTER EDGE OF THE HAZ OF THE HH RAIL OF WELD 7. 4500X.

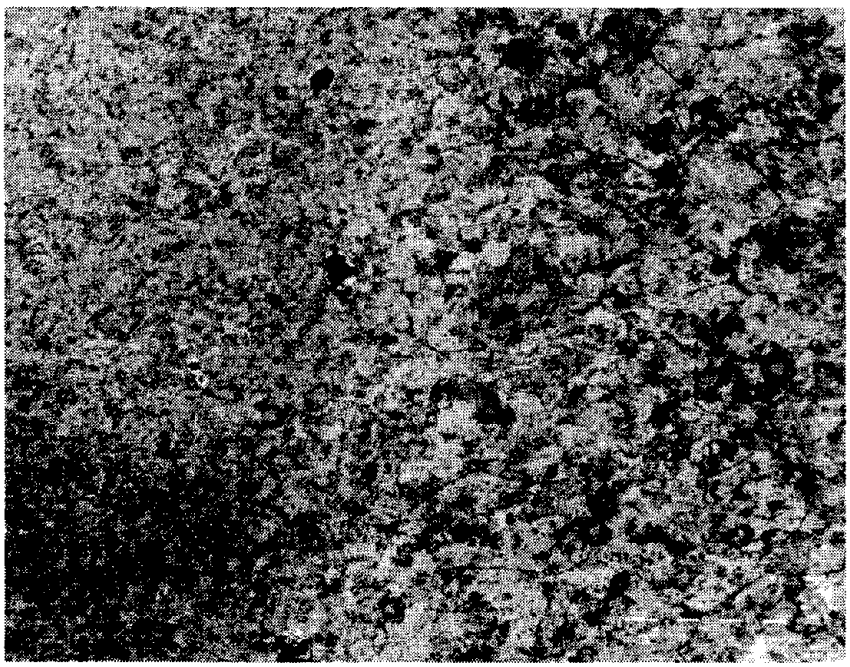

FIGURE 30: ALUMINA (WITH SILICA) INCLUSIONS IN THE CrV FUSION ZONE OF WELD 6. THE WELD METAL IS TO THE RIGHT OF THE INCLUSIONS. 32X.

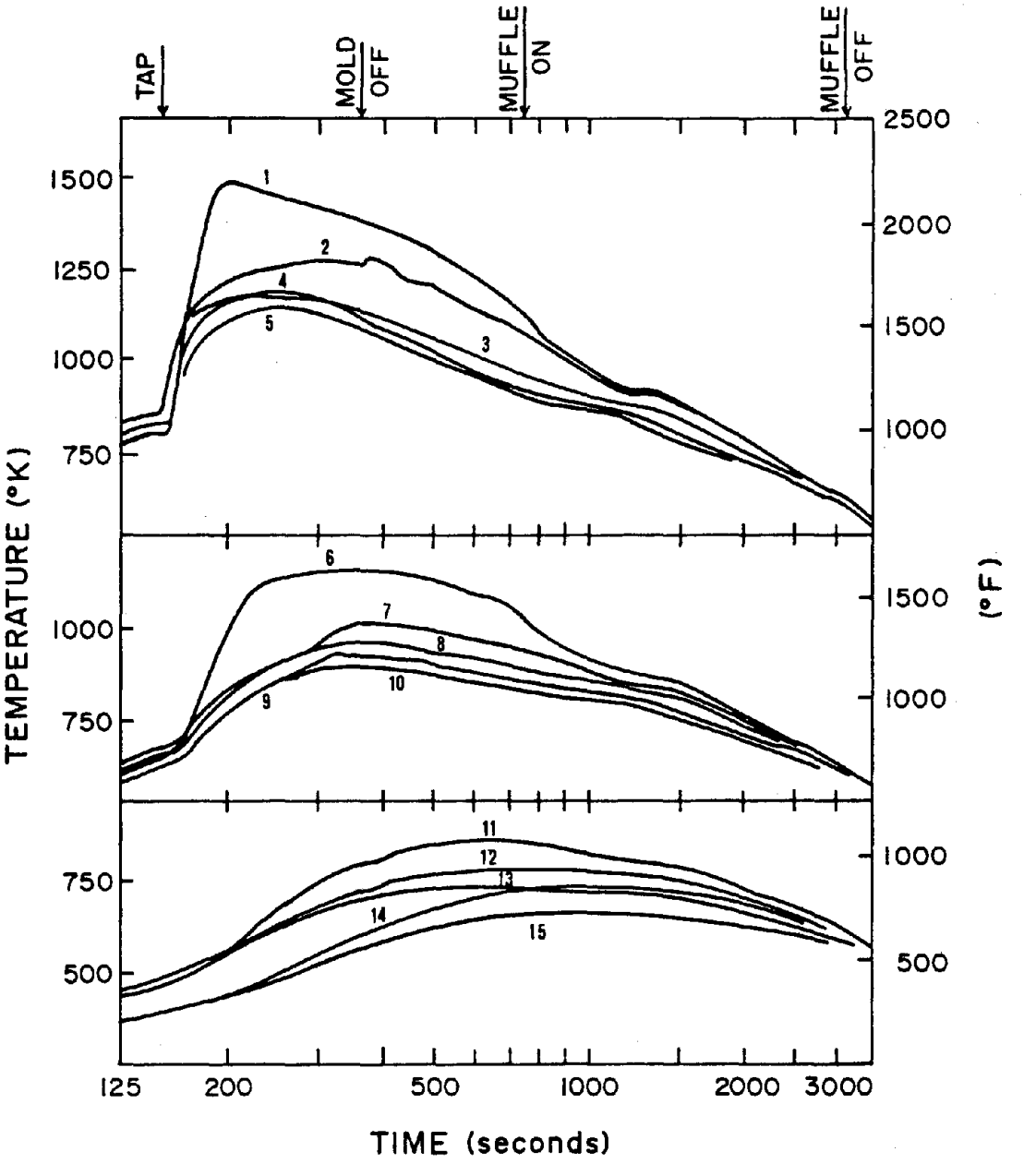

FIGURE 31: TEMPERATURE AS A FUNCTION OF TIME AND POSITION IN THE RAIL DURING THE WELDING PROCESS FOR WELD 1. REFER TO FIGURE 3 FOR THE LOCATIONS OF THE THERMOCOUPLES.

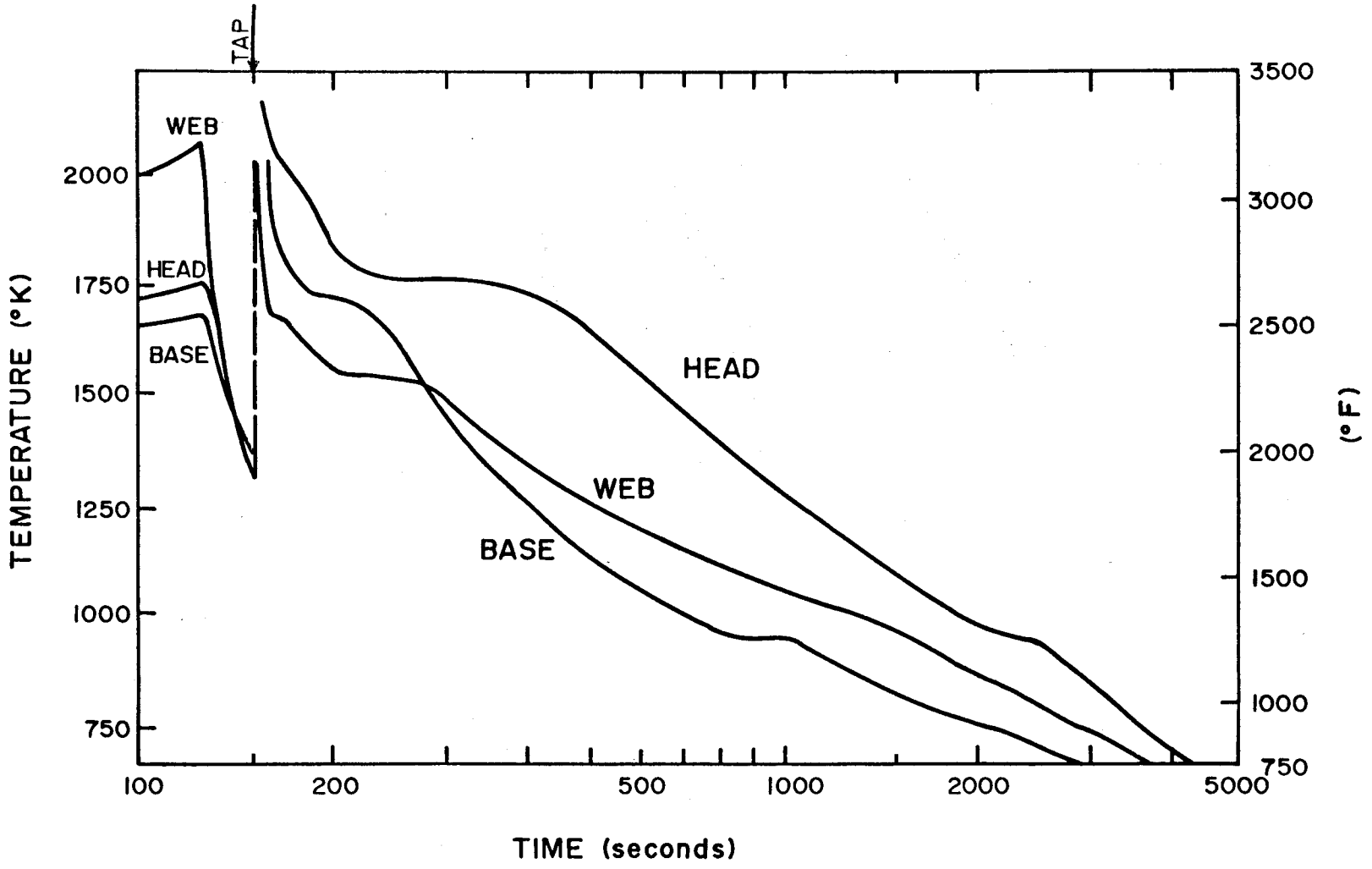

FIGURE 32: TEMPERATURE AS A FUNCTION OF TIME AND POSITION IN THE WELD METAL OF WELD 9. REFER TO FIGURE 4 FOR THE LOCATIONS OF THE THERMOCOUPLES.

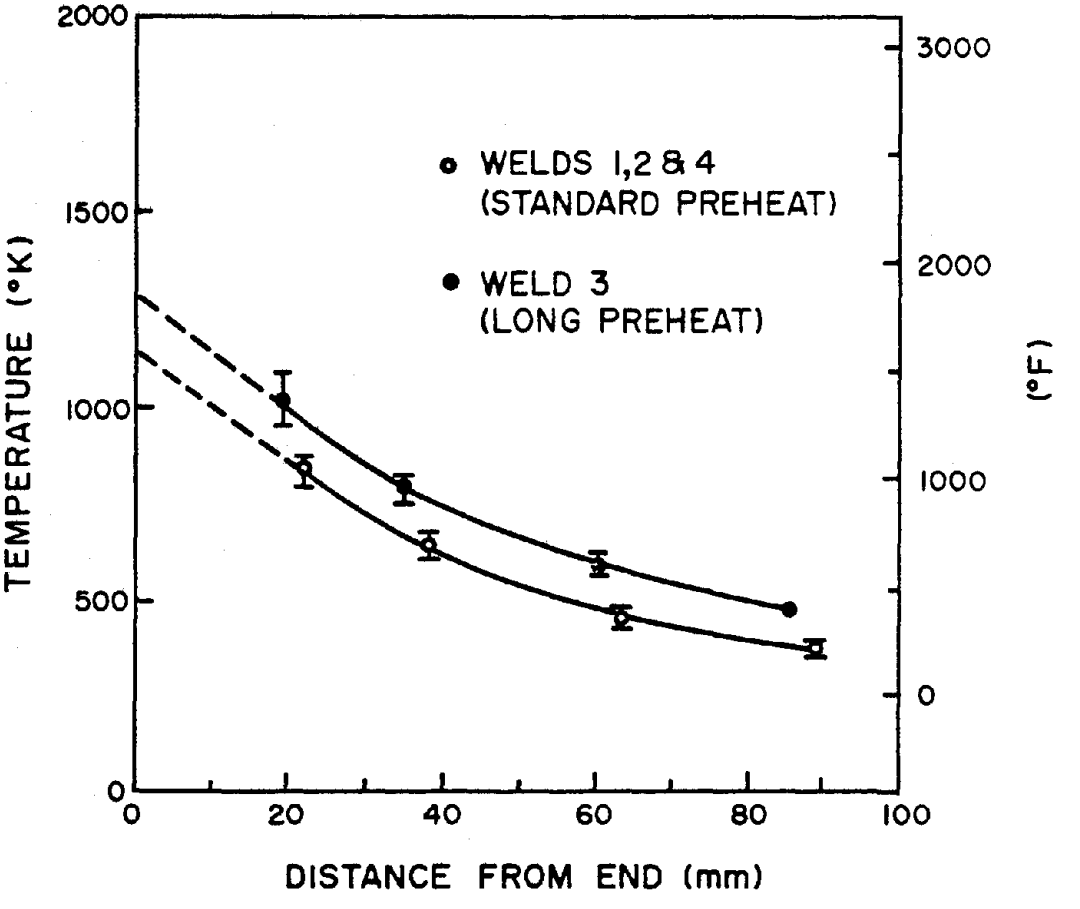

FIGURE 33: RAIL TEMPERATURE DISTRIBUTIONS AT THE END OF PREHEAT. CURVES ARE EXTRAPOLATED TO THE RAIL END.

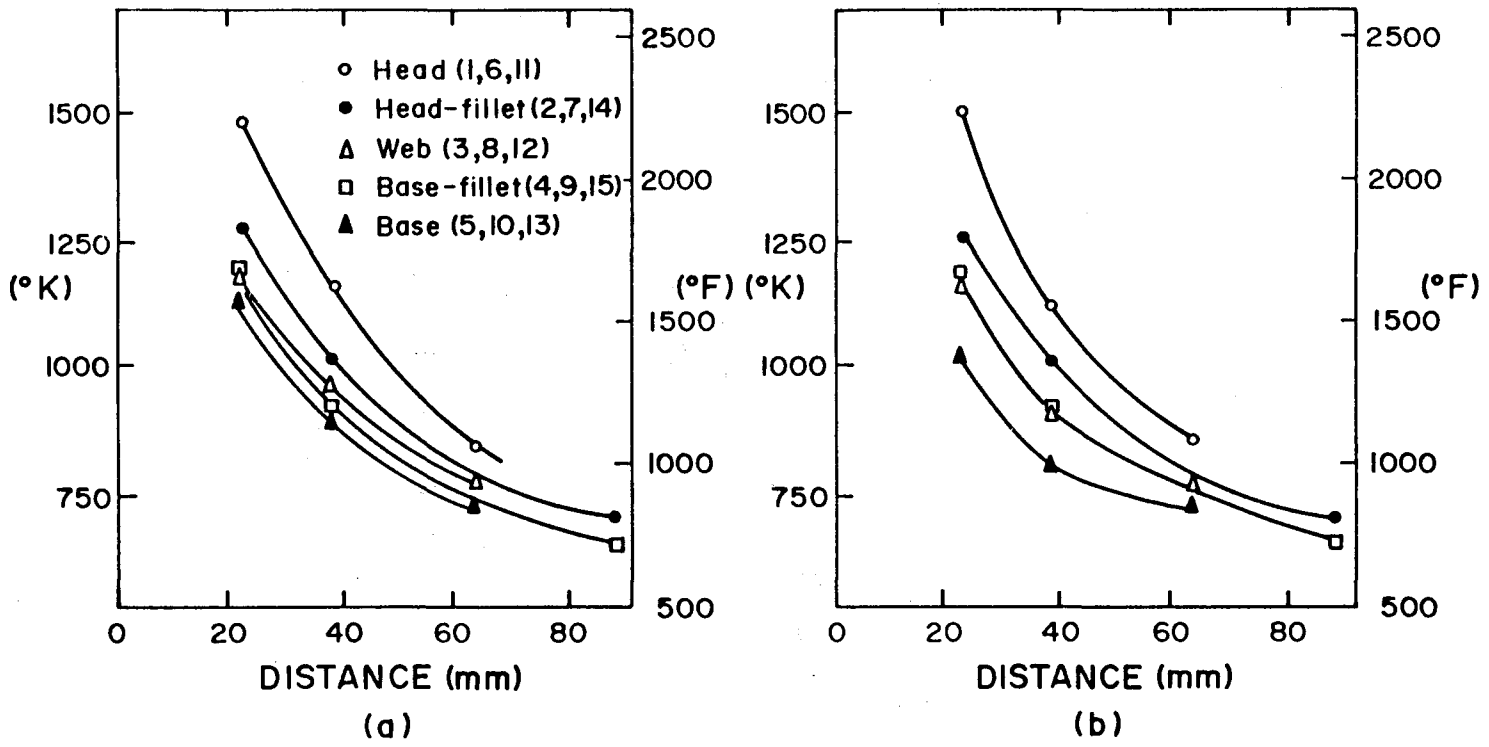

FIGURE 34: PEAK TEMPERATURES AS A FUNCTION OF DISTANCE FROM THE RAIL END: (a) WELD 1; (b) WELD 2. STANDARD PREHEATS. THE NUMBERS IN PARENTHESES IDENTIFY THE THERMOCOUPLE LOCATIONS SHOWN IN FIGURE 3.

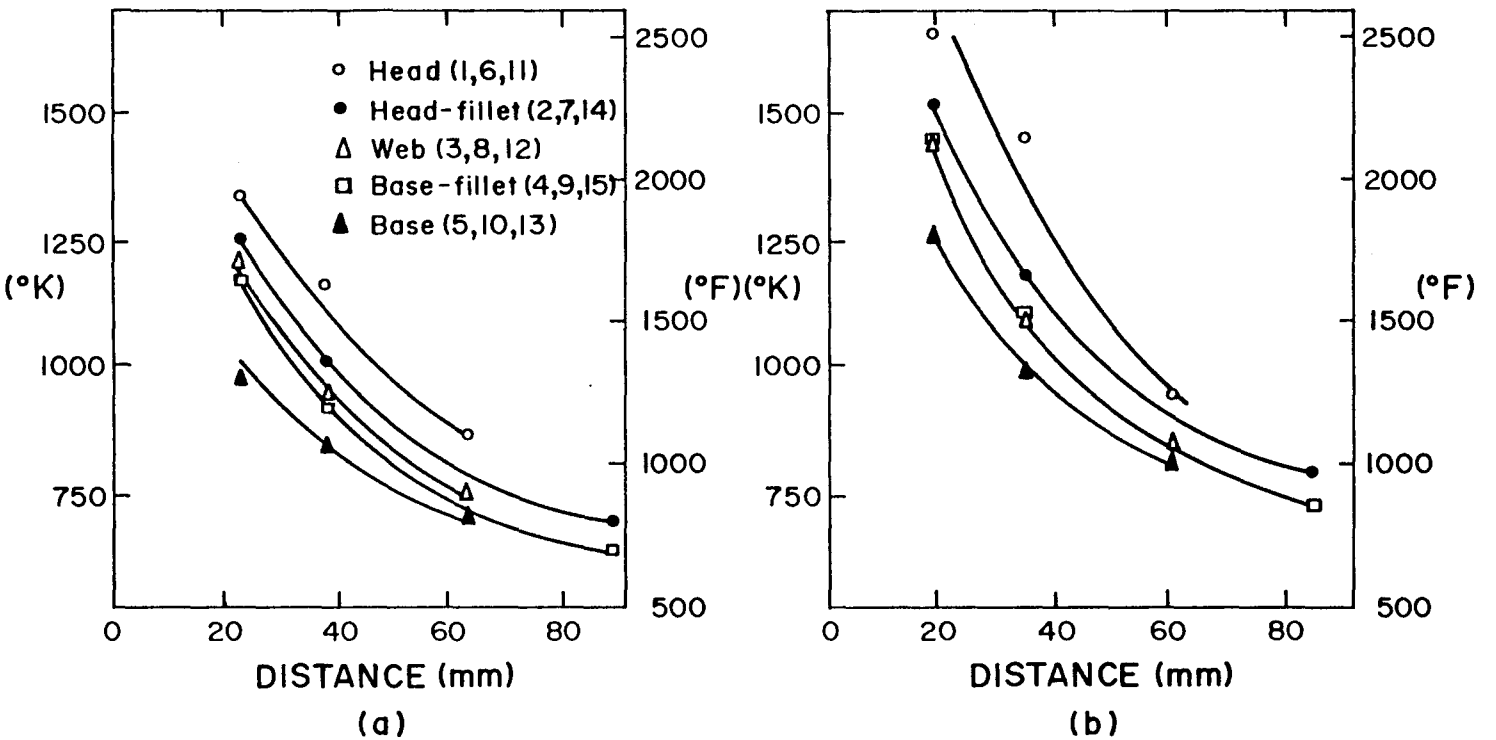

FIGURE 35: PEAK TEMPERATURES AS A FUNCTION OF DISTANCE FROM THE RAIL END: (a) WELD 4 - STANDARD PREHEAT, (b) WELD 3 - LONG PREHEAT. THE NUMBERS IN PARENTHESES IDENTIFY THE THERMOCOUPLE LOCATIONS SHOWN IN FIGURE 3.

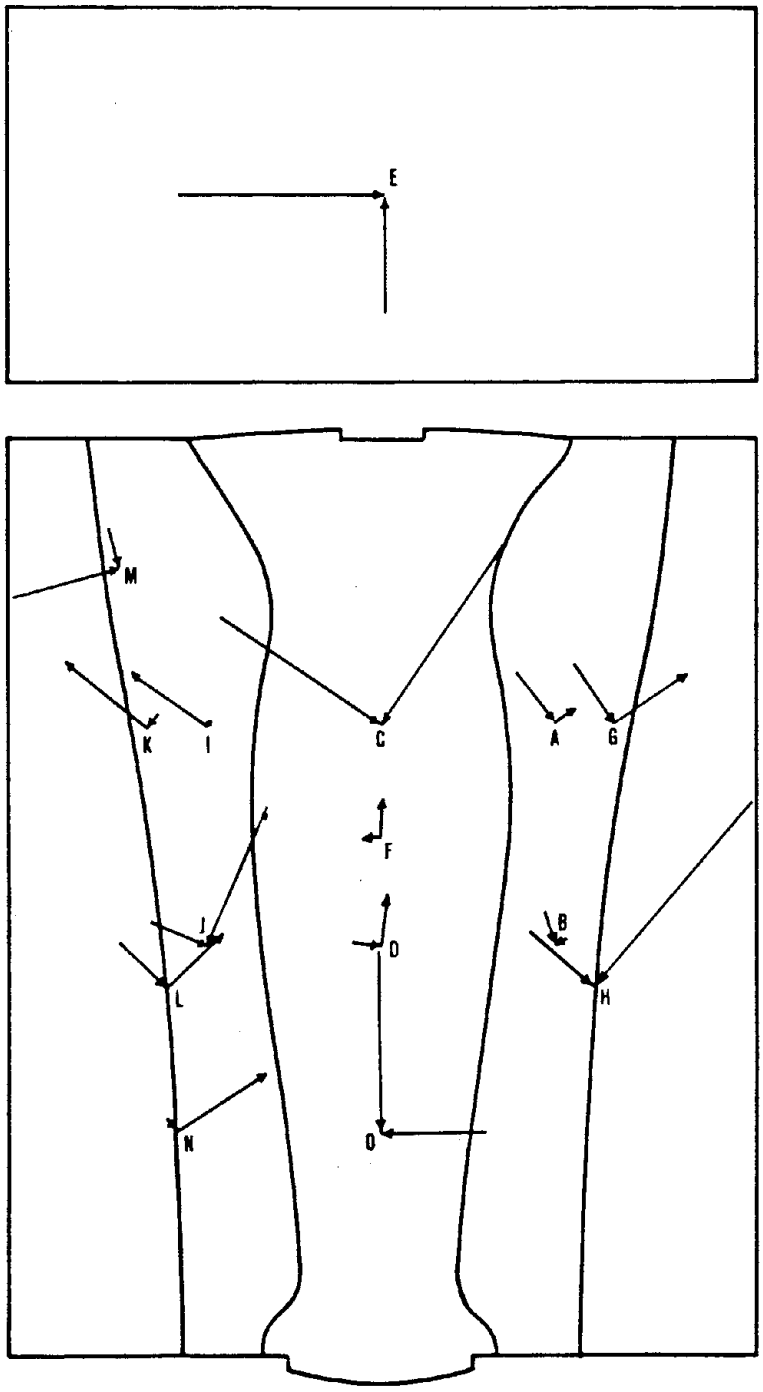

FIGURE 36: PRINCIPAL RESIDUAL STRESSES IN WELD 11. THE LENGTHS OF THE VECTORS ARE PROPORTIONAL TO THE MAGNITUDES OF THE STRESSES. THE LETTERS CORRESPOND TO THE LOCATIONS OF THE ROSETTES SHOWN IN FIGURE 6.

TABLE 1 - MECHANICAL PROPERTIES FROM BEND TESTS ON RAIL AND ON WELDED RAIL.

RAIL SIZE Kg/m	(lb/yd)	WELD	LOADING	MAX. LOAD KN	(kip)	MAX. DEFLECTION cm	(in)	REFERENCE
65	(131)	NONE	HEAD DOWN	1334	(300)	5.3	(2.1)	5
65		EFB	HEAD DOWN	1401	(315)	6.4	(2.5)	5
65		Thermite	HEAD DOWN	1148-1757	(258-395)	1.0-3.6	(0.4-1.4)	5
68	(136)	None	BASE DOWN	1334	(300)*	13.7	(5.4)	23
68		EFB	BASE DOWN	890-1334	(200-300)	1.8-7.6	(0.7-3.0)	23
68		THERMITE	BASE DOWN	712-979	(160-220)	1.3-2.5	(0.5-1.0	23
68	(136)	NONE	LATERAL	445	(100)*	22.6	(8.9)	23
68		EFB	LATERAL	445	(100)*	19.8	(7.8)	23
68		THERMITE	LATERAL	178-298	(40-67)	1.0-3.8	(0.4-1.5	23

*DID NOT FRACTURE.

TABLE 2 - EXPERIMENTAL CONDITIONS FOR WELDS.

WELD NUMBER	RAIL TYPE A	RAIL TYPE B	THERMITE PORTION ALLOY	THERMITE TYPE ST'D	PREHEAT TIME (SEC)* ST'D	PREHEAT TIME (SEC)* LONG	TAP TIME (SEC)Δ	COOLING WITH MUFFLE	COOLING WITHOUT MUFFLE	THERMAL DATA RECORDED
1	Cr	CrMo	X		120		25	X		X
2	Cr	CrMo	X		124		27		X	X
3	Cr	CrMo	X			184	23	X		X
4	ST'D	CrV		X	128		25	X		X
5	ST'D	CrV		X	120		24		X	
6	ST'D	CrV		X		180	25	X		
7	CrMo	HH		X	120		21	X		
8	CrMo	HH		X	131		21		X	
9	Cr	CrV	X		125		25	SEE NOTE		X
10	Cr	CrV	X			180	22		X	
11	ST'D	ST'D		X	120		24		X	
12	CrMo	CrMo	X		124		12+	X		
13	CrMo	CrMo	X		121		24		X	
14	CrMo	CrMo	X			183	24	X		

*SPECIFIED PREHEAT TIMES: STANDARD-2 MIN., LONG-3 MIN.
ΔTOLERANCE ON AUTOMATIC TAP TIME: 18-28 SEC.
NOTE: PRESENCE OF THERMOCOUPLES RESULTED IN WELD 9 BEING COOLED WITH THE MOLD LEFT IN PLACE.
+PREMATURE TAP.

TABLE 3 - NOMINAL COMPOSITIONS OF RAILS AND OF WELD METAL.

ELEMENT	RAIL*			AREA STANDARD AND HH	THERMITE WELD METAL**	
	CrMo	Cr	CrV		ALLOY	STANDARD
C	.70-.80	.73	.72	.69-.82	.61	.53
Mn	.50-.70	1.30	1.27	.70-1.00	1.47	1.28
P	.030 MAX	.023	.014	.04 MAX	--	.036
S	.025 MAX	.026	.03	.05 MAX	--	.019
Si	.20-.25	.30	.22	.10-.25	.17	.13
Cr	.50-.70	1.25	1.04	--	.08	.05
Mo	.16-.20	--	--	--	--	--
V	--	--	.087	--	.10	.065
Ti	--	--	--	--	.02	.025
Al	--	--	--	--	.36	.48
Ni	--	--	--	--	--	<.01
Cu	--	--	--	--	--	.06

*CrMo, Cr, CrV FROM REF. (49).
AREA STANDARD AND HH FROM REF. (50).
**FROM REF. (51).

TABLE 4 - HARDNESSES OF THE HEAT-AFFECTED ZONES

RAIL ALLOY	WELD	PREHEAT, MIN.	USE OF MUFFLE	HARDNESS IN HAZ, R_C MAXIMUM	HARDNESS IN HAZ, R_C MINIMUM	HARDNESS IN RAIL, R_C
CrMo	1	2	YES	40	25	34
	7	2	YES	32	20	30
	12*	2	YES	38	23	33
	2	2	NO	40	22	33
	8	2	NO	41	23	32
	13*	2	NO	41	23	32
	3	3	YES	37	23	33
	14*	3	YES	38	23	32
						Avg: 32.4
CrV	9	2	YES	38	22	32
	4	2	YES	40	22	33
	5	2	NO	40	25	32
	6	3	YES	39	24	33
	10	3	NO	39	23	32
						Avg: 32.4
Cr	9	2	**	38	22	33
	1	2	YES	39	23	34
	2	2	NO	40	24	32
	3	3	YES	38	22	32
	10	3	NO	40	26	32
						Avg: 32.6
ST'D	4	2	YES	32	20	25
	5	2	NO	34	23	28
	6	3	YES	28	20	23
						Avg: 25.3
HH	7	2	YES	27	20	29
	8	2	NO	29	20	20
						Avg: 24.5

*BOTH SIDES OF THE WELD WERE CrMo RAIL STEEL.
**THE MOLD WAS LEFT INTACT FOR THIS WELD.

TABLE 5 - IMPACT ENERGIES OF THE WELD AT 20°C

WELD	A-RAIL HAZ J	A-RAIL HAZ ($ft\text{-}lb_f$)	B-RAIL HAZ J	B-RAIL HAZ ($ft\text{-}lb_f$)	C-RAIL HAZ J	C-RAIL HAZ ($ft\text{-}lb_f$)
St'd MIX						
4	5.6	(4.1)	2.7	(2.0)	6.8	(5.0)
5	4.8	(3.5)	2.4	(1.8)	5.2	(3.8)
6	5.2	(3.8)	2.8	(2.1)	6.9	(5.1)
7	6.5	(4.8)	2.3	(1.7)	2.8	(2.1)
8	6.5	(4.8)	2.6	(1.9)	2.6	(1.9)
ALLOY MIX						
1	6.1	(4.5)	2.0	(1.5)	5.7	(4.2)
2	5.2	(3.8)	1.8	(1.3)	6.8	(5.0)
3	4.3	(3.2)	1.5	(1.1)	4.3	(3.2)
9	5.2	(3.8)	1.6	(1.2)	9.6	(7.1)*
10	5.3	(3.9)	2.0	(1.5)	6.9	(5.1)
12	5.6	(4.1)	1.6	(1.2)	6.8	(5.0)
13	6.5	(4.8)	1.8	(1.3)	5.4	(4.0)
14	6.8	(5.0)	1.5	(1.1)	5.2	(3.8)

*ONLY 10 PERCENT OF HAZ IN FRACTURE.

TABLE 6 - TENSILE PROPERTIES OF THE WELDS

WELD	SPECIMEN LOCATION AND RAIL	BHN	YIELD STRENGTH 0.2% OFFSET MPa	(ksi)	ULTIMATE STRENGTH MPa	(ksi)	TRUE FRACTURE STRENGTH MPa	(ksi)	PERCENT ELONGATION**	PERCENT REDUCTION OF AREA
St'd MIX										
4	A(HAZ)-St'd		476	(69)	855	(124)	1103	(160)	6.8	25.3
	C(WELD)	236	469	(68)	772	(112)	814	(118)	2.7	4.7
	B(HAZ)-CrV		558	(81)	924	(134)	1475	(214)	11.9	58.3
5	A-St'd		552	(80)	883	(128)	1048	(152)	4.9	16.8
	C	255	538	(78)	800	(116)	821	(119)	1.5	2.4
	B-CrV		534	(78)	924	(134)	945	(137)*	9.0	20.5
6	A-St'd		462	(67)	855	(124)	1041	(151)	5.7	18.9
	C	227	462	(67)	786	(114)	834	(121)	3.8	5.5
	B-CrV		579	(84)+	958	(139)	938	(136)*	10.6	25.9
7	A-CrMo		545	(79)+	952	(138)	1565	(227)	10.0	54.7
	C	233	586	(85)	800	(116)	814	(118)	1.3	1.6
	B-HH		469	(68)+	862	(125)	1344	(195)	9.9	46.0
8	A-CrMo		588	(81)+	952	(138)	1372	(199)	10.4	49.1
	C	244	572	(83)	841	(122)	869	(126)	2.6	3.2
	B-HH		476	(69)+	869	(126)	1317	(191)	10.1	44.1

**1.0 in. (25.4 mm) GAGE LENGTH.
*FAILED OUTSIDE NECKED REGION, WITH 0.1 in (2.5 mm).
+YIELD POINT DISPLAYED.

CONTINUED

TABLE 6 - CONTINUED

WELD	SPECIMEN LOCATION AND RAIL	BHN	YIELD STRENGTH 0.2% OFFSET MPa	(ksi)	ULTIMATE STRENGTH MPa	(ksi)	TRUE FRACTURE STRENGTH MPa	(ksi)	PERCENT ELONGATION**	PERCENT REDUCTION OF AREA
ALLOY MIX										
1	A-Cr		558	(81)+	931	(135)	1048	(152)	7.6	24.1
	C	310	683	(99)	1000	(145)	1027	(149)	3.2	2.4
	B-CrMo		510	(74)+	931	(135)	1110	(161)	7.2	33.0
2	A-Cr		586	(85)+	931	(135)	1544	(224)	10.3	43.2
	C	290	669	(97)	938	(136)	965	(140)	1.0	2.4
	B-CrMo		552	(80)	952	(138)	1041	(151)	10.0	45.2
3	A-Cr		593	(86)+	945	(137)	1262	(183)	9.5	50.0
	C	268	558	(81)	889	(129)	931	(135)	1.6	2.4
	B-CrMo		531	(77)+	938	(136)	1489	(216)	10.8	54.8
9	A-Cr		558	(81)+	889	(129)	1517	(220)	10.9	57.3
	C	286	620	(90)	979	(142)	1020	(148)	2.1	3.9
	B-CrV		545	(79)+	883	(128)	1496	(217)	13.0	61.2

**1.0 in (25.4 mm) GAGE LENGTH.
+YIELD POINT DISPLAYED.

CONTINUED

TABLE 6 - CONTINUED

WELD	SPECIMEN LOCATION AND RAIL	BHN	YIELD STRENGTH 0.2% OFFSET MPa	(ksi)	ULTIMATE STRENGTH MPa	(ksi)	TRUE FRACTURE STRENGTH MPa	(ksi)	PERCENT ELONGATION**	PERCENT REDUCTION OF AREA
ALLOY MIX										
10	A-Cr		531	(77)+	945	(137)	1096	(159)	8.4	25.8
	C	286	634	(92)	979	(142)	1007	(146)	1.8	3.2
	B-CrV		565	(82)+	958	(139)	1069	(155)	7.4	23.9
12	A-CrMo		717	(104)	931	(135)	1627	(236)	9.9	59.4
(two sets)	C	296	572	(83)	938	(136)	972	(141)	1.2	3.2
	B-CrMo		607	(88)	924	(134)	1565	(227)	11.0	57.6
	A-CrMo		620	(90)	938	(136)	1034	(150)*	8.3	29.4
	C		607	(88)	931	(135)	958	(139)	1.0	2.4
	B-CrMo		510	(74)	910	(132)	1551	(225)	10.1	54.5
13	A-CrMo		552	(80)+	952	(138)	1613	(234)	10.3	56.4
	C	314	696	(101)	979	(142)	1007	(146)	1.3	2.4
	B-CrMo		558	(81)+	958	(139)	1462	(212)	9.6	51.4
14	A-CrMo		820	(119)	1000	(145)	1455	(211)	11.6	47.2
	C	282	614	(89)	924	(134)	958	(139)	1.1	
	B-CrMo		531	(77)+	945	(137)	1503	(218)	10.0	54.3

**1.0 in (25.4 mm) GAGE LENGTH.
*FAILED OUTSIDE NECKED REGION, WITHIN 2.5 mm (0.1 in).
+YIELD POINT DISPLAYED.

TABLE 7 - FRACTURE CHARACTERISTICS OF TENSILE SPECIMENS OF THE HEAT AFFECTED-ZONES

FRACTURE TYPE	SPECIMEN	RAIL TYPE	RANGE OF REDUCTION OF AREA (%)
1. CLEAVAGE WITH SHEAR LIP	1-A, 10-A, 5-B*, 6-B*, 10-B, 12-A* (LOWEST RA)	Cr CrV CrMo	20.5 - 29.4
2. NO SHEAR LIP, CLEAVAGE WITH FIBROUS CENTRAL REGION	4-A, 5-A, 6-A	STANDARD	16.8 - 25.3
3. "CUP AND CONE," FIBROUS CENTRAL REGION WITH SHEAR LIP	1-B 7-B, 8-B	CrMo HH	33.0 - 46.0
4. "CUP AND CONE" WITH RADIAL FEATURES JOINING FIBROUS CENTRAL REGION TO SHEAR LIP	2-A, 3-A, 9-A 4-B, 9-B 2-B, 3-B, 7-A 8-A, 12-A (HIGHEST RA), 12-B (BOTH) 13-A,B, 14-A,B	Cr CrV CrMo	43.2 - 61.2

*FAILED OUTSIDE NECKED REGION, WITHIN 2.5 mm.

TABLE 8 - FRACTURE CATEGORIES OF TENSILE SPECIMENS IN THE REGION OF MINIMUM HARDNESS

RAIL	NUMBER OF SPECIMENS	LOW DUCTILITY FRACTURE TYPE 1	LOW DUCTILITY FRACTURE TYPE 2	HIGH DUCTILITY FRACTURE TYPE 3	HIGH DUCTILITY FRACTURE TYPE 4
STANDARD	3		3		
HEAD-HARDENED	2			2	
Cr	5	2			3
CrMo	13	1		1	11
CrV	5	3			2

cf. page 29 for description of types.

TABLE 9 - EDS ANALYSES OF THE SURFACES OF THE AS-CAST COLUMNAR STRUCTURE IN STANDARD WELD METAL

ELEMENT	COUNT RATIOS (Fe = 1) WELD 4	WELD 8	WELD 6	WELD 7
Fe	1	1	1	1
Ni	0.49	1.33	0.36	0.35
Cu	0.21	0.64	0.15	0.14
Zn	0.13	0.37	0.09	0.09
Al	0.03	0.16	0.03	0.03
Mn	0.06	0.09	0.05	0.05
Si	0.03	0.07	0.04	0.03
P	0.05	0.14	0.05	0.05

TABLE 10 - EDS ANALYSES OF THE SURFACES OF DENDRITES IN ALLOY WELD METAL

ELEMENT	COUNT RATIOS (Fe = 1) WELD 10	WELD 3
Fe	1	1
Ni	0.42	0.36
Cu	0.31	0.16
Zn	0.18	0.1
Al	0.03	0.03
Mn	0.06	0.05
Si	0.04	0.04
P	0.06	0.05
Cr	0.05	0.04

TABLE 11 - INCLUSION CONTENT OF WELD METAL

MAGNIFICATION: 400X, FIELDS PER SAMPLE: 10
AREA PER FIELD: 257,600 μ^2 (0.26 mm^2)
FEATURE AREA RANGE: 0-400 μ^2

WELD	TOTAL NO. OF FEATURES OBSERVED, n	No. of FEATURES WITH AREA >400 μ^2*	SIZE: (μ^2) MEAN, $\bar{x}$	ST'D DEVIATION	MAX.	VOLUME FRACTION, V_V (%)	95% CONFIDENCE LIMITS ON V_V (%)
5	196	11	38.7	52.4	280.7	0.294	$0.239 < V_V < 0.350$
6	162	10	69.4	86.3	371.5	0.436	0.353 0.520
7	162	3	57.6	77.7	369.2	0.362	0.287 0.437
12+	157	4	45.2	67.8	379.8	0.276	0.211 0.340
13	151	9	40.8	63.2	327.3	0.239	0.180 0.299
14	168	9	75.3	91.4	383.0	0.491	0.401 0.581

*PRIMARILY MICROPOROSITY.
+PREMATURE TAP.

TABLE 12 - TIME IN THE TRANSFORMATION RANGE DURING COOLING

POSITION		DISTANCE FROM END, mm	TIME BETWEEN 1000°K AND 810°K; SECONDS WELD 1 (MUFFLE)	WELD 2 (NO MUFFLE)	WELD 3 (MUFFLE)	WELD 4 (MUFFLE)	WELD 9 (MOLD IN PLACE)
HEAD	1	19*	920	590	1000	690	--
	6	35*	940	600	1020	790	--
HEAD-FILLET	2	22	960	620	960	660	--
	7	38	1100	700	1020	960	--
WEB	3	22	1040	720	1010	870	--
	8	38	--	--	1050	--	--
BASE-FILLET	4	22	900	770	950	800	--
	9	38	--	--	1050	--	--
BASE	5	22	840	720	910	--	--
	10	38	--	--	--	--	--
WELD MET.							
HEAD			--		--		1380
WEB			--		--		1140
BASE			--		--		880

*IN WELD 3, THE THERMOCOUPLES WERE LOCATED AT 19 and 35 mm; IN WELDS 1, 2 AND 4, THEY WERE LOCATED AT 22 AND 38 mm.

TABLE 13 - PRINCIPAL RESIDUAL STRESSES IN WELD 11

GAGE LOCATION	PRINCIPAL STRESSES MPa (ksi) s_p		s_q		ORIENTATION OF s_p FROM THE WELD VERTICAL CENTERLINE θ, +ccw, -cw, DEGREES	LOCATION
E	-285.4	(-41.4)	-160.6	(-23.2)	+1.3*	HEAD RUNNING SURFACE
M	-56.5	(-8.2)	-154.4	(-22.4)	+15.9	HEAD SIDE
K	-22.8	(-3.3)	+147.6	(+21.4)	-38.7	HEAD-WEB FILLET
I	+3.4	(+0.5)	+129.6	(+18.8)	-36.2	HEAD-WEB FILLET
C	-229.2	(-43.4)	-271.0	(-39.3)	-34.0	HEAD-WEB FILLET
A	-88.3	(-12.8)	+33.8	(+4.9)	+36.9	HEAD-WEB FILLET
G	-96.5	(-14.0)	+128.2	(+18.6)	+34.6	HEAD-WEB FILLET
L	+109.6	(+15.9)	-94.5	(-13.7)	-44.3	WEB
J	-206.8	(-30.0)	-82.7	(-12.0)	-23.6	WEB
F	+52.4	(+7.6)	+26.2	(+3.8)	-1.95	WEB
D	+69.6	(+10.1)	-40.0	(-5.8)	-7.25	WEB
B	-48.3	(-7.0)	-12.4	(-1.8)	+17.45	WEB
H	-336.5	(-48.8)	-115.8	(-16.8)	-40.4	WEB
N	-18.6	(-2.7)	+151.0	(+21.9)	+33.9	BASE-WEB FILLET
O	-251.	(-36.4)	-146.2	(-21.2)	+0.75	BASE-WEB FILLET

*ccw wrt LONGITUDINAL CENTERLINE OF RAIL WHEN VIEWED FROM ABOVE.